Analysis of Type Three System Transport Mechanism in Gram-negative Bacteria

Dissertation

Zur Erlangung des akademischen Grades

doctor rerum naturalium
(Dr. rer. nat.)

im Fach Biologie
eingereicht an der

Mathematisch-Naturwissenschaftlichen Fakultät I
der Humboldt Universität zu Berlin

von

Kim Stephanie Dohlich

Präsident der Humboldt Universität zu Berlin
Prof. Dr. Jan-Hendrik Olbertz

Dekan der Mathematisch-Naturwissenschaftlichen Fakultät I
Prof. Stefan Hecht, Ph.D.

Gutachter: Prof. Arturo Zychlinsky, Ph.D.
Prof. Dr. Kai Matuschewski
Prof. Dr. Gerhard Wolber

Tag der mündlichen Prüfung: 17.12.2013

The Road not Taken

Two roads diverged in a yellow wood,
And sorry I could not travel both
And be one traveler, long I stood
And looked down one as far as I could
To where it bent in the undergrowth;

Then took the other, as just as fair,
And having perhaps the better claim,
Because it was grassy and wanted wear;
Though as for that the passing there
Had worn them really about the same,

And both that morning equally lay
In leaves no step had trodden black.
Oh, I kept the first for another day!
Yet knowing how way leads on to way,
I doubted if I should ever come back.

I shall be telling this with a sigh
Somewhere ages and ages hence:
Two roads diverged in a wood, and I -
I took the one less traveled by,
And that has made all the difference.

Robert Frost (1920)

Disclaimer

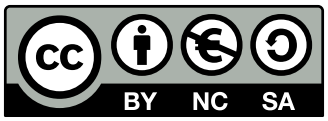

This work has partially been published as a research manuscript:
Dohlich K, Zumsteg AB, Goosmann C, Kolbe M (2014) A Substrate-Fusion Protein Is Trapped inside the Type III Secretion System Channel in Shigella flexneri. PLoS Pathog 10(1): e1003881. doi:10.1371/journal.ppat.1003881

Zusammenfassung

Das Typ III Sekretionssystem (T3SS) ist ein makromolekularer Proteinkomplex den Gram-negative Bakterien nutzen um in einem Schritt Effektorproteine (Effektoren) aus dem Zytosol über die Doppelmembran zu sekretieren. Für viele Bakterien ist das T3SS ein essenzieller Virulenzfaktor, der es ihnen erlaubt mit ihrem Wirt zu interagieren und diesen zu manipulieren. Charakteristisch für das T3SS ist die membrangebundene strukturelle Komponente, der sogenannte Nadelkomplex. Der Nadelkomplex ähnelt in seiner Struktur einer Spritze, deren Basalkörper die bakteriellen Membranen und das Periplasma durchspannt und einer Nadel, die vom Basalkörper aus dem Bakterium hervorragt. Basierend auf dem Modell einer Spritze wird angenommen, dass Effektoren entfaltet und anschließend durch Basalkörper und Nadelkanal sekretiert werden. Trotz der kontinuierlichen Forschung an T3SS entbehrt dieses Modell einer experimentellen Grundlage und der Sekretionsmechanismus ist nicht vollständig erklärt.

Ziel der Arbeit war es, eine experimentelle Basis für den Sekretionsmechanismus des T3SS zu schaffen um die Funktionsweise des T3SS besser zu erfassen. Um zu verstehen, wie das T3SS Effektoren sekretiert, wurden zunächst Fusionsproteine konstruiert, welche aus einem Effektor und einem stabil gefalteten Knotenprotein bestehen. Die Effektorfunktion wird durch die Fusion nicht beeinflusst und der Knoten faltet nativ innerhalb des Fusionsproteins. Aufgrund der Position des Knotens in der Fusion ist davon auszugehen, dass der Knoten während der Sekretion nicht entfalten kann. Die Effektordomäne wird sekretiert, der Knoten verbleibt jedoch im Kanal und verstopft das T3SS. Zusätzlich wurden die blockierten Nadelkomplexe mittels Immunodetektion im Elektronenmikroskop untersucht und das Fusionsprotein am isolierten Nadelkomplex lokalisiert. Nach dem derzeitigen Stand der Forschung und unserem Wissen ist diese Arbeit die erste Visualisierung von Effektorfusionen an isolierten Nadelkomplexen. Die Effektorfusion wird N-terminal voran durch den Kanal sekretiert, wobei der Kanal das Substrat umschließt und gegen Proteasen und chemische Modifikationen abschirmt. Die Ergebnisse dieser Arbeit untermauern ein elementares Verständnis über die Funktionsweise des T3SS und liefern eine vielversprechende Strategie für zukünftige *in situ*-Strukturanalysen. Dieser Ansatz lässt sich auch auf andere Proteinsekretionssysteme übertragen, bei welchen Substrate vor dem Transport entfaltet werden müssen.

Abstract

The Type III Secretion System (T3SS) is a macromolecular complex used by Gram-negative bacteria to secrete effector proteins from the cytoplasm across the bacterial envelope in a single step. For many pathogens, the T3SS is an essential virulence factor that enables the bacteria to interact with and manipulate their respective host. A characteristic structural feature of the T3SS is the needle complex (NC). The NC resembles a syringe with a basal body spanning both bacterial membranes and a long needle-like structure that protrudes from the bacterium. Based on the paradigm of a syringe-like mechanism, it is generally assumed that effectors are unfolded and secreted from the bacterial cytoplasm through the basal body and needle channel. Despite extensive research on T3SS, this hypothesis lacks experimental evidence and the mechanism of secretion is not fully understood.

This work aimed to provide an experimental basis for the model of the T3SS mechanism for a better comprehension of how secretion by T3SS works. In order to elucidate details of the effector secretion mechanism, fusion proteins consisting of an effector and a bulky protein containing a knotted motif were generated. The functionality of the effector domain within the fusion was tested, as well as the folding status of the knotted domain. It is assumed that the knot cannot be unfolded during secretion of the chimera. Consequently, these fusions are accepted as T3SS substrates but remain inside the NC channel and obstruct the T3SS. Furthermore, the obstructed T3SS channel was analyzed by immuno-labeling combined with electron microscopy. This is, to our best knowledge, the first time effector fusions have been visualized together with isolated NCs and it demonstrates that effector proteins are secreted directly through the channel with their N-terminus first. The channel physically encloses the fusion protein and shields it from a protease and chemical modifications. These results corroborate an elementary understanding of how the T3SS works and provide a powerful tool for *in situ*-structural investigations in the future. This approach might also be applicable to other protein secretion systems that require unfolding of their substrates prior to secretion.

Contents

1 Introduction

1.1 *Shigella* - a model for type III secretion

Shigella are the causative agent of bacillary dysentery (Shigellosis). They are Gram-negative γ-proteobacteria which are rod-shaped, non-flagellated and thus non-motile (Peng *et al.*, 2009). The genus *Shigella* contains four species, namely *S. dysenteriae*, *S. flexneri*, *S. sonnei* and *S. boydii*, all of which are able to cause disease in humans which are *Shigella*s only natural hosts. First descriptions date back to the late 19^{th} century where the Japanese scientist Kiyoshi Shiga reported a bacterium being responsible for a dysenteric epidemic with over 89.000 cases of which more than 22.000 were fatal. *Shigella* are very similar to *Escherichia coli*, but were classified into a different genus because of their medical significance in the 1940s. In fact, they are so similar that sequence analysis revealed *Shigella* being clones of *E. coli* species and that enteroinvasive *E. coli* and *Shigella* share a common pathovar (Lan & Reeves, 2002). Although distinct phylogeny is kept merely for traditional and medical reasons, bacteria will be regarded as independent species throughout this work.

The lack of clean water, hygiene and malnutrition are contributing factors to higher incidents in developing countries. In addition, the bacteria are highly contagious: oral uptake of 10-100 bacteria is sufficient to cause disease (DuPont *et al.*, 1989), which is at least partially because of their resistance to acidic conditions (Gorden & Small, 1993; Jennison & Verma, 2007). With regards to acquisition of antibiotic resistances (von Seidlein *et al.*, 2006; Shiferaw *et al.*, 2012), infections with *Shigellae* are in need for alternative medical strategies, especially since there is no vaccine available yet (Sansonetti, 2006; Phalipon *et al.*, 2008). In the developed world, *S. sonnei* is the predominant isolate (77% of all cases) whereas *S. flexneri* is endemic in developing countries and the most frequent isolate of bacillary dysentery worldwide (WHO on diarrhoeal diseases/Shigellosis, 2009). *Shigella*-caused dysentery

is characterized by an inflammatory response with major pathology in the colon and rectum where the bacteria invade the epithelial cells (Sansonetti *et al.*, 1999). As the epithelial lining is protected by a thick layer of mucus and a brush border, bacteria cannot enter directly from the lumen through the apical side but have to cross the epithelium and infiltrate epithelial cells from the basolateral side.

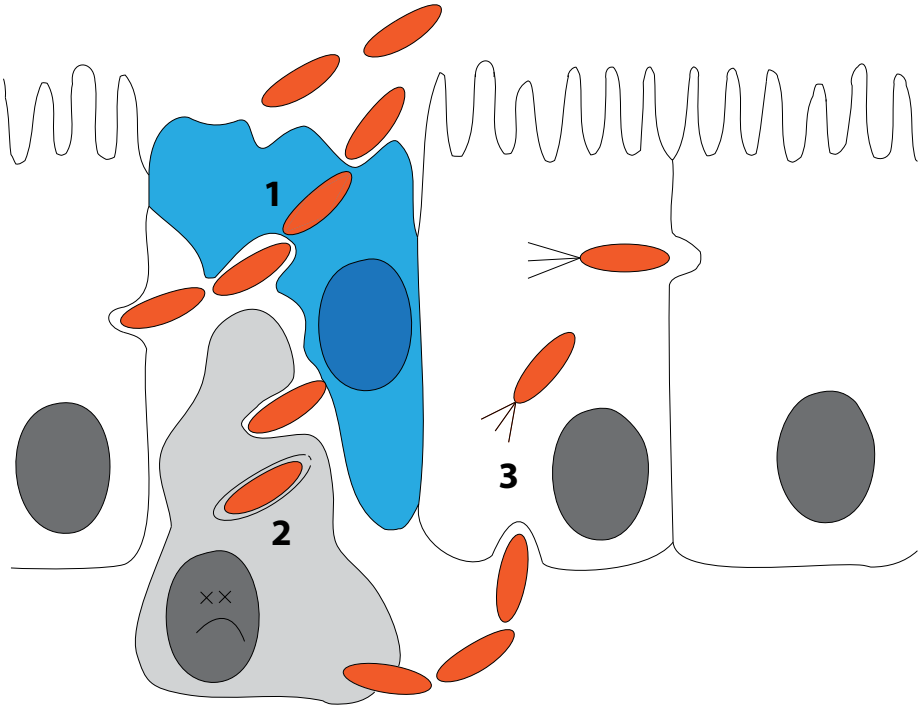

Figure 1.1: Early steps in *Shigella flexneri* infection. Bacteria (orange) traverse the epithelial cell line (white) through M-cells (blue, **1**) where they encounter macrophages (grey). The bacteria then escape the phagolysosome and induce pyroptosis (**2**). Subsequently, bacteria evade the macrophage and enter the epithelial cells from the basolateral side, where they hijack the actin network for actin-based motility (**3**).

Three major steps take place before invasion of epithelial cells by *S. flexneri*: First, bacteria cross the epithelium through microfold cells (M-cells) that constantly sample macromolecules and bacteria from the gut lumen (Wassef *et al.*, 1989; Perdomo *et al.*, 1994)(Fig. 1.1, **1**). Next, resident macrophages engulf the bacteria which subsequently escape the phagosome and activate Caspase-1. By induced cell death, the bacteria evade phagocytic killing (**2**) (Zychlinsky *et al.*, 1992, 1994; Schroeder & Hilbi, 2008; Senerovic *et al.*, 2012). Membrane disruption of macrophages leads to release of mature Interleukin-1β, thereby stimulating the inflammatory response. As a consequence, tissue destruction further destabilizes the epithelial lining which in turn favors bacterial infiltration of the lamina propria (Perdomo *et al.*, 1994). The bacterium invades the epithelium by stimulating phagocytosis (High *et al.*, 1992), escapes the phagosome and hides inside the cytoplasm of epithelial cells. After entering from the basolateral side, bacteria spread intracellularly to neighboring cells

by hijacking the actin-network of the host. This exploitation of host factors is displayed by the formation of actin tails which confer motility to the bacteria (Fig. 1.1, **3**) (Mounier *et al.*, 1992; Vasselon *et al.*, 1992; Prevost *et al.*, 1992). Once inside a host cell, *S. flexneri* replicates remarkably fast with a doubling time of 40 min, pointing out the efficient adaptation of the bacterium to the host environment (Sansonetti *et al.*, 1986; Ray *et al.*, 2009).

Most of these steps depend on a functional Type III Secretion System (T3SS) which is encoded on an extrachromosomal 200 to 220 kb plasmid (Venkatesan *et al.*, 2001; Buchrieser *et al.*, 2000). This plasmid is present in all virulent *Shigella flexneri* isolates (Sansonetti *et al.*, 1982). Specifically a 31 kb core region, called the entry region, is indispensable and sufficient for invasion of epithelial cells (Maurelli *et al.*, 1985). This region encodes genes for structural components of the T3SS, most of the substrates, chaperones and regulators. Apart from its role as a highly prevalent human pathogen, *Shigella flexneri* is a model organism for understanding the T3SS.

1.2 Type III Secretion Systems: Syringes mediating bacterial virulence

The T3SS is metaphorically described as a molecular syringe that *S. flexneri* and other Gram-negative bacteria use to inject effector proteins into their hosts (Fig. 1.2). The T3SS enables delivery of effector proteins into eukaryotic cells and is an important instrument in host-pathogen interaction (Cornelis, 2006; Galan & Wolf-Watz, 2006). Some of the worst pandemics in human history, for example plague and cholera, were caused by bacteria that are known to utilize a T3SS. Recently, the T3SS has been also focused on as it might serve as a target for novel anti-infective therapies (Clatworthy *et al.*, 2007).

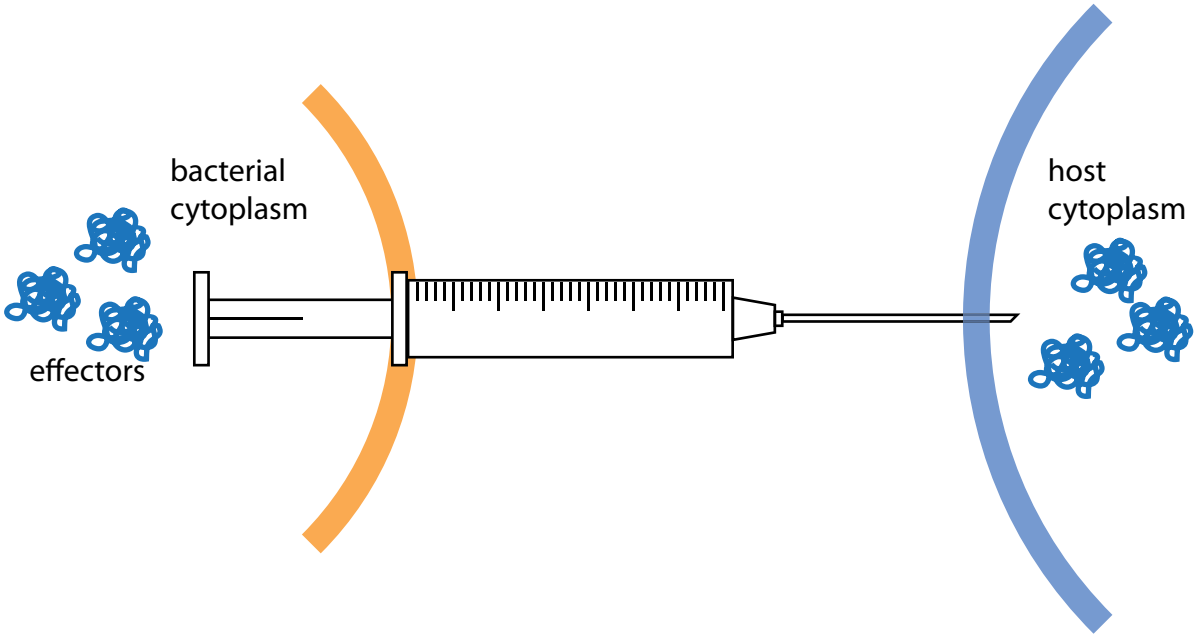

Figure 1.2: Paradigm of type III secretion. Bacterial effector proteins (blue) are secreted across the bacterial membrane (orange) and injected into the host cell (light blue). The T3SS (syringe) forms a continuous channel connecting both cytoplasms.

More than 20 years ago, the T3 secretion pathway was discovered by analysis of *Yersinia* outer proteins (Yops) as it was distinguished from the type I transporters and the sec-dependent type II pathway (Salmond & Reeves, 1993). The independence from a Sec-signal peptide as seen for type I but also the dependency on a different gene cluster for secretion like type II secretion led to the definition of a third bacterial secretion pathway.

By the end of the 20th century, the structural component had been identified in *Salmonella* and *Shigella* and isolated from the bacterial envelope (Kubori *et al.*, 1998; Blocker *et al.*, 2001). This syringe-like needle complex (NC) is the structural hallmark of the T3SS pathway. The T3SS bridges the gap between the bacterium and the host cell as it is thought to provide

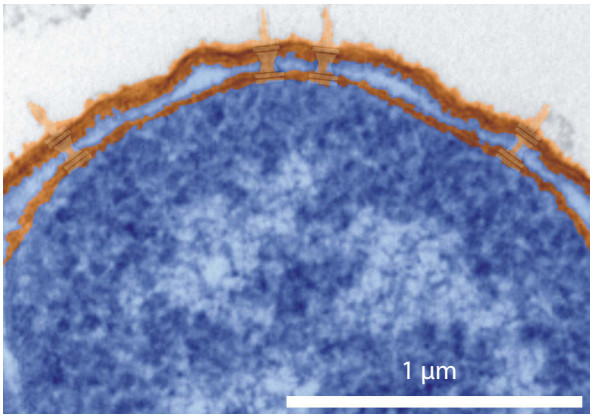

Figure 1.3: Type III needle complexes in the bacterial cell wall. Artificially coloured transmission electron-micrograph of a bacterial cross-section. The needle complexes embedded into the bacterial membranes (orange) are highlighted. Image courtesy of Ulrike Abu Abed, Diane Schad and Michael Kolbe.

a continuous channel between the bacterial and host cytosol (Büttner & He, 2009). Consisting of more than 25 structural proteins, the syringe is a complex export system spanning the bacterial membranes and the periplasm (Fig. 1.3).

Both pathogens and symbionts use T3SS to establish a trans-kingdom relationship with one or more eukaryotic organisms by secreting proteins via the T3SS pathway, which are stored in the bacterial cytoplasm prior to secretion (Hueck, 1998; Soto *et al.*, 2006; Preston, 2007; Büttner & He, 2009). These proteins are collectively termed effectors, which includes general effectors that target pathways in the host cell, and translocators that play an additional role in effector translocation into the host cytoplasm. Effectors are thought to be delivered unidirectionally in a single step into the host cytoplasm, where they then manipulate host cell biology, metabolism and defense pathways (Rosqvist *et al.*, 1994; Ghosh, 2004; Dean, 2011).

T3SS are thought to have appeared in bacteria just after the evolution of eukaryotes as these systems are dedicated to trans-kingdom interaction (Troisfontaines & Cornelis, 2005). Since then, the T3SS have been shaped by evolution depending on the pathogens or symbionts niche. The T3SS was most likely spread by horizontal gene transfer, resulting in a phylogeny tree completely different from the 16S rRNA-based tree which assigns bacterial phyla. The T3SS is very similar to the flagellar apparatus in Gram-negative bacteria and it is assumed that both systems share a common ancestor (Galan & Collmer, 1999; Erhardt *et al.*, 2010). Based on sequence analysis of non-flagellar and flagellar T3SS proteins, seven T3SS subfamilies have been identified (Troisfontaines & Cornelis, 2005). Despite the distribu-

tion of T3SS among bacteria living under completely different environmental conditions, the principle of effector secretion through the NC is thought to happen by a common mechanism.

1.2.1 Architecture of T3SS

The NC structure is remarkably conserved among the T3SS-positive bacteria. Of the seven structural families, the Inv-Mxi-Spa subfamily including T3SS from *S. flexneri* and *Salmonella enterica* and the Ysc subfamily from *Yersinia* have been extensively studied (Troisfontaines & Cornelis, 2005). Cryo-EM analysis of the NC structure of *Salmonella enterica* serovar Typhimurium SPI-1 and *S. flexneri* revealed structural details up to subnanometer resolution (Schraidt & Marlovits, 2011; Hodgkinson *et al.*, 2009). Assembly of the NC occurs in a stepwise manner starting with embedding protein rings into the bacterial membrane (Galan & Wolf-Watz, 2006; Chatterjee *et al.*, 2013). The first proteins to build the NC are pilotins and secretins, which are secreted via the sec-pathway across the inner membrane and are essential building blocks for type III and also type II or type IV secretion systems (Bayan *et al.*, 2006). The pilotin helps with insertion of the secretin into the outer bacterial membrane which in turn provides a structural basis for attachment of additional protein multimers (Bayan *et al.*, 2006; Chatterjee *et al.*, 2013). Rings of variable stoichiometry are stacked on top of each other until the membrane-spanning part is completed. This unit is the basal body and has an inner diameter of about 30 to 40 nm. In *S. flexneri*, the basal body consists of rings of MxiG and MxiJ in the inner and MxiD in the outer membrane, where MxiD is a secretin that targets the outer membrane with the assistance of the pilotin MxiM (Schuch & Maurelli, 2001). Together, these rings enclose a central tube-like structure, called the inner rod, which is formed by MxiI (Fig. 1.4).

Once the basal body is complete, the needle is formed by numerous copies of a small protein with a hairpin structure (MxiH in *S. flexneri*). The yet unfinished system secretes the structural needle-protein during assembly of the extracytosolic appendage (Erhardt *et al.*, 2010). The hollow needle grows at the distal end and usually ranges between 45 and 50 nm in length, which is regulated by Spa32 in *S. flexneri* (Tamano *et al.*, 2000, 2002). The inner diameter of the needle is about 2-3 nm and is considerably smaller than the basal body. Recently, a channel of 2.5 nm has been confirmed in *Salmonella* SPI-1 which is conserved in *S. flexneri* and thereby seems to be a universal feature of the Inv-MxiG-Spa T3SS (Loquet *et al.*, 2012; Demers *et al.*, 2013). The assembly of the central channel is assisted by the

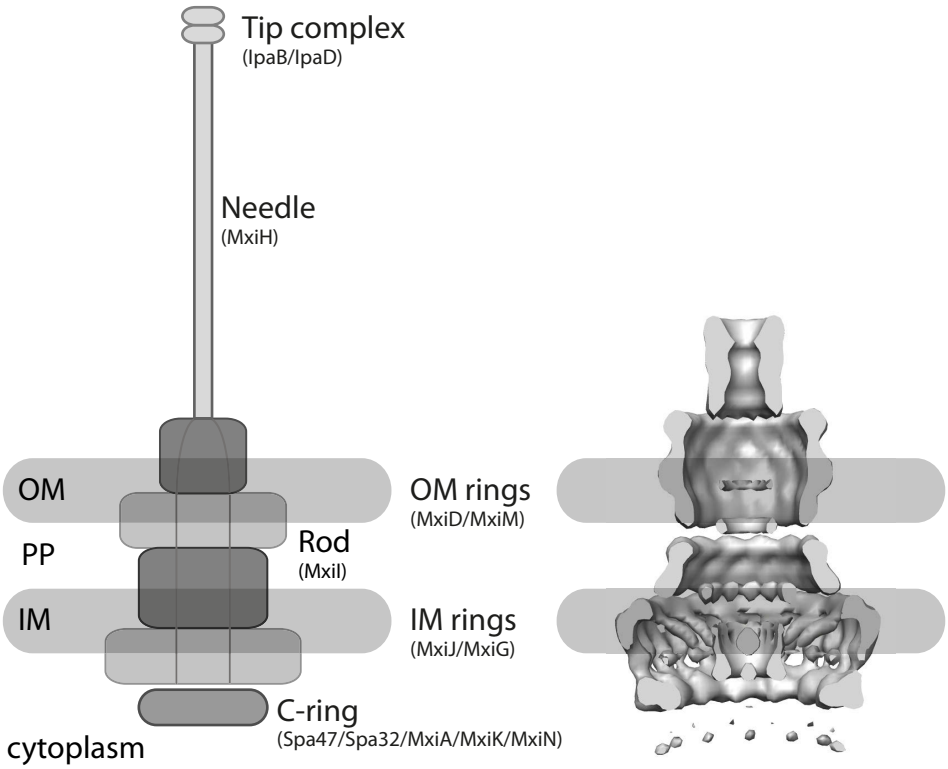

Figure 1.4: *Shigella flexneri* needle complex scheme and model. Left: Schematic of the T3SS embedded in the bacterial envelope, denotations for constituent proteins are given in brackets. Right: Model of the *S. flexneri* NC in a lateral section with schematic membranes (modified from Hodgkinson *et al.* (2009)). OM = outer membrane, PP = periplasm, IM = inner membrane.

cytosolic proteins MxiN and MxiK, as mutants lacking these proteins did not form secretion-competent needles (Jouihri *et al.*, 2003). These proteins interact with the ATPase (Spa47 in *S. flexneri*) which is an essential component of the basal body and is part of a cytoplasmic ring (C-ring). Through the interaction with cytoplasmic and structural T3SS components, the C-ring is thought to orchestrate assembly and substrate secretion (Morita-Ishihara *et al.*, 2006).

1.2.2 The repertoire of T3SS substrates

Compared to the conserved structural part, the repertoire of effectors is highly diverse as they shape the interaction between bacterium and host (Preston, 2007). Effector proteins thereby constitute the armory of pathogenic and symbiotic bacteria and they often mimic or modify host factors (Galan, 2009). Phosphorylation and ubiquitinylation pathways are common targets for bacterial effectors that covalently modify host factors, including pathways regulating the actin network and immune response (Dean, 2011). The variety of interactions underlines the flexibility in bacterial adaptation to widespread ecological niches where effectors serve as an extensive toolbox to support the bacterium in the host environment.

Despite this variety, most effectors share the pattern of an N-terminus dedicated to secretion of the protein and downstream domains that provide the actual effector activity. Bioinformatic studies developed prediction tools for T3SS signal sequences based on amino acid composition and structure prediction (Arnold *et al.*, 2009; Lower & Schneider, 2009; Samudrala *et al.*, 2009; Yang *et al.*, 2010), although the signal itself is not completely characterized yet. Many effectors require chaperones for their cytoplasmic stability which bind to their N-terminal region downstream of the signal peptide. For the *S. flexneri* effector and translocator IpaB, two chaperone binding domains have been identified (Lunelli *et al.*, 2009; Lokareddy *et al.*, 2010), the first of which overlaps with the secretion signal (Fig. 1.5). To prevent aggregation or effector activity in the bacterium, IpaB stays bound to the chaperone IpgC in a partially unfolded conformation. Without IpgC, IpaB is degraded and recombinant expression of IpaB requires co-expression of IpgC (Menard *et al.*, 1994b; Page *et al.*, 1999; Lunelli *et al.*, 2009).

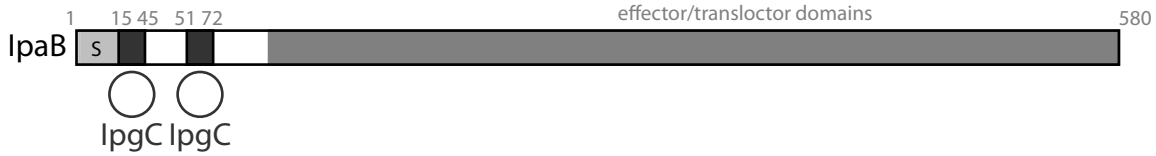

Figure 1.5: Schematic of the effector and translocator IpaB. IpaB has an N-terminal signal in the first 15-20 amino acids that overlaps with the first chaperone binding domain (IpgC binding site). An additional IpgC binding site is further downstream and followed by effector domains. Numbers indicate amino acids, S = signal sequence.

For reaching the host cytoplasm, effectors require the help of translocator proteins. Translocators are thought to mediate contact with the host-cell membrane where they insert to form a pore and mediate translocation of other effectors (Müller *et al.*, 2008). Therefore, translocators like IpaB and IpaC in *S. flexneri* are also situated at or recruited to the tip of the needle forming a complex that is thought to sense and establish contact with the host (Blocker *et al.*, 1999; West *et al.*, 2005; Espina *et al.*, 2006; Veenendaal *et al.*, 2007) (Fig. 1.4). IpaD assists translocon formation and interacts with the needle subunit MxiH and IpaB, thereby connecting the two (Johnson *et al.*, 2007; Epler *et al.*, 2012). IpaB is a multifunctional protein and has, in addition its translocator activity, at least four different eukaryotic targets. First, it activates Caspase-1 in phagocytes, thereby stimulating an inflammatory response (Hilbi *et al.*, 1998; Zychlinsky *et al.*, 1994). Second, it has been shown that IpaB can oligomerize to form ion channels in the endolysosomal membrane. Subsequent leakage of potassium activates the

IPAF inflammasome and leads to pyroptosis (Senerovic *et al.*, 2012). Third, there is evidence for IpaB mediating disruption of the Golgi network, possibly by its CD44/cholesterol-binding activity (Skoudy *et al.*, 2000; Lafont *et al.*, 2002; Mounier *et al.*, 2012). Last but not least, IpaB can arrest the host cell cycle by interacting with Mad2L2, an activtiy that possibly decelerates the otherwise rapid epithelial cell turnover (Iwai *et al.*, 2007).

1.2.3 Through the eye of a needle: Effector secretion by T3SS

Since it is energetically costly to express the T3SS and effectors, the T3SS is strictly regulated at the level of transcription and secretion. T3SS components are only synthesized at 37 °C and effectors are stored within the cytosol in an inactive state until a host cell is encountered (Menard *et al.*, 1994a). The tip complex formed by IpaB and IpaD regulates secretion and in the absence of host cells *Shigella* leaks minimal amounts of Ipa proteins into culture supernatants (Parsot *et al.*, 1995). Mutants of either *ipaB* or *ipaD* fail to establish a regulatory tip complex and hypersecrete effectors without induction. The interaction between IpaB and IpaD is crucial, as deletion of the 3 C-terminal amino acids in IpaB causes a hypersecretory phenotype (Roehrich *et al.*, 2010). Secretion can be artificially induced *in vitro* by addition of Congo Red (Bahrani *et al.*, 1997), although it remains unclear how the dye acts on the T3SS. When *S. flexneri* establishes contact with a host cell, effector pools of IpaB and IpaC are released entirely into the host cell with a half-time of five minutes (Enninga *et al.*, 2005). Other effectors are not transcribed until IpaB and IpaC are secreted, as they are regulated by a feedback loop mediated by IpgC. When IpaB and IpaC are secreted, IpgC is released and can associate with MxiE. IpgC and MxiE together induce transcription of a second set of effectors, termed late effectors (Parsot, 2009). Timely regulation of effector expression provides an efficient way to maintain a secretion hierarchy that is adapted to the pathogens needs.

Besides temporal regulation, hierarchy of effector secretion occurs through substrate specificity (Ghosh, 2004; Barison *et al.*, 2013). In *S. flexneri*, Spa32 is involved in the switch from basal body components to needle subunits, while MxiC regulates the switch to translocator secretion after the needle is completed (Magdalena *et al.*, 2002; Botteaux *et al.*, 2009; Martinez-Argudo & Blocker, 2010). Furthermore, a recently discovered protein complex in *Salmonella* termed sorting platform was proposed to order substrates prior to secretion by

the T3SS (Lara-Tejero *et al.*, 2011; Osborne & Coombes, 2011). The protein complex, partially cytosolic and partially associated with the T3SS, delivers the effectors to the T3SS NC by interacting with the effector-associated chaperone. The sorting platform components are conserved in other T3SS and shown to interact in *Shigella* (MxiN, MxiK and Spa47 (Jouihri *et al.*, 2003)), but thus far, function of this complex has only been investigated in *Salmonella*. Once an effector reaches the entry port of the NC, effectors are required to unfold in order to fit the narrow dimensions of the needle. The inner diameter of the needle is 2.5 nm which only allows secretion of secondary structures or simple structural motifs. As effectors are shown to be folded prior to secretion (Wilharm *et al.*, 2004b), activity of an unfoldase is required. This function is mediated by the ATPase which associates with the NC and the sorting platform (Akeda & Galan, 2005; Lara-Tejero *et al.*, 2011).

The driving mechanism of effector secretion is not fully elucidated. The ATPase, which localizes close to the entry port of the NC in the bacterial cytoplasm, has been shown to be essential for secretion and it is possible that it might be fueling the secretion process. Secretion also depends on a proton motive force (PMF) as the PMF inhibitor CCCP abolished secretion in *Yersinia* and *Shigella* (Wilharm *et al.*, 2004a; Schroeder *et al.*, 2007). A recent alternate model proposed rotation of the needle involved in effector secretion (Ohgita *et al.*, 2013). Based on the similarity to the rotating flagellar export apparatus, structural components of the NC needle tip in *Pseudomonas aeruginosa* have been labeled and rotation has been observed by microscopy. Whether this is a general feature of secretion mechanism is not clear. However, rotation fits into the context of the needle being a helical structure with effectors moving in a screw-like manner through the channel (Wilharm *et al.*, 2007).

1.3 Fusion proteins as tools for secretion analysis

Substrate proteins fused to reporter domains are powerful tools for investigations of secretion mechanisms. The substrate, an effector in case of T3SS, is a carrier for the reporter which serves as a readout for translocation or localization studies (Fig. 1.6*A*). In *Shigella*, this approach has been used to study kinetics of secretion with effectors that were labeled with small fluorescent dyes or linked to small enzymatic domains (Schesser *et al.*, 1996; Enninga *et al.*, 2005). Another possibility is to specifically inhibit transport or system assembly by

fusing domains that clearly exceed the channel dimensions and cannot be unfolded prior to secretion (Fig. 1.6*B*). This leads to obstruction of the channel, preventing secretion of other effectors. Consequently, only effectors that were secreted before the channel was occluded are found in culture supernatants or the host.

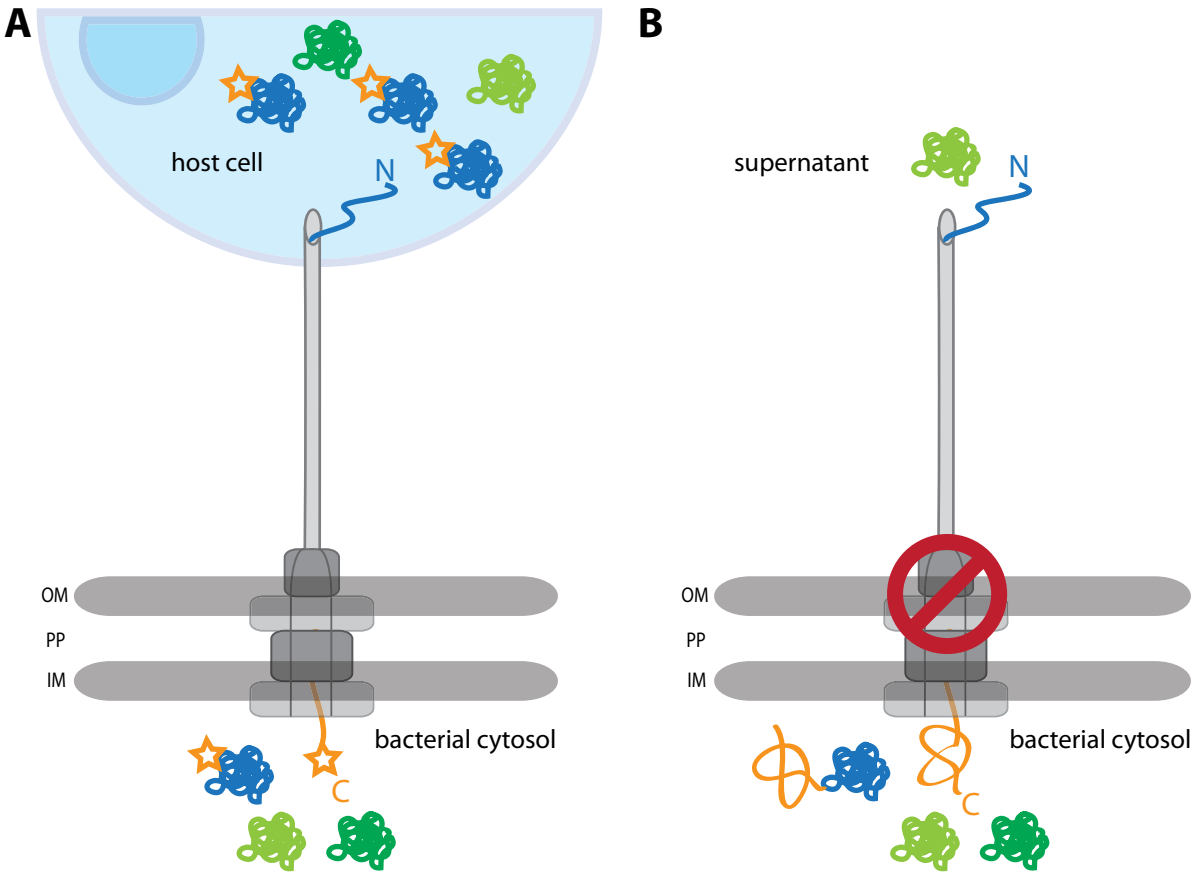

Figure 1.6: Monitoring secretion with engineered effectors.(*A*) Schematic of secretion with labeled effectors (blue molecule with star) that can be transported into the host. (*B*) Schematic of effector impassable for the T3SS that blocks secretion of other effectors, effector in the supernatant (light green) was transported before the channel was obstructed. OM = outer membrane, PP = periplasm, IM = inner membrane.

The T3SS with its narrow channel has been the subject of many studies with either reporter fusions or blocking fusions for gaining mechanistic insights. Many of these experiments have been carried out in *Yersinia* where the T3SS was first discovered. The N-terminal secretion signal was defined by fusion of truncated effectors to β-galactosidase or alkaline phosphatase (Michiels & Cornelis, 1991) and could be further specified for YopE fusions where the N-terminal 11 amino acids were sufficient for secretion (Sory & Cornelis, 1994; Schesser *et al.*, 1996).

Other experiments have attempted to obstruct the channel using murine dihydrofolate reductase (DHFR) as a fusion partner for effectors. This approach derived from studies in

eukaryotic cells where a mitochondrial targeting peptide fused to DHFR directed DHFR to the mitochondrial compartment (Hurt *et al.*, 1984). DHFR folding can be stabilized by its ligand methotrexate, making it impassable for translocation and thereby occluding the mitochondrial import channel (Eilers & Schatz, 1986). In *Yersinia*, DHFR was fused to YopE and the fusion protein was secreted very little already in the absence of methotrexate (Lee & Schneewind, 2002). Additional studies revealed that effector fusions including the signal sequence and the chaperone binding domain were secreted depending on the presence of the cognate chaperone SycE (Feldman *et al.*, 2002). In line with these findings was the secretion of a truncated and thereby destabilized DHFR mutant. Therefore, the chaperone mediates unfolding of domains downstream of its binding site in the effector. It is noteworthy that DHFR has been shown to be folded in these fusions prior to secretion (Wilharm *et al.*, 2004b). This suggests that further active unfolding by the T3SS required, a task probably seen to by the ATPase and that fusion proteins are indeed unfolded by the T3SS (Wilharm *et al.*, 2007). In agreement with the ATPase being the potential unfolding component was another study with *Yersinia* effectors fused to gluthatione-(S)-transferase. Upon blocking the T3SS, the ATPase was detected in effector fusion-pulldown assays (Riordan *et al.*, 2008). In summary, the T3SS has complex unfolding capacities that at least partially depend on the ATPase.

1.4 Knotted proteins - Non-linear folds as common motifs

Our general understanding of protein folding is that a linear peptide chain folds into intricate structures, but, like knit-wear, can be unraveled if we pull on both termini. This understanding has been challenged by the observation of proteins that do not comply with this model and have a knot as a structural motif. A knot is practically defined as a crossing of threads which remain folded when a pull is applied to both ends (Virnau *et al.*, 2011). In particular, knots are technically defined only in closed circles where there is no option for the ends to slip and untie the knot. Therefore, algorithms for knot identification include artificial joining of the protein termini, a process that resembles the circle being closed as if we pick up a string (Taylor, 2000; Yeates *et al.*, 2007). Despite the tendency of long collapsed chains to form knots, the knotted fold in a protein seemed unlikely at first, as a computational analysis of the entire protein data bank (PDB, 400 proteins at the time of the analysis) did not reveal any knots (Mansfield, 1994). This result was challenged by structural data of

an *S*-adenosyl methionine-synthetase that obviously contained a knotted motif (Takusagawa & Kamitori, 1996). An improved analysis of the PDB revealed more than 10 different knotted proteins and already distinguished between simple trefoil knots and more sophisticated figure-of-eight knots (Taylor, 2000). By now, knotted topologies in proteins are accepted as common structural motifs and have opened new possibilities for studying protein folding dynamics. Although the purpose of knotted folds is not clear, the fact that methyltransferases with trefoil knots have been found predominantly in extremophiles indicates that knots might confer additional structural stability (Taylor, 2007).

One example of a knotted methyltransferase is RrmA from *Thermus thermophilus*, a thermophilic eubacterium. RrmA has a trefoil-knot in the active site and the position of the knot implies that it is of a deeply-folded nature, meaning that it is unlikely to slide off the chain (Virnau *et al.*, 2011; Nureki *et al.*, 2002). RrmA was the first protein where a deeply-folded trefoil knot was discovered. Homologs of RrmA are YibK from *Haemophilus influenza* and YbeA from *Escherichia coli*, which, together with RrmA and other methyltransferases containing knots, have been assigned to the α/β-superfamily of knotted proteins in the Pfam protein database (Bateman *et al.*, 2004; Mallam & Jackson, 2007b). These proteins usually form homodimers and bind *S*-adenosyl methionine as a ligand in their active center. Folding studies revealed that the knotted motif can refold *in vitro* without need for chaperones and it was suggested that the folding process takes place when the chain is largely unfolded (Mallam & Jackson, 2007a). Fusion experiments with these proteins showed that knots still form when either one or both termini are fused to ThiS from *Archeoglobus fulgidus* (Mallam *et al.*, 2008). These findings underlined the intricate folding properties of knotted proteins and suggested that the knot is formed when the protein is in a largely denatured state.

1.5 Injection revisited: Does the syringe function as a syringe?

With its defined role as a device that mediates bacterial virulence, T3SS have been the subject of extensive research in the past 25 years. Early studies with fusion proteins clearly elucidated a correlation between the fold of a domain and its ability to be secreted. Furthermore, effector proteins from *Yersinia* were only active when injected into the respective host

cell *in vitro*. These findings led to the common hypothesis that effectors are injected into the host by the bacterium. The discovery of the NC further substantiated this idea. NCs were isolated from bacterial membranes and were shown to be essential for effector secretion. In addition, a central channel across the NC was discovered by electron microscopy averaging. The channel discovery lead to the common belief that effector proteins are delivered by the means of the NC into the bacterium in a single step, however, this hypothesis has not been confirmed experimentally.

Regarding studies using effector fusions, it is still possible that these fusions constantly occupy the ATPase which hampers secretion, leading to an absence of secreted effectors interpreted as channel obstruction. Thus, these experiments do not prove secretion through the channel. Opposing the injection model, a recent study in *Yersinia* demonstrated the presence of effector proteins which are stored on the outer membrane of the bacterium and are found in the host cell in later stages of the infection (Akopyan *et al.*, 2011)(Fig. 1.7). These findings contradict the model of single-step translocation from one cytoplasm to the other, although effector assembly on the bacterial surface was shown to be a T3SS-dependent process. Even if this study did not exclude the idea of secretion through the NC channel, it raised questions concerning the purpose of the syringe. An alternative model considers the syringe as an anchoring device that mediates intimate contact between the bacterium and the host. Importantly, the authors pointed out that there is no experimental evidence of effectors being secreted through the NC channel (Edgren *et al.*, 2012).

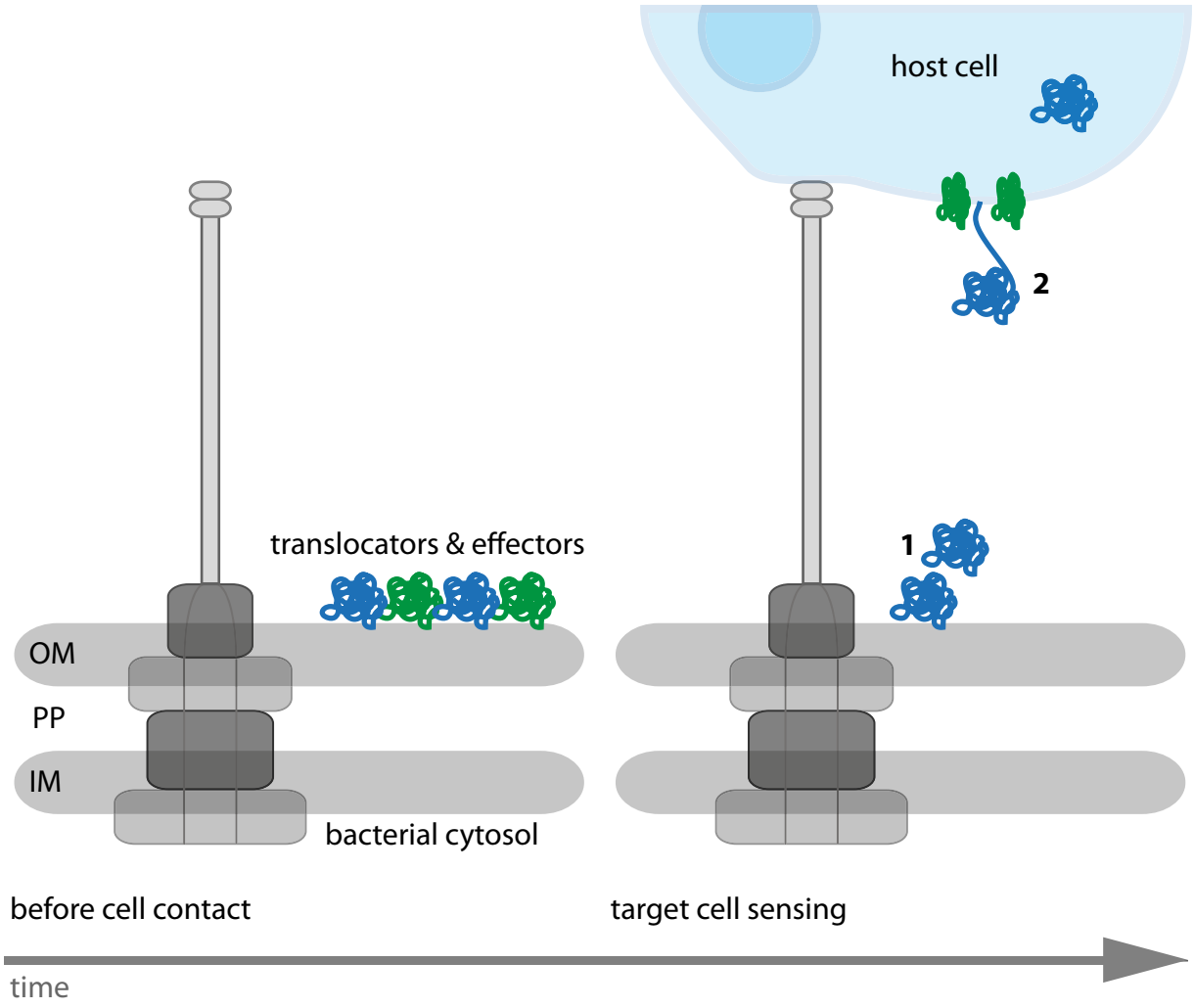

Figure 1.7: Model of protein translocation in distinct steps. Bacterial translocators and effectors are stored on the bacterial cell wall and released only upon host cell contact (*1*). Translocators (green) form a pore in the host cell membrane where effectors (blue) are secreted into the target cell (*2*). OM = outer membrane, PP = periplasm, IM = inner membrane. Adapted from Edgren *et al.* (2012).

1.6 Aim of the study

The aim of the study was to answer the question whether or not effector proteins are secreted through the T3SS channel. Secretion through the NC has two major consequences: First, effectors need to be unfolded in order to be secreted, as bulky domains are impassable for the narrow channel. Second, the NC channel shields the substrate from the environment as it physically surrounds the effector. We proposed that if an effector protein were fused to a stably folded knotted motif, it could not be unfolded by the T3SS during secretion. The trefoil knot-motif is a good candidate for blocking the T3SS because first, its size does not fit the restricted dimensions of the channel and second, it stably folds in the absence of chaperones. The knotted protein was fused to the effector IpaB, which is one of the first effectors being secreted by the bacterium. IpaB is well characterized and protocols for protein purification

and testing functionality are available, which would enable us to study the fusion protein outside the bacterium.

If the fusion protein were trapped in the NC, it would prevent passage of other native effector proteins. This approach also provides the opportunity to analyze the occupied NC in more detail and localize the effector protein in an isolated NC. Furthermore, combination of biochemical assays, like protease treatment and chemical modification, might elucidate whether the effector fusion protein was accessible or trapped within the NC. While the protease should not be able to reach the cleavage site if buried inside the channel, the chemical modification indicates which sites of the protein are still accessible on isolated NCs. Taken together, this work aims to experimentally address the secretion mechanism in T3SS. This approach might serve as a convenient tool to study secretion mechanisms of other systems which require unfolding of their substrates.

2 Results

2.1 Knotted proteins - candidates for blocking T3 secretion

Selection of proteins containing knots as candidates for effector fusions was based on protein size and structural data available. Both proteins were smaller than 30 kDa and contained a simple trefoil-knot in the C-terminal region (Fig. 2.1). One protein (Knot 1, Fig. 2.1*A*) is a hypothetical protein from the archaeal bacterium *Methanobacterium thermoautotrophicum* (PDB 1K3R) (Zarembinski *et al.*, 2003), the other (Knot 2, 2.1*B* and *C*, Fig. 2.2) a methyl transferase RrmA from the eubacterium *Thermus thermophilus* (PDB 1IPA) (Nureki *et al.*, 2002). The topology plot shows the trefoil-knot motif highlighted in green, which results from three peptide crossings in the C-terminal region of RrmA (Fig. 2.2).

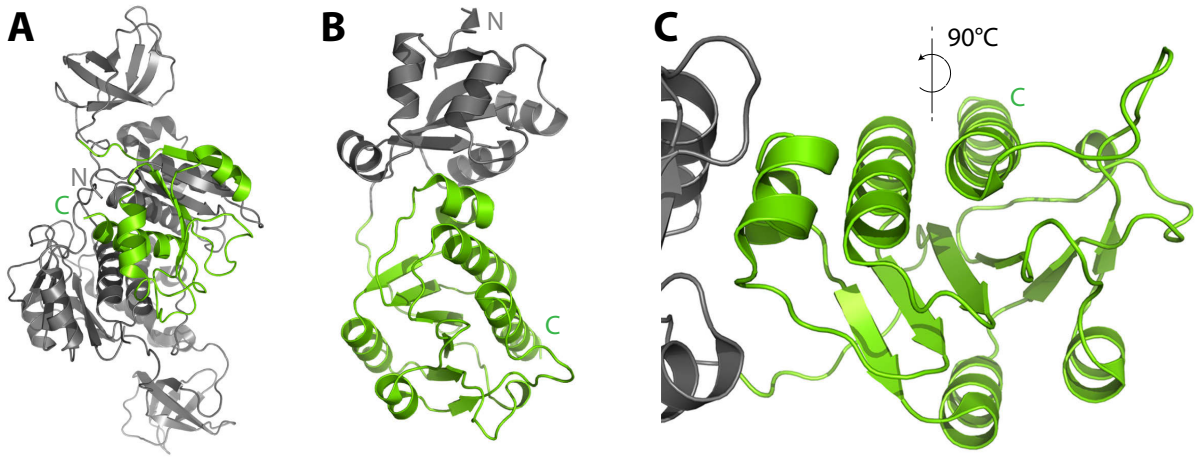

Figure 2.1: 3D structures of the knotted proteins. Full length structural data of Knot 1 (*A*) and Knot 2 (*B*) with the trefoil-knot domains highlighted in green. A close-up of the knotted region in *B* is given in *C*.

As the knot locates in the C-terminal part of each protein, it was assumed that knot folding should be autonomous from an N-terminal fusion to the effector IpaB. Thus, both proteins appeared to be suitable candidates for stably-folded domains that might obstruct the T3SS channel.

The influence on effector secretion by these proteins was tested by expressing both knot

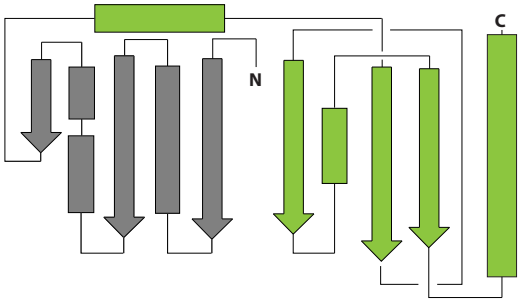

Figure 2.2: Topology of Knot 2/RrmA. Topology plot of Knot 2/RrmA, adapted from Nureki *et al.* (2002). The trefoil knot is highlighted in green analog to figure 2.1*B* and *C*.

protein-encoding genes without a fusion in the Δ*ipaB* strain and comparing secretion of induced and non-induced cultures before and after induction.

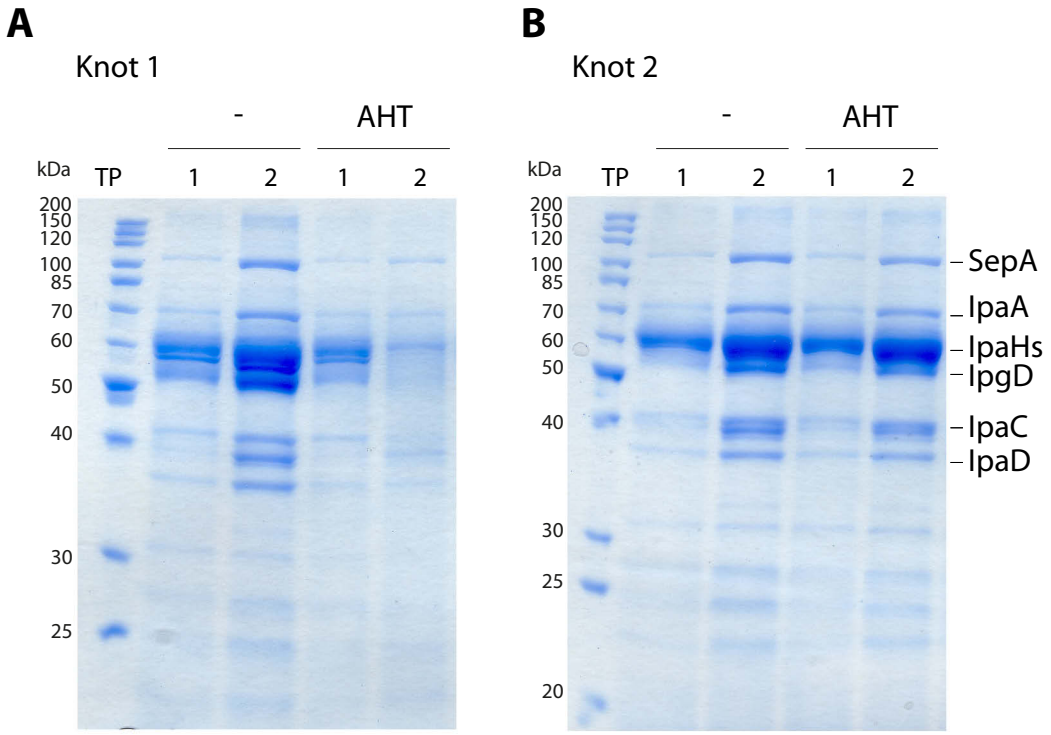

Figure 2.3: Secretion assay of Δ*ipaB* with Knot 1 and Knot 2. Bacterial supernatants were analyzed by Coomasssie stain before (1) and after (2) induction time points (TP). Cells were left untreated (-) or protein expression was induced with AHT (AHT). Knot 1 is shown in (*A*), Knot 2 in (*B*).

Aliquots of culture supernatants that contain secreted proteins were precipitated with TCA and analyzed by SDS PAGE and Coomassie stain. A typical effector pattern for hypersecretory strains was seen for the *ipaB* mutant as effector proteins accumulated in the supernatants during the logarithmic growth phase of the culture (Fig. 2.3, lanes TP 1). The protein level was increased as bacteria were allowed to secrete an additional hour (Fig. 2.3, lanes TP 2) without induction of expression of the knots. Expression of *knot1* influenced the T3SS pathway as the amount of secreted effectors was decreased after induction (Fig. 2.3*A*, AHT, TP

2). This decrease was not observed for the other Knot from *T. thermophilus* (Fig. 2.3*B*, AHT). The protein from *M. thermoautotrophicum* was therefore excluded from further experiments. Knot 2 was chosen as a fusion partner for IpaB and is henceforth termed "Knot" (or *knot*, for genes). The Knot was fused to the C-terminus of IpaB, resulting in the fusion protein IpaB-Knot.

2.2 Purified IpaB-Knot induces pyroptosis in macrophages

As an initial step for characterizing the fusion protein, the functionality of IpaB fused to Knot was tested using purified protein. Expression of *ipaB* is toxic to *E. coli* BL21 and toxicity can be circumvented by co-expression of the cognate chaperone *ipgC* (Lokareddy *et al.*, 2010). IpgC stabilizes IpaB in the cytoplasm and thereby prevents IpaB degradation (Menard *et al.*, 1994b). Therefore, IpaB-Knot was co-purified after expressing it together with *ipgC* in *E. coli* BL21. The purification strategy for IpaB is based on purifying the IpgC/IpaB complex *via* a His-tag in IpgC and subsequent destabilization of the interaction with LDAO. This destabilization lead to elution of monomeric IpaB (Birket *et al.*, 2007; Senerovic *et al.*, 2012). Additional affinity purification using Strep-Tactin resin prior to gelfiltration of the protein resulted in the purification of only full-length IpaB-Knot (Fig. 2.4*A*), as the Strep-tag of the fusion is C-terminal. Gelfiltration separated aggregated protein from monomeric IpaB-Knot (Fig. 2.4*B*).

To ensure that IpaB-Knot remains a functional T3SS effector, IpaBs capability to induce pyroptosis in murine bone marrow macrophages (mBMM) was analyzed using purified IpaB-Knot. IpaB is a multifunctional effector and translocator and the induction of pyroptosis is well documented (Zychlinsky *et al.*, 1994; Senerovic *et al.*, 2012; Lunelli *et al.*, 2009) and can be assessed with a colorimetric assay. Upon macrophage disintegrity, lactate dehydrogenase (LDH) is released into the supernatant. Activity of LDH is quantified in a colorimetric reaction, where LDH reduces a yellow tetrazolium salt (2-(4-Iodophenyl)-3-(4-nitrophenyl)-5-phenyl-2H-tetrazolium chloride) into a red formazan product. The accumulation of red dye is proportional to the amount of cells lysed and was quantified in a 96-well plate spectrometer.

IpaB exerts cytotoxicity at concentrations as low as 0.4 µM (Senerovic *et al.*, 2012) and a

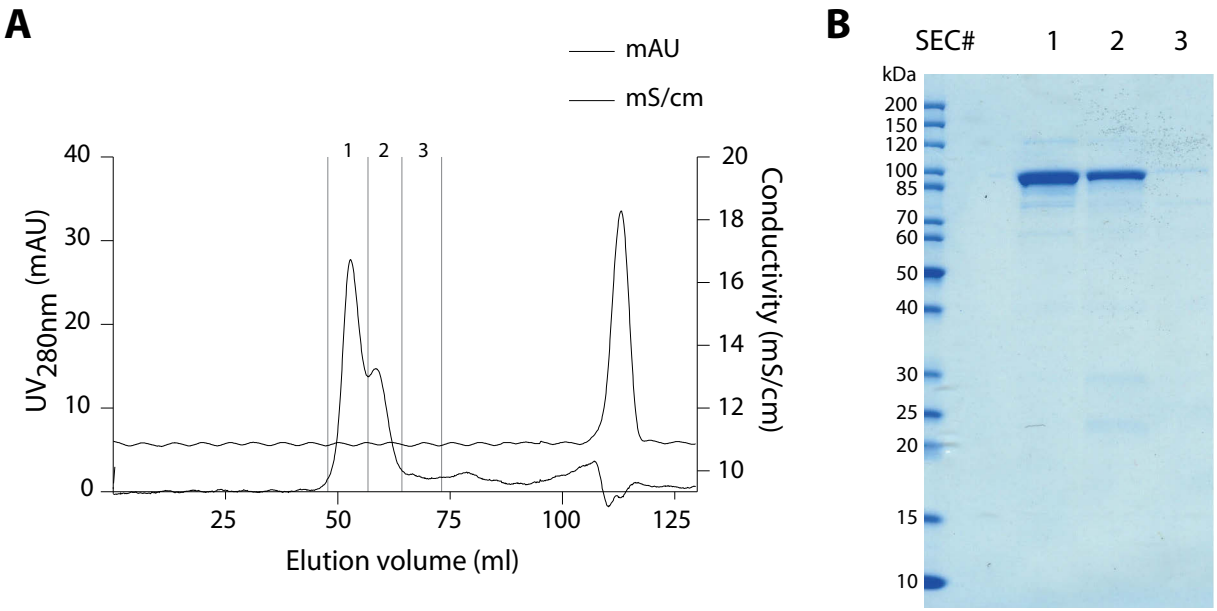

Figure 2.4: Size-exclusion chromatography and analytical SDS PAGE/Coomassie of recombinant IpaB-Knot. (*A*) Elution profile of IpaB-Knot. 1, 2 and 3 indicate fractions collected which were analyzed in (*B*).

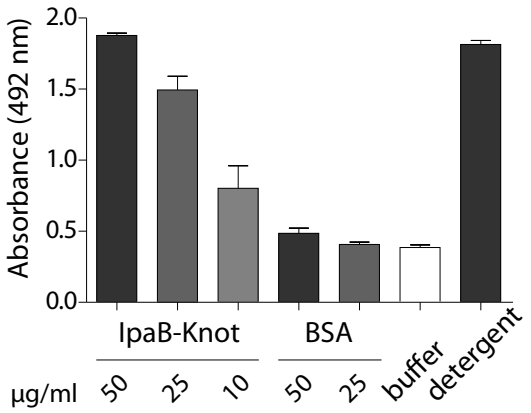

Figure 2.5: Induction of cell death in macrophages by IpaB-Knot. Cell death was measured by release of LDH from mBMM in a colorimetric assay. Error bars indicate SD, n=3 independent experiments.

similar result was obtained for IpaB-Knot, where cytotoxicity was already seen at 0.25 µg/ml (0.26 µM) (Fig. 2.5). At 0.5 µg/ml (0.53 µM), cell lysis was as efficient as disruption with 1 % detergent (Triton X-100). Since IpaB-Knot is concentrated in the presence of LDAO, the detergent might accumulate during protein concentration and enhance cytotoxicity. To rule out a cytotoxic effect of LDAO, the non-toxic protein bovine serum albumin (BSA, 66 kDa) was concentrated under same conditions as IpaB-Knot and added to mBMM. No cellular disintegration was detected in samples with 50 µg/ml (0.75 µM) BSA. Thus, disruption was caused by a functional IpaB domain in IpaB-Knot. This confirmed that IpaB maintains effector function inside the fusion protein.

2.3 The Knot is folded within IpaB-Knot

For efficient obstruction of the NC channel by IpaB-Knot, the Knot has to be tightly folded when fused to IpaB. Since IpaB is stored in complex with IpgC in the bacterial cytoplasm, the complex of IpaB-Knot and IpgC represents the conformation of IpaB-Knot prior to secretion. As the Knot needs to fold prior to secretion, folding analysis was carried out on IpaB-Knot bound to IpgC by means of fluorescence spectrometry and limited proteolysis.

2.3.1 Fluorescence spectrometry

Fluorescence spectrometry measures the intrinsic fluorescence of the protein which largely depends on tryptophan residues and their molecular environment. Thereby, different folding states of the protein can be compared as the emission spectrum changes when tryptophans are exposed to solvent upon unfolding. The folding status of the Knot-domain in IpaB-Knot was addressed by measuring the change in tryptophan fluorescence under native and denaturing conditions (Fig. 2.6). IpaB contains a single tryptophan whereas the Knot domain has four tryptophans, three of which are part of the trefoil knot in the C-terminal region, indicating that the fluorescence is mainly derived from folding status of the Knot. Fluorescence of IpaB-Knot in complex with the chaperone IpgC was recorded. IpgC does not contain tryptophans and was included in the blank buffer as a control.

Spectra of purified IpaB-Knot complex were compared to spectra of the Knot alone, either in buffer or in the presence of the chaotropic salt guanidine hydrochloride (GuHCl). The native

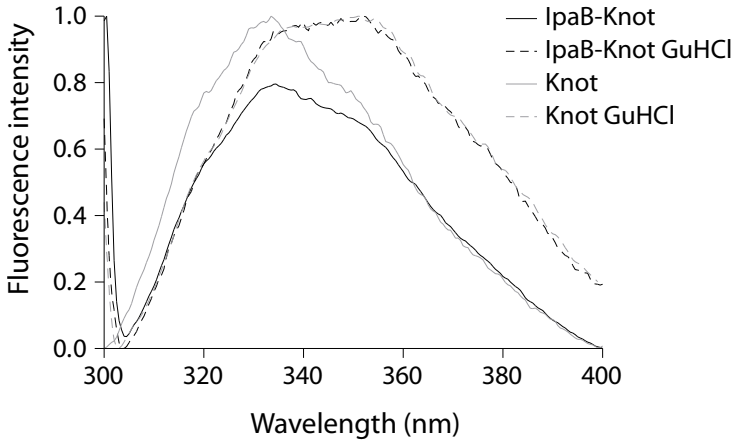

Figure 2.6: Fluorescence spectra of IpaB-Knot and Knot. Solid lines represent native conditions, dashed lines show spectra under the influence of 6 M guanidine hydrochloride.

Knot protein had a fluorescence emission peak at 335 nm which represents tryptophans in the folded protein (Fig. 2.6, solid grey line). The fluorescence spectrum of IpaB-Knot was similar to the native Knot spectrum with an emission peak at 335 nm (Fig. 2.6, solid black line). This similarity of fluorescence spectra suggests folding of Knot in IpaB-Knot analog to native Knot. Treatment with 6 M GuHCl lead to unfolding represented by a red shift of emission peaks from 335 nm to 355 nm. This shift indicated a change of the molecular environment due to exposure of the respective tryptophans to solvents in both IpaB-Knot and Knot alone. Thus, the change in fluorescence derived from GuHCl-induced structural alterations of the Knot domain confirms that this domain was folded under the tested conditions.

2.3.2 Protease treatment reveals a folded core including the trefoil knot

Folding of a protein can be analyzed in more detail with treatment by unspecific proteases. Under native conditions, the protein fold prevents cleavage by proteases. Only free structures can be accessed by the enzyme and the folded parts remain intact over time.

For the Knot protein alone, protein fragments were obtained by treatment with the non-specific protease Proteinase K and separated by SDS PAGE (Fig. 2.7*A*).

Already after a few minutes of incubation, treatment led to a product of approximately 25 kDa which is no further digested. The cleavage product was stable because of its native fold, as total cleavage of Knot occurred in the presence of the denaturing detergent SDS, a condition where Proteinase K is active (Hilz *et al.*, 1975). The obtained fragment was analyzed by mass spectrometry (MS) (Fig. 2.7*B*) and mapped on the known structure for RrmA (Fig. 2.7*C*). Only the terminal helices were cleaved whereas the trefoil knot remained intact.

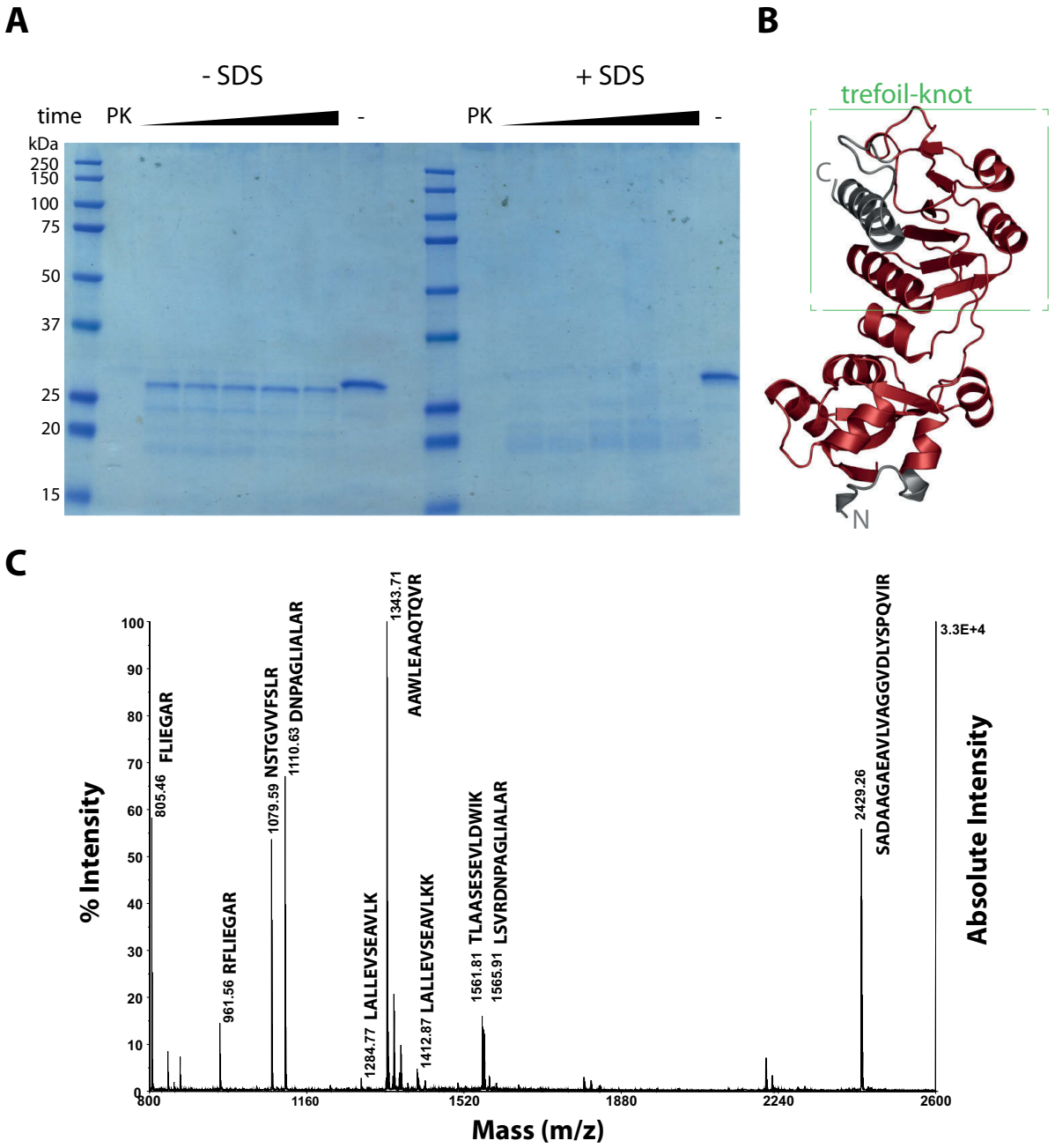

Figure 2.7: Protease K treatment of Knot under native and denaturing conditions. (*A*) SDS PAGE and Coomassie stain of Knot treated with Proteinase K (PK) or untreated (-) under native (-SDS) and denaturing (+SDS) conditions, where Proteinase K is still active. (*B*) 3D structure of Knot mapped with fragment identified by MS from the stable band in (*A*). The trefoil knot is indicated by a green box. (*C*) MS spectrum of the stable fragment. Peptides are indicated on peaks, see Fig. 2.10 for Knot sequence. MS analysis was performed by Monika Schmid, MPIIB.

Like treatment of Knot, IpaB-Knot (in complex with IpgC) was digested with Proteinase K and the sample was analyzed by 2D-electrophoresis in order to obtain a better resolution of IpaB fragments and the Knot (Fig. 2.8). Protein spots that appeared after digest were further analyzed by MS and MS/MS. Some peptides resulted from digestion of the IpaB domain, which, in complex with IpgC, was partially unfolded when treated with Proteinase K (Fig. 2.8, Box 1). As seen for the Knot, polypeptides that cover almost the entire sequence of the Knot domain and the complete sequence of the trefoil-knot motif were detected (Fig. 2.8, Box 2).

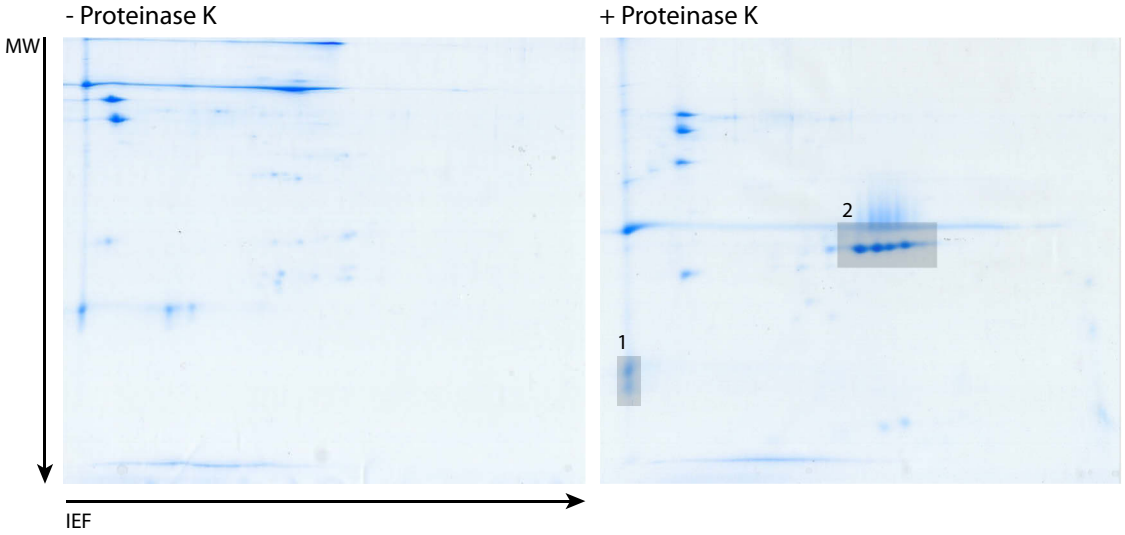

Figure 2.8: 2D-electrophoresis of IpaB-Knot. IpaB-Knot was separated by isoelectric focus (IEF) and molecular weight (MW) as a second dimension without Proteinase K (left) or after Proteinase K treatment. Protein fragments after Proteinase K digest were analyzed by mass spectrometry. Electrophoresis was performed by Ursula Zimny-Arndt, MPIIB.

Subfragments from these spots were confirmed by MS/MS analysis (Fig. 2.9). y and b ions have been mapped to fragments with the respective charge retained either at the N-terminus (b) or C-terminus (y). Although the spectrum for the IKELAR-peptide was of low quality (Fig. 2.9*A*), the FLIEGAR peptide matched the N-terminal peptide of the Knot in IpaB-Knot (Fig. 2.9*B*) and the LLRDL peptide confirmed the C-terminal fragment (Fig. 2.9*C*). Again, only the C-terminal helix and N-terminal parts of the Knot domain, but not the trefoil knot, were cleaved, suggesting that this motif is folded and consequently inaccessible to Proteinase K (Fig. 2.10).

Fluorescence analysis and mass spectrometry after limited proteolysis substantiate a folded core domain of Knot in IpaB-Knot. This includes the trefoil-knot motif which was unfolded by GuHCl and resistant to proteolysis by Proteinase K under native conditions.

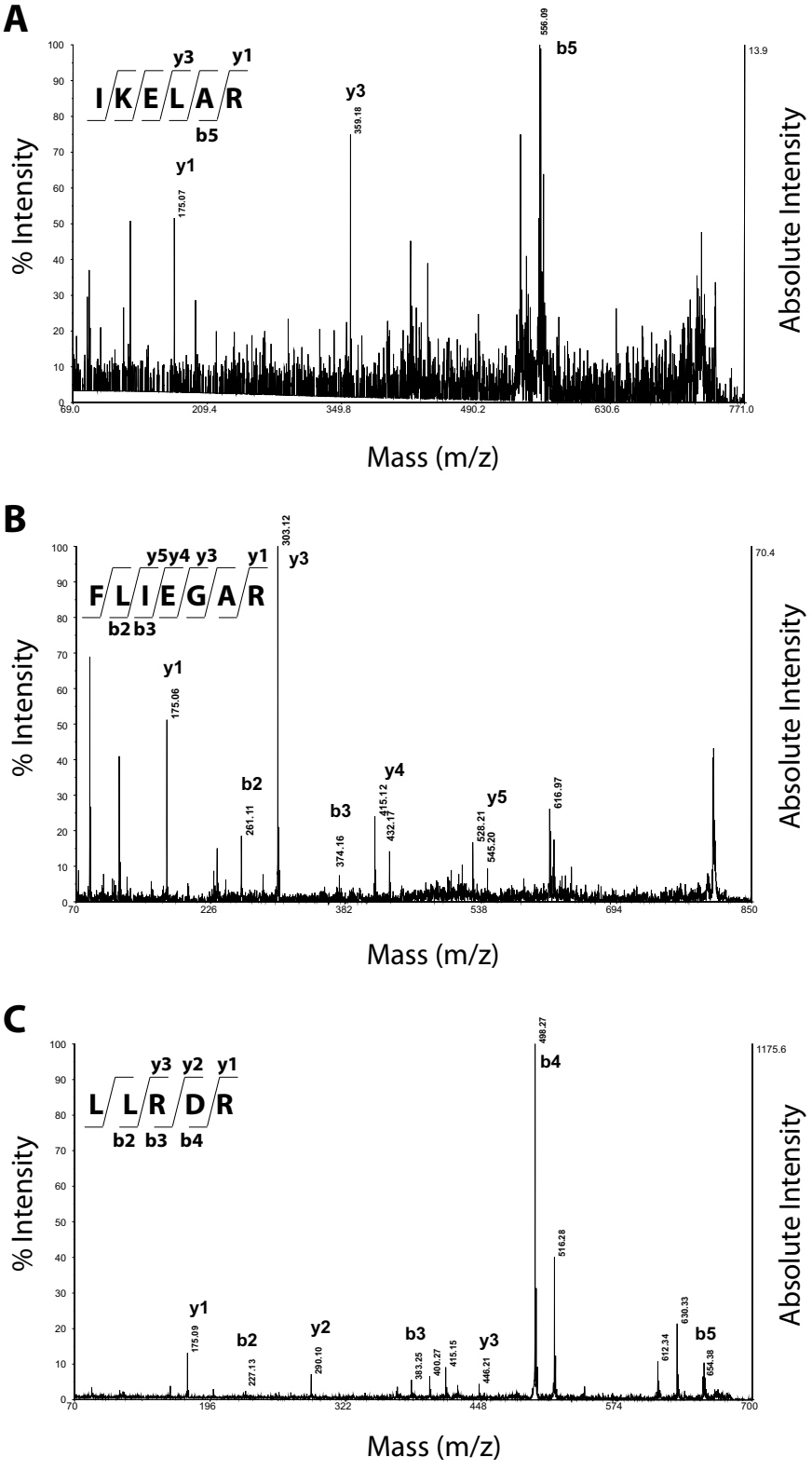

Figure 2.9: MS/MS analysis of IpaB-Knot. Spectra for N-terminal and C-terminal fragments of Knot after Proteinase K digest of IpaB-Knot and separation of peptides by 2D gel electrophoresis (analysis of Box 2 from Fig. 2.8). b and y anions correspond to amino acids with charge retained on the N-terminus (y) or C-terminus (b). Analysis was performed by Monika Schmid, MPIIB.

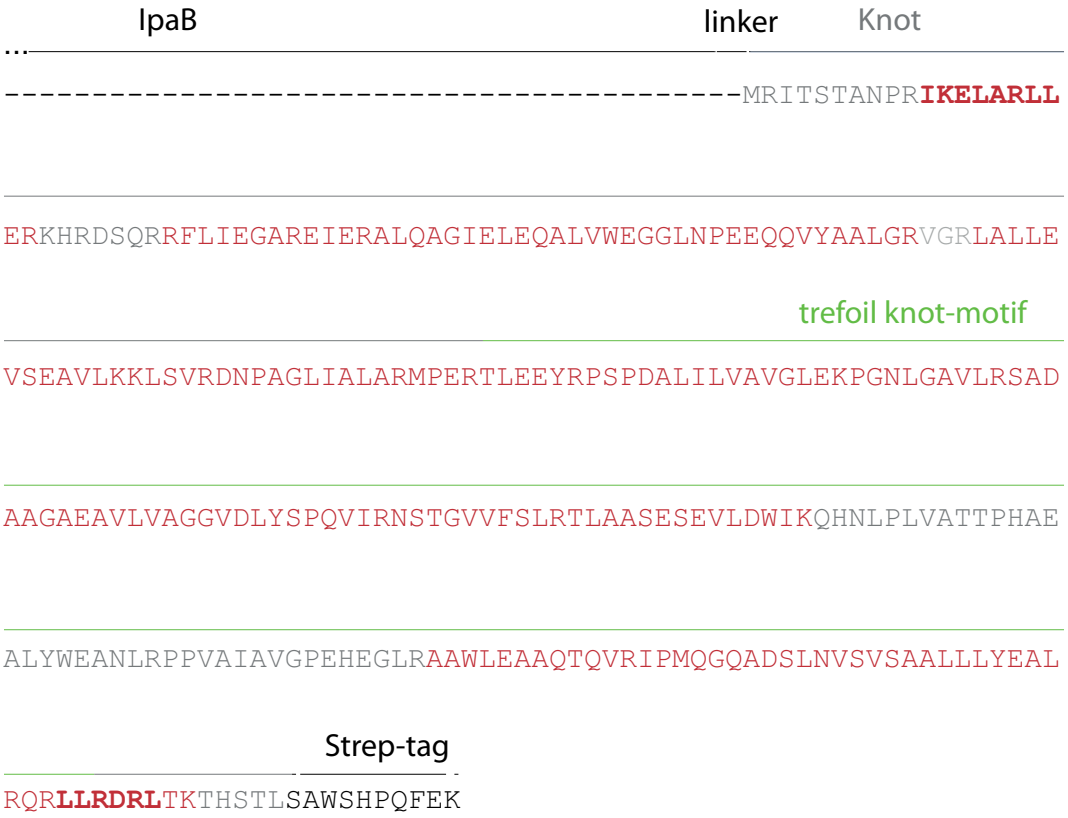

Figure 2.10: MS and MS/MS analysis of IpaB-Knot. Identified peptides by MS are highlighted in red in the Knot sequence and fragments confirmed by MS/MS are highlighted bold. The Knot is indicated by a green line above the amino acid sequence.

2.4 Plasmid-encoded IpaB-Knot: effects on hypersecretion

The fusion protein was introduced into hypersecretory strains, the Δ*ipaB* or Δ*ipaD* strain in order to analyze effects on T3SS. In the initial approach, fusion genes were expressed from inducible plasmids with a tetracycline-promoter after bacteria had grown into the logarithmic phase.

2.4.1 Induced expression in Δ*ipaB*

The Δ*ipaB* strain was complemented with plasmids containing either p*ipaB* or p*ipaBknot* and secretion was analyzed by SDS PAGE and silver stain (Fig. 2.11). Induced cultures were washed and splitted and leaky secretion (-CR) was differentiated from Congo Red-induced secretion (+CR) (Fig. 2.11*A*). Effector secretion in the Δ*ipaB* strain is not affected by Congo Red-addition except for one band missing at 40 kDa. In comparison, expression of p*ipaB* leads to absence of a doublet at 60 kDa and a band at 38 kDa. Secretion could be enhanced by Congo Red, as additional bands appeared (e.g. 50 kDa, 52 kDa, 60 kDa and 70 kDa). For complementing Δ*ipaB* with p*ipaBknot*, no secretion was observed after adding Congo Red. Secretion was analyzed in more detail by Western blotting. For the Δ*ipaB* + p*ipaB* strain, IpaB was detected in supernatants after gene expression of p*ipaB* was induced. In this strain, secretion was enhanced in the presence of Congo Red (Fig. 2.11*B*). This was not observed for Δ*ipaB* complemented with p*ipaBknot*, although intracellular protein levels were equal for both IpaB and IpaB-Knot (Fig. 2.11*C*). The intracellular chaperone DnaK in supernatants served as a marker for cellular disintegrity. DnaK was not detected in the supernatants which confirms bacterial viability in this experiment. Furthermore, IpaB-Knot was not secreted in this strain and also influenced secretion of other effectors when expressed from a plasmid.

2.4.2 Induced expression in Δ*ipaD*

Since the aim was to block the T3SS channel with the fusion, expressing the fusion in the background of a strain that secretes the effector IpaB in the absence of Congo Red induction was considered. The Δ*ipaD* strain has a hypersecreting phenotype similar to Δ*ipaB*, secretes IpaB as well as other effectors without Congo Red (Menard *et al.*, 1994a) and IpaB does not contribute to regulation of secretion in Δ*ipaD*. Unlike in the Δ*ipaB* strain, expression of p*ipaB* or p*ipaBknot* should not restore wildtype secretion, thus no Congo Red-induction is needed.

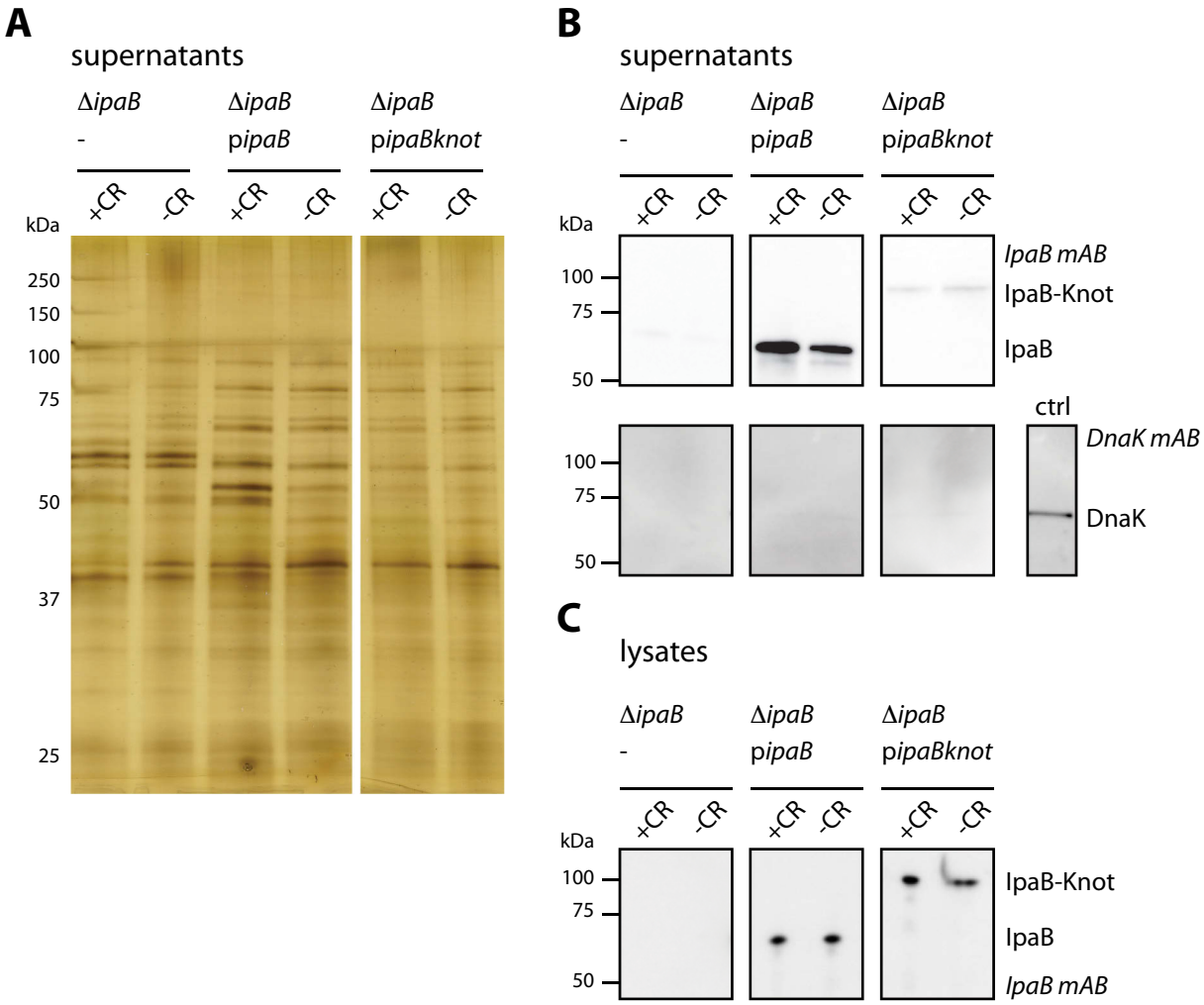

Figure 2.11: Secretion assay of Δ*ipaB* with IpaB-Knot. (*A*) Bacterial supernatants were analyzed by silver stain after induction with AHT or without induction (Δ*ipaB* / -). Induced samples were further grown in the presence of Congo Red (CR+) or without Congo Red (CR-). (*B*) Supernatants analyzed by Western blotting with IpaB and DnaK mouse monoclonal antibodies. One lysate was included as an DnaK antibody control (ctrl). (*C*) Bacterial lysates analyzed by Western blotting with IpaB mouse monoclonal antibody.

Expression of either p*ipaB* or p*ipaBknot* in Δ*ipaD* was investigated in comparison to an *mxiH* mutant (secretion deficient) and the untransformed Δ*ipaD* strain. These strains served as controls to monitor effects of AHT (+) or DMF (-, vehicle), as secretion was analyzed from overnight-grown cultures in order to accumulate more effector proteins in culture supernatants (Fig. 2.12*A*).

For induced expression of p*ipaB*, analysis of SDS PAGE and Coomassie stain showed a slight reduction in secretion compared to the Δ*ipaD* control but the typical pattern of secreted effector proteins was retained (Fig. 2.12*A*, middle panel). With regards to the effector proteins secreted, the Δ*ipaD* strain with induced p*ipaBknot* was completely deficient in secretion and only residual proteins were detected in the supernatant (Fig. 2.12*A*, right panel).

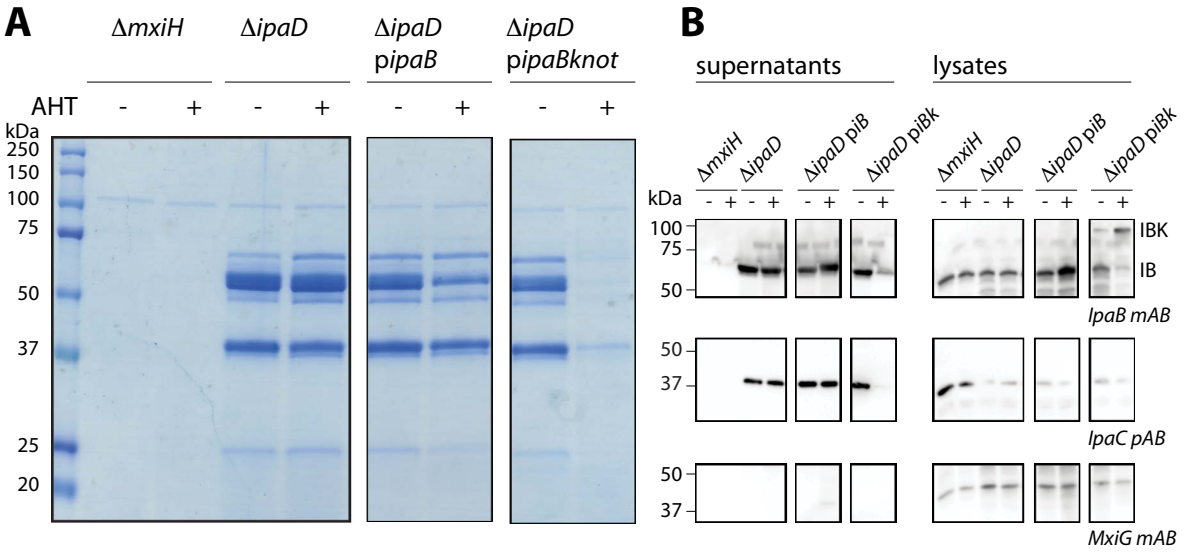

Figure 2.12: Secretion assay of Δ*ipaD* with IpaB or IpaB-Knot. (*A*) Coomassie stain of precipitated culture supernatants of Δ*mxiH*, Δ*ipaD* and Δ*ipaD* plus plasmid-encoded p*ipaB* or p*ipaBknot*. All strains tested were treated with DMF (-) or AHT in DMF (+). Supernatants were normalized. (*B*) Western blot analysis of strains from *A*, probed with anti-IpaB mouse mAB, anti-IpaC rabbit pAB, anti-MxiG mouse mAB, piB: plasmid-*ipaB*, piBk: plasmid-*ipaBknot*, IB: IpaB, IBK: IpaBKnot.

The effect on secretion by p*ipaBknot* and lack of effector synthesis due to regulatory effects were further differentiated. Western blot analysis of IpaB in supernatants and lysates showed that the Δ*ipaD* strain secreted IpaB whereas the Δ*mxiH* did not and both strains had equal levels of IpaB in the cytoplasm (Fig. 2.12*B*, supernatants and lysates, upper left panels). The level of IpaB in Δ*ipaD* represents the basal intracellular amount of IpaB for this bacterial background. This level, as well as the amount of secreted IpaB, was increased by additional expression of p*ipaB* (supernatants and lysates, middle panels). In Δ*ipaD* expressing p*ipaBknot*, the amount of secreted IpaB as well as the intracellular level of endogenous IpaB were reduced and cytoplasmic levels of IpaB-Knot (IBK) were comparable to IpaB (IB) in Δ*ipaD*. Again, IpaB-Knot was not secreted. IpaC was analyzed as an additional effector protein. Levels of IpaC in supernatants and cytoplasm were reduced compared to Δ*ipaD* + p*ipaB*. This only applied to effector proteins, as levels of MxiG, a structural component of the NC basal body, were not altered in bacterial lysates.

2.5 Insertion of *knot* into pWR100

Expression of p*ipaB-knot* influenced the cytoplasmic level of effectors, including IpaB, which is due to the regulatory function of IpaB. Therefore, the strategy for *ipaBknot* expression in the bacterium was changed and *ipaBknot* was expressed under the native promoter of *ipaB*. The gene encoding *ipaB* was fused to the *knot* gene by insertion of the coding sequence into the virulence plasmid in *S. flexneri*, together with the codons for a *strep*-tag (Fig. 2.13*A*). The gene was placed 3' in the *ipaB* open reading frame, resulting in *ipaBknot*, which was then expressed under the control of the native promoter in the *ipgCipaBCDA* operon. The insertion was verified by colonyPCR with oligonucleotides (half arrows in Fig. 2.13*A*) that annealed up- and downstream of the insertion site. In the wildtype, the PCR product was about 300 bp, whereas insertion of *knot* together with the chloramphenicol cassette (cam) resulted in a product of about 2 kb (Fig. 2.13*B*).

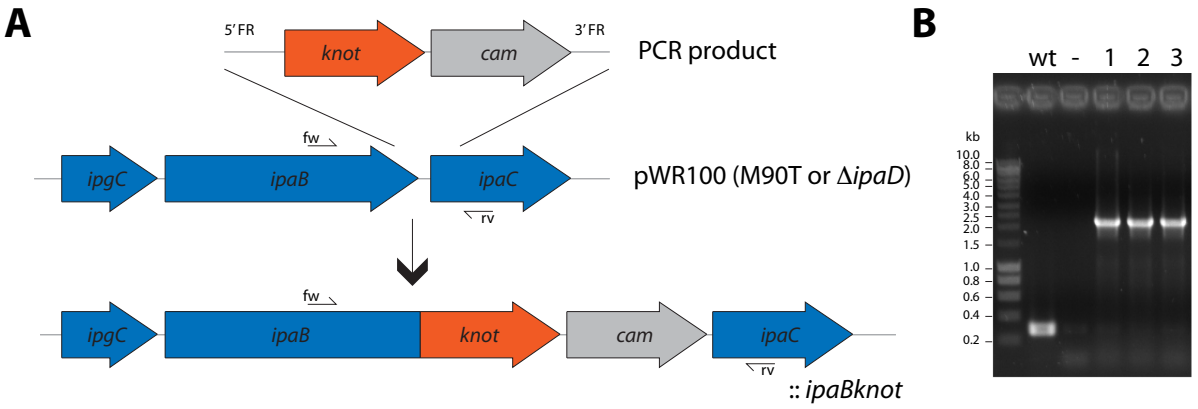

Figure 2.13: *knot* insertion in the virulence plasmid pWR100. (*A*) Schematic of homologous recombination mediated by Flp recombinase. (*B*) Agarose-gel of PCR products from genotyping of M90T (wt) or M90T::*ipaBknot* (1-3).

IpaB was thereby replaced by IpaB-Knot (with a C-terminal Strep-tag, 93 kDa). This strategy was applied to both M90T wildtype and the hypersecretor Δ*ipaD*.

2.6 IpaB-Knot does not complement IpaB in invasion

IpaB plays an essential role during bacterial invasion of epithelial cells (Menard *et al.*, 1993), and since it was shown before that IpaB is functional in fusion with Knot, effects on invasion caused by the fusion protein were analyzed.

Invasiveness was quantified in a gentamicin protection assay (Sansonetti *et al.*, 1982) by

comparing invasion of M90T::*ipaBknot* to wildtype M90T and the Δ*ipaB* mutant (Fig. 2.14). M90T::*ipaBknot* showed a 1000-fold decreased invasion phenotype comparable to the negative control Δ*ipaB* (Fig. 2.14*A*).

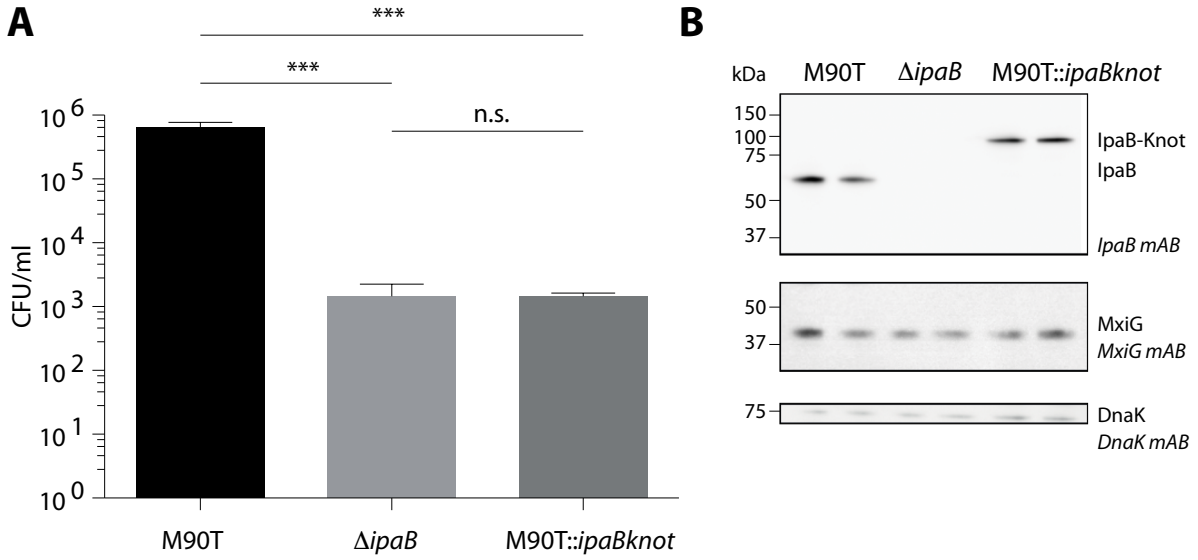

Figure 2.14: Invasion assay with *S. flexneri* strains and Western blot analysis. (*A*) Invasiveness quantified by colony-forming units (CFU) per ml culture. Two clones were grouped, each as a technical triplicate, and compared by multiple t-test. (*B*) Western blot analysis of IpaB, MxiG and DnaK (loading control) in whole cell lysates.

The observed deficiency in invasion was not based on altered expression of *ipaBknot* when protein levels were compared to wildtype IpaB in M90T (Fig 2.14*B*). A deficit in expressing structural components of the NC was excluded by Western blot, which revealed equal levels of MxiG in all three strains. As previous results demonstrated a functional IpaB domain in IpaB-Knot, it is likely that the phenotype of decreased invasion is based on IpaB-Knot affecting the T3SS pathway.

2.7 IpaB-Knot influences regulation of effector secretion

Since bacteria expressing *ipaBknot* are not invasive despite normal expression of functional IpaB-Knot and T3SS components, effects on secretion were investigated. Secretion of bacteria that carry the fusion allele *ipaBknot* was analyzed in comparison to wildtype M90T (with or without Congo Red induction), the hypersecretory mutant Δ*ipaB* as a positive control and Δ*mxiH* as a negative control (Fig. 2.15). The Coomassie stain in Fig. 2.15 shows effector proteins from culture supernatants that were secreted by the indicated bacterial strain.

Compared to M90T and the *ipaB*-deficient strain, M90T::*ipaBrrmA* phenocopied both strains. Secretion comparable to Δ*ipaB* was observed already without induction of Congo Red. With

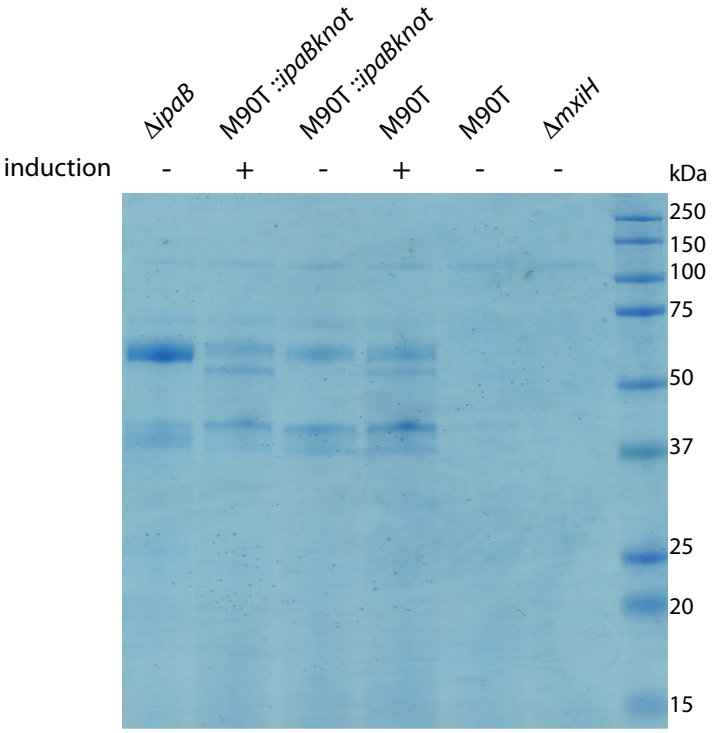

Figure 2.15: Coomassie stain of effector proteins (secretion assay). Amounts were normalized to culture density. Induction with Congo Red is indicated by +, or - for no induction, respectively.

induction, the number of proteins in the supernatant increased by an additional band visible at about 55 kDa and the pattern resembled M90T under the influence of Congo Red. This suggests that secretion is deregulated when IpaB is replaced by IpaB-Knot in M90T.

2.8 IpaB-Knot impedes T3SS secretion

2.8.1 The effect of IpaB-Knot on effector secretion

For further analysis of effects on the T3SS pathway and better comparison of secretion phenotypes, an *ipaD*-deficient strain (Δ*ipaD*) was used as a background for the expression of genomic *ipaBknot*. Secretion of Δ*ipaD* (Δ), Δ*ipaD*::*ipaBknot* (Δ+) strain and of a secretion-deficient negative control (Δ*mxiH*Δ*ipaD*, ΔΔ) were compared in overnight cultures and amounts of secreted proteins were monitored by SDS PAGE and Coomassie stain (Fig. 2.16*A*) or Western blotting (Fig.2.16*B*).

Opposing hypersecretion in Δ*ipaD*, the amount of proteins secreted by Δ*ipaD*::*ipaBknot* was merely residual. In contrast, SepA, an autotransporter and substrate to a type V secretion system (Henderson *et al.*, 2004), was equally present in all strains (Fig. 2.16*A*, 110 kDa and *B*, upper panel). This lead to the conclusion that only amounts of T3SS-dependent pro-

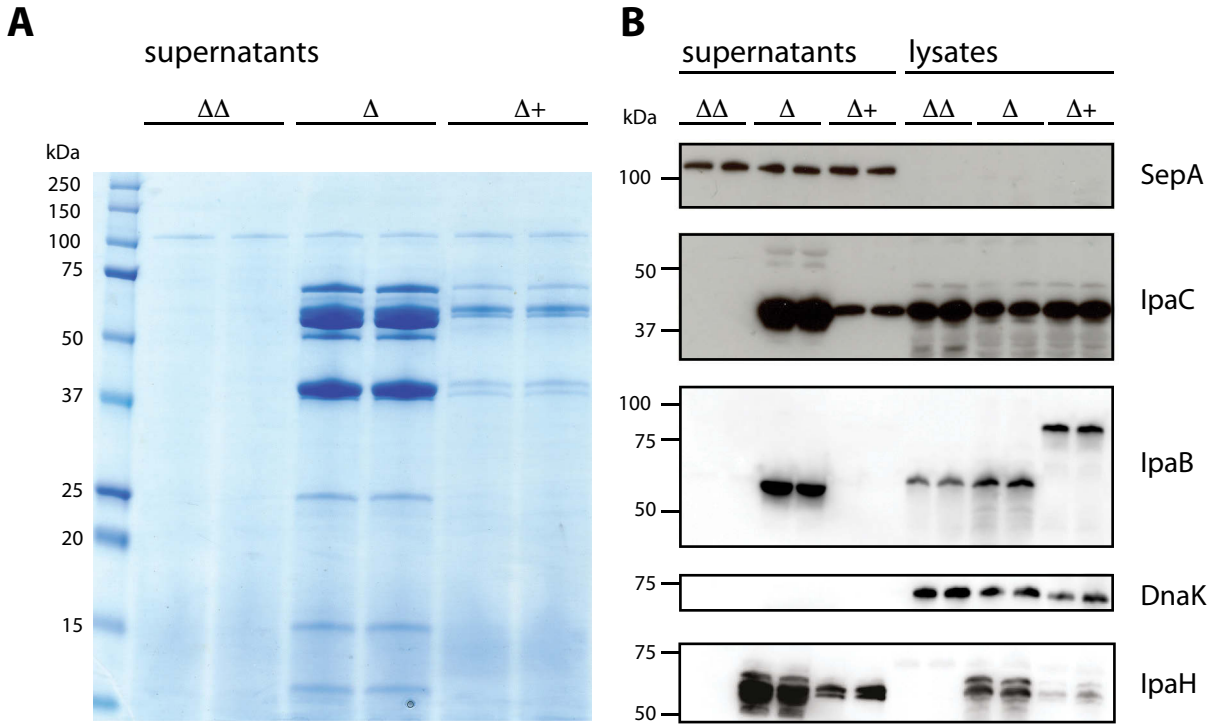

Figure 2.16: Secretion assay with *S. flexneri* strains and Western blot analysis. (*A*) SDS PAGE and Coomassie stain of precipitated proteins from either Δ*mxiH*Δ*ipaD* (ΔΔ), Δ*ipaD* (Δ) or Δ*ipaD*::*ipaBknot* (Δ+) shown for two clones. (*B*) Western blot analysis from (*A*) of proteins secreted or bacterial lysates using different antibodies as indicated.

teins were decreased in supernatants of Δ*ipaD*::*ipaBknot*.

The limited secretion in Δ*ipaD*::*ipaBknot* was confirmed by more specific Western blot analysis (Fig. 2.16*B*). IpaB was found in supernatants of Δ*ipaD* which contrasts the entirely cytoplasmic localization of IpaB-Knot in Δ*ipaD*::*ipaBknot*. The supernatants and bacterial lysates from Δ*ipaD* and Δ*ipaD*::*ipaBknot* were tested for the translocator IpaC and the effector IpaH. The amount of secreted IpaC was reduced in supernatants of Δ*ipaD*::*ipaBknot* but not in Δ*ipaD*. Furthermore, cytoplasmic levels of IpaC showed equal protein synthesis which underlines an effect on the secretion pathway but not expression. IpaH belongs to the second set of effectors (late effectors) which are regulated by the IpgC/MxiE feedback loop (Schroeder & Hilbi, 2008). Representing one late effector, IpaH was found to be reduced in the supernatants as well as in bacterial lysates. Hence, the observed reduction of T3SS-dependent proteins in supernatants resulted from less secretion as well as downregulation of late effector genes.

2.8.2 Expression of *knot* has no effect

As a control, the Knot-encoding gene was expressed by insertion into pWR100 together with the *ipaC* ribosomal binding site between *ipaB* and *ipaC*. As in the previous experiment, proteins from bacterial supernatants were analyzed by Coomassie-stained SDS PAGE and Western blotting. The effector pattern observed resembles the secreted proteins of the Δ*ipaD* mutant strain and did not show deficits in protein secretion (Fig. 2.17, left panel). As the intracellular levels of IpaC were not reduced in the Δ*ipaD*::*ipaBknot* strain, *knot* mRNA should be translated under the control of the *ipaC* ribosomal binding site. Production of Knot was detected in the bacterial cytoplasm using an anti-Strep tag antibody. The Knot was found in the cytoplasm only and was not secreted (Fig. 2.17, right panel).

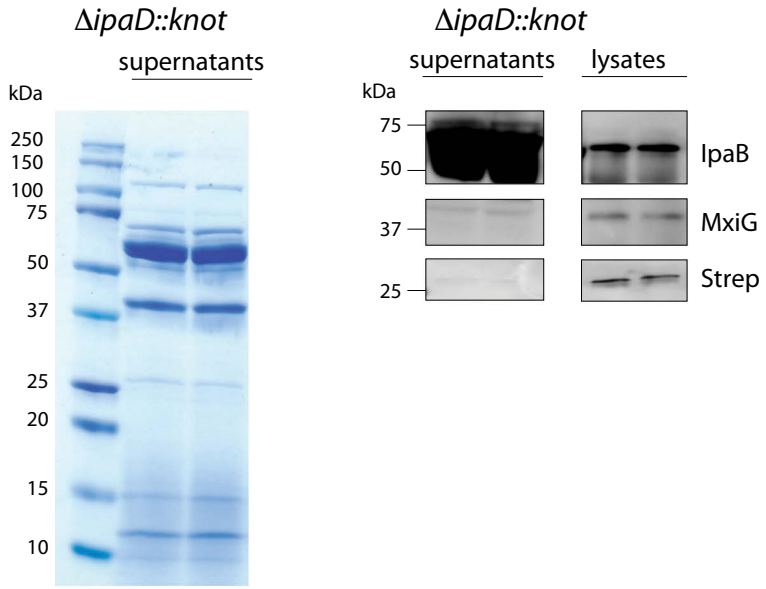

Figure 2.17: Secretion assay with *S. flexneri* strains and Western blot analysis. Two clones are shown with effector proteins secreted (left) and specific Western blot analysis with anti-IpaB, anti-MxiG and anti-Strep antibody (detection of Knot).

In agreement with the expression of *knot* from the inducible plasmid system in figure 2.3, expression of *knot* without fusion under the native promoter of the *ipaB*- and *ipaC*-including operon did not affect the T3SS pathway. Neither effector synthesis nor bacterial integrity were influenced, as levels of IpaB and MxiG were equal to Δ*ipaD* (Fig. 2.17, right panel, compared to 2.16*B*). In summary, fusion of IpaB to the Knot but not unfusioned Knot reduced T3SS-dependent effector secretion and synthesis (late effectors) in the hypersecretor Δ*ipaD*.

2.9 Needle complexes co-purify with IpaB-Knot

Next, the question emerged if attenuated secretion was the result of IpaB-Knot interacting with the NC. Interaction of IpaB-Knot and NCs were studied on NC isolates from Δ*ipaD*::*ipaBknot* using cesium chloride density fractionation where a continuous salt gradient is built over time by centrifugal force and large protein complexes are separated from smaller soluble proteins. Isolated NCs were detected with an anti-MxiG antibody, as MxiG constitutes the inner membrane ring which is an integral part of the NC (Blocker *et al.*, 2001). Residual IpaB was separated from the NCs which is in agreement with the observation that IpaB is unable to bind to the NC in the Δ*ipaD* mutant (Veenendaal *et al.*, 2007). In contrast to IpaB which remained in the low-density fraction, NCs migrated to high-density fractions (Fig. 2.18*A*). This migration pattern was opposed by isolates from Δ*ipaD*::*ipaBknot* where IpaB-Knot migrated with isolated NCs to high-density fractions (Fig. 2.18*B*).

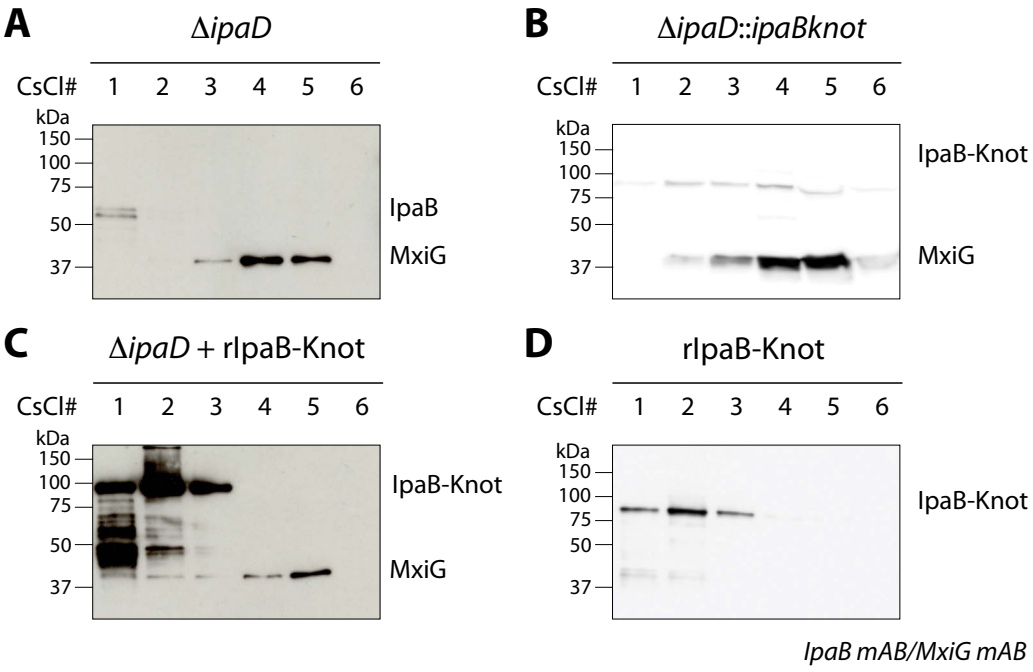

Figure 2.18: Density gradient fractionation of needle complexes and IpaB or IpaB-Knot. Separation of NC isolates from Δ*ipaD* (*A*), Δ*ipaD*::*ipaBknot* (*B*), Δ*ipaD* plus purified IpaB-Knot (*C*) or purified IpaB-Knot only (*D*). Western blot analysis of fractions (CsCl# 1 to 6) with 1 being the low density fraction. anti-IpaB mAB and anti-MxiG mAB were used simultaneously.

IpaB-Knot from recombinant expression (rIpaB-Knot) was added to purified NCs from Δ*ipaD* cells (Fig. 2.18*C*) to further characterize the nature of potential interaction. Purified IpaB-Knot remained in low-density fractions and did not migrate with NCs to high-density fractions, which was also seen for purified IpaB-Knot without isolated NCs (Fig. 2.18*D*) and therefore aggregation as a cause for migration to higher densities was excluded. This co-

migration suggests interaction between the NC and IpaB-Knot in the Δ*ipaD*::*ipaBknot* strain which might result from attempted secretion and subsequent obstruction of the T3SS by IpaB-Knot.

2.10 Localization of IpaB-Knot at isolated needle complexes (overall NC population)

Based on previous results, IpaB-Knot was localized at the isolated NCs. Localization of IpaB-Knot at NCs was investigated after density fractionation using immuno-electron microscopy (iEM). Fractions that contained both IpaB-Knot and MxiG (Fig. 2.18*B*, fractions 4 and 5) were further purified by gelfiltration as cesium chloride interfered with visualization due to its high electron density. After gelfiltration and subsequent concentration of NCs, the samples were stained on grids with an anti-IpaB monoclonal antibody (mAB), which binds to an N-terminal epitope between the residues 118 and 179 (Barzu *et al.*, 1993). Using this antibody, the IpaB epitope of IpaB-Knot could be detected either at needle tips or at the basal side of isolated NCs (Fig. 2.19*A*-*D*).

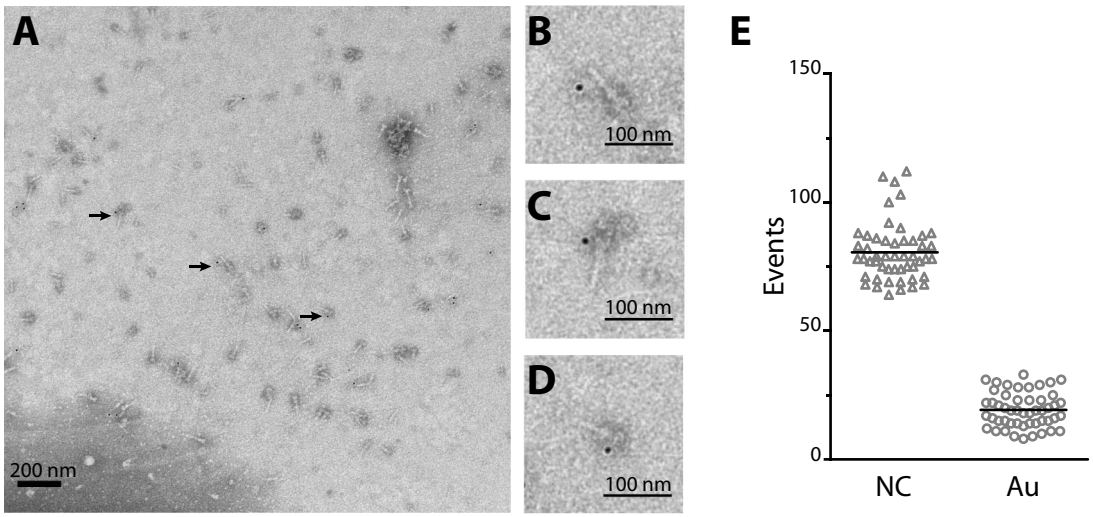

Figure 2.19: Gold labeling of IpaB-Knot at isolated NC. IpaB was detected with anti-IpaB mAB and goat anti-mouse, 12 nm gold conjugate. (*A*) Example iEM image of anti-IpaB labeling in isolated NCs with magnified details (indicated by arrows in (*A*)) in (*B*-*D*). (*E*) Distribution of distances between NCs and gold particles in 50 images, including (*A*).

IpaB was not detected in samples of isolated NCs from the Δ*ipaD* strain which is consistent with IpaB being separated from NCs in these samples (Fig. 2.18*A*). To assess whether the observed co-localization between IpaB-Knot and NC is specific, 50 random iEM images were quantified and coordinates for gold labeling IpaB and NCs were recorded manually. Average

counts comprised of 80 NC and 20 labels per image (Fig. 2.19*E*).

In order to obtain a random distribution of gold and NCs, respective coordinate X and Y values were randomized according to counts per image within the range of the image dimensions. Both counted and simulated coordinates were subjected to a nearest-neighbor analysis, quantifying distances between NC centers and the closest adjacent gold particles (Fig 2.20*A*).

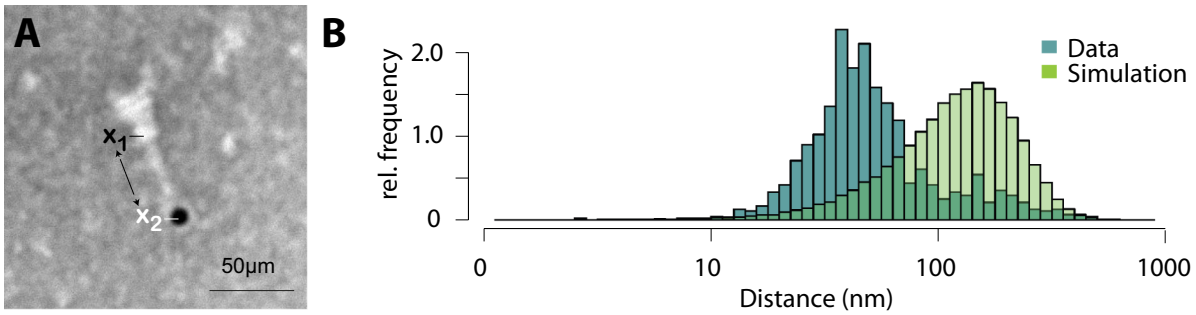

Figure 2.20: Nearest-neighbor analysis of isolated NCs and gold. IpaB was detected with anti-IpaB mAB and goat anti-mouse, 12 nm gold conjugate. (*A*) Coordinates for NC centers (x_1) and gold particles (x_2) were manually selected. (*B*) Distribution of distances between NCs and gold particles in 50 images.

The distribution of counted NC/gold distances shows a maximum around 30 to 50 nm, whereas distances from a random distribution of according gold and NC numbers per image peaked around 100 nm to 120 nm (Fig. 2.20*B*).

2.11 Detection of IpaB-Knot C-terminus in occupied NCs

About 25 % of the NC were positive for gold labeling of the IpaB-Knot N-terminus. Since it cannot be distinguished if only 25 % interact with IpaB-Knot or if this is a technical limitation, NCs occupied by IpaB-Knot were specifically enriched. Purified NCs from solubilized membrane fractions were immobilized on sepharose using Strep-Tactin resin which binds to the C-terminal Strep-tag of IpaB-Knot. NCs eluted from the resin after treatment with desthiobiotin, however, some NCs were still bound to the resin (Fig. 2.21*A*) The purification using resin lead to the elution of partially damaged NCs, as many NCs were deficient for basal body rings of the inner membrane (Fig. 2.21*B*) and consisted merely of the central channel.

The isolated channels were still positive for IpaB-Knot. Regarding the bilateral labeling seen for IpaB, labeling of the C-terminus of IpaB-Knot occurred mostly at the basal side of the isolated NC (Fig. 2.22*B*, *C* and *D*) with rare exceptions (Fig. 2.22*E*). For isolated channels

with an incomplete base, the basal side was distinguished from the distal side by localizing the long needle on the distal side of the NC.

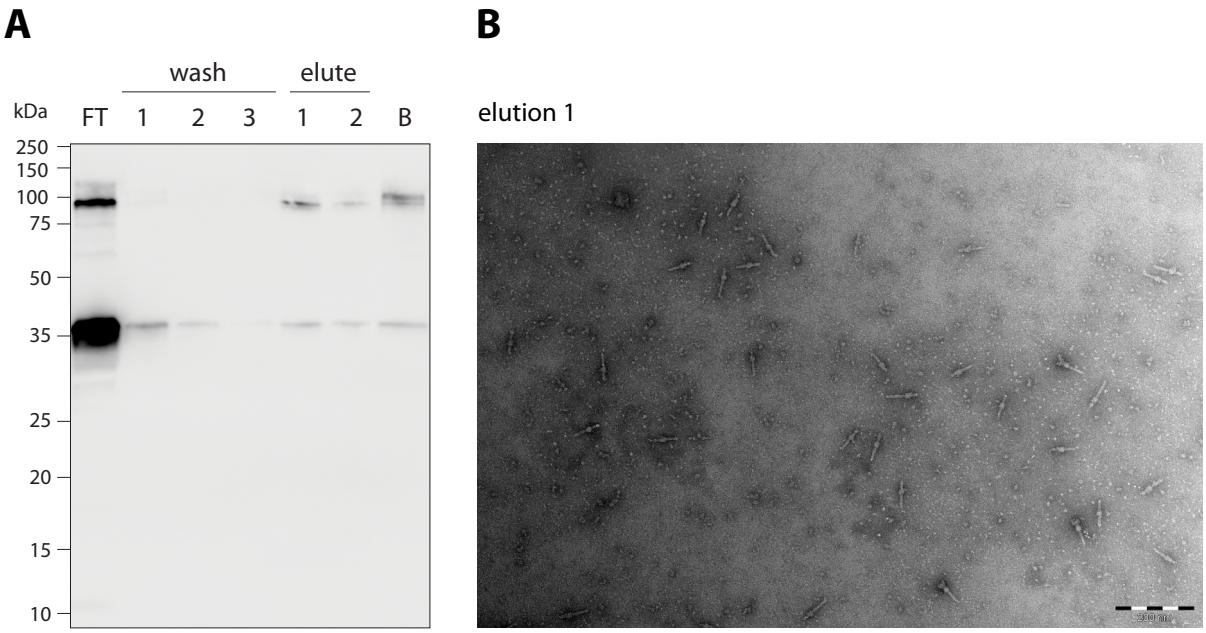

Figure 2.21: Batch purification of NCs using Strep-Tactin resin. (*A*) Western blot analysis of batch purification detecting IpaB-Knot (93 kDa) and MxiG (42 kDa) simultaneously; FT: Flow through, B: beads. (*B*) TEM of elution fraction 1 from batch purification.

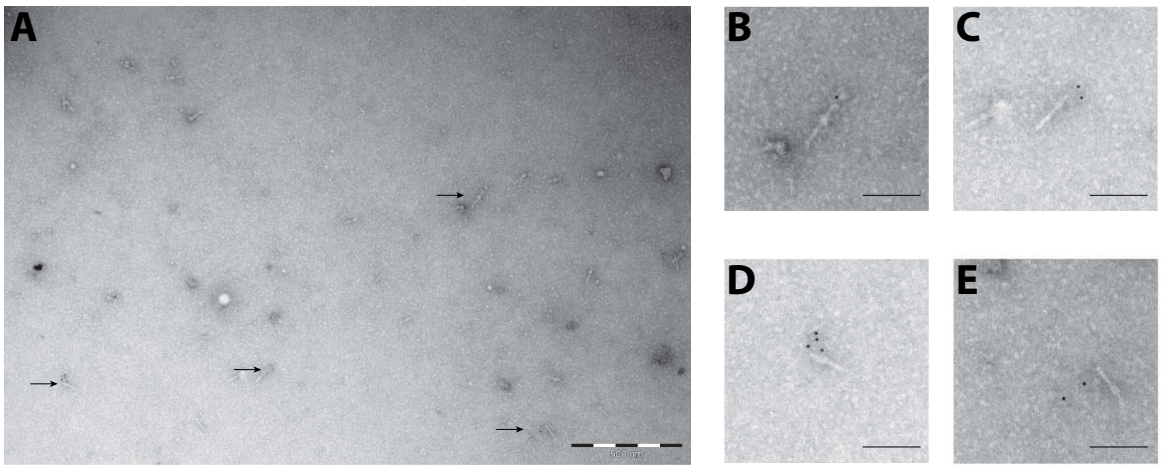

Figure 2.22: anti-Strep tag labeling on isolated NCs. (*A*) Overview of labeled NCs and magnifications shown in (*B-E*); scale bars indicate 100 nm.

2.11.1 Production of humanized IpaB mAB

Labeling with different gold-conjugated secondary antibodies enables distinguishing between epitopes, if different species of primary antibodies are used. Each secondary antibody is coupled to gold colloids of defined diameters. Since both the IpaB mAB and the Strep-tag mAB are murine antibodies, the IpaB mAB was expressed as a human IgG1.

The hybridoma H16 is based on a spleen cell line fused to the IpaB mAB-producing B cell (Barzu *et al.*, 1993). After obtaining H16 cDNA, the B cell receptor (BCR) genes encoding the variable regions were amplified, resulting in two overlaying sequences. One represents the genomic BCR of the spleen cell, the other sequence contains information on the variable segment of the IpaB-specific BCR. Since the variable region of the spleen BCR is known, the sequence of the IpaB-specific BCR was extracted from the overlaying signal (by manually subtracting the spleen BCR signals) and an IpaB-BCR specific primer was chosen for subcloning of the respective variable segment. The plasmids contain human constant regions of IgG1 heavy and light chains. By insertion of the murine variable region, an IpaB-specific human monoclonal antibody (hmAB) was generated.

Purified IpaB hmAB was tested for specificity by Western blot analysis (Fig. 2.23). Bacterial lysates of Δ*ipaD*::*ipaBknot* were probed for IpaB-Knot with combinations of either IpaB mAB and goat-anti mouse horse-radish peroxidase (HRP), IpaB hmAB and goat-anti mouse HRP, IpaB mAB and goat-anti human HRP or IpaB hmAB and goat-anti mouse HRP. Signals were obtained only for matches of primary antibodies with species-specific secondary antibodies (Fig. 2.23*A* and *C*). This demonstrated suitability of the IpaB hmAB for concomitant detection of the IpaB-epitope and the Strep-tag by the Strep-tag mouse mAB, as non-matching secondary antibodies did not evoke unspecific signals.

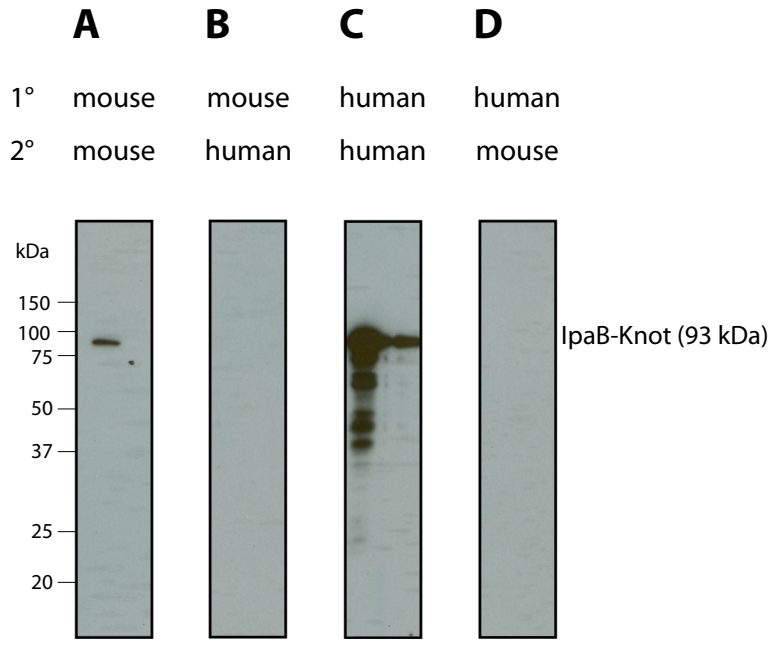

Figure 2.23: Western blot analysis of mouse and human anti-IpaB. Primary (1) and secondary (2) antibodies were combined as indicated.

2.11.2 Simultaneous detection of IpaB-Knot N- & C-terminus

Labeling both the IpaB epitope and the Strep-tag on enriched occupied NCs was performed with the IpaB hmAB and the Strep-tag mAB simultaneously. In a few cases, NCs were labeled on both sides with the IpaB epitope detected at the tip and the Strep-tag epitope at the base (Fig. 2.24). Compared to single labeling, this was a rare event compared to single labeling, but was reproducable when both antibodies were used. Also multiple gold particles for each epitope were detected (Fig. 2.24*B-D*). Importantly, only labeling of one epitope occurred if one primary antibody was used together with both secondary gold-conjugated antibodies.

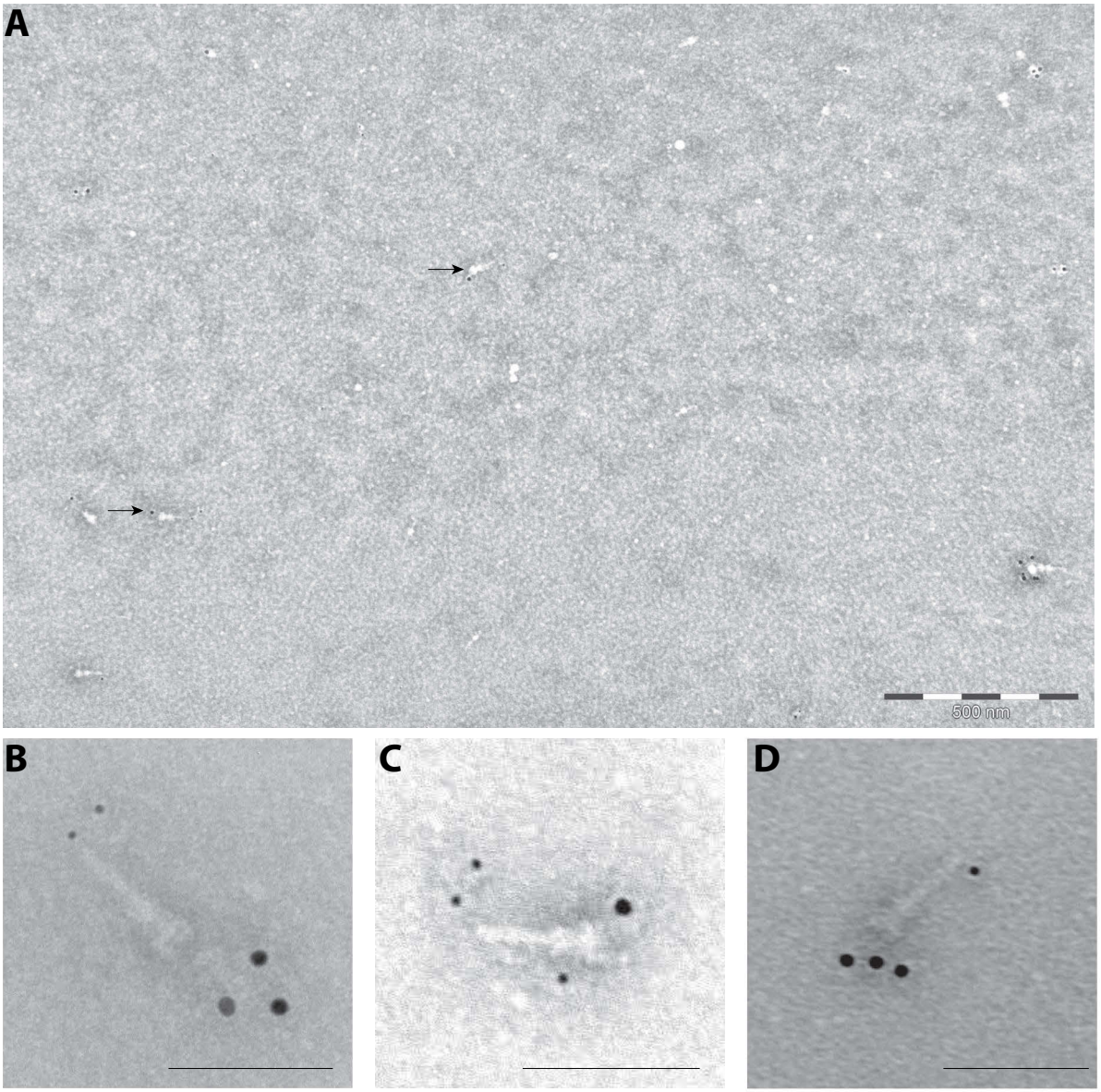

Figure 2.24: Double labeling of IpaB N-terminus and C-terminal Strep-tag on isolated NCs. (*A*) Overview image with two double labeled NCs. (*B-D*) Magnified double-labeled NCs chosen from different images; scale bars indicate 100 nm.

2.12 The T3SS channel shields parts of IpaB-Knot

It was examined whether IpaB-Knot was inserted into the NC channel by testing the accessibility of the fusion protein. According to a conduit model for T3SS where effectors are secreted through the NC, part of IpaB-Knot should be enclosed by the NC channel. After obstruction, the effector should remain inside the needle and would be shielded from enzymatic modifications or crosslinking chemicals that cannot penetrate into the channel.

2.12.1 The fusion protein is inaccessible to TEV protease

The IpaB-Knot fusion was modified with a TEV protease-specific cleavage site between both domains of IpaB-Knot. Δ*ipaD*::*ipaBTEVknot* NC isolates occupied with IpaB-TEV-Knot and IpaB-TEV-Knot purified from *E. coli* BL21 were coupled to Strep-Tactin sepharose beads via the Strep-tag and subsequently treated with TEV protease.

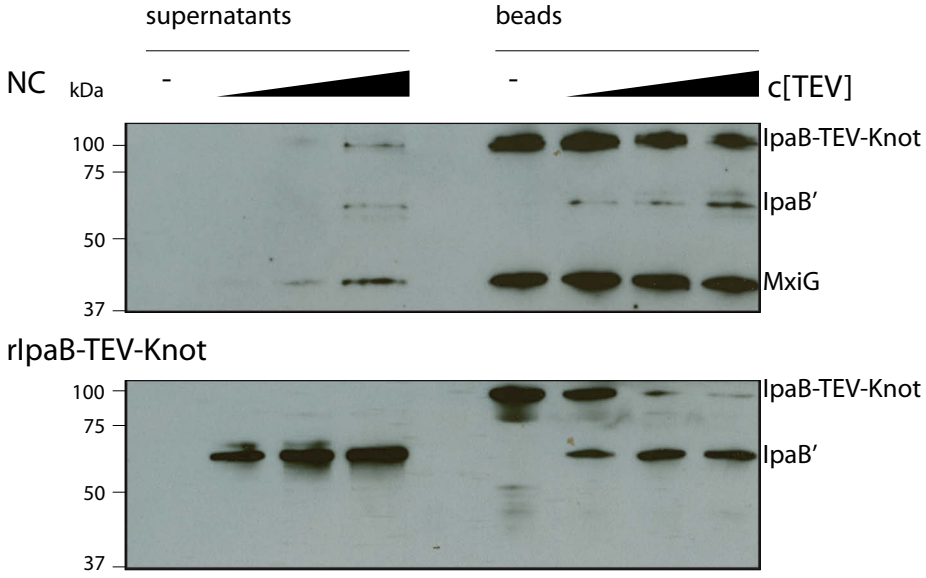

Figure 2.25: TEV protease treatment of isolated NCs and purified IpaB-TEV-Knot. Isolated NCs are shown in the upper panel and purified protein in the lower panel. Western blot analysis was performed with anti-IpaB mAB and anti-MxiG mAB simultaneously.

Supernatants with enriched cleavage products and bead fractions were analyzed by Western blotting after protease treatment. IpaB-TEV-Knot co-purified with NCs showed almost no cleavage products (IpaB') after treatment with increasing concentrations of TEV protease (Fig. 2.25, upper panel). In comparison, control IpaB-TEV-Knot purified from *E. coli* was entirely cleaved by TEV protease (Fig. 2.25, lower panel). Purified IpaB-TEV-Knot decreased in direct correlation with released IpaB' accumulating in supernatants. Cleavage efficiency depended on the amount of TEV protease, however, already at low concentrations, almost

all IpaB-TEV-Knot was digested. Some IpaB' was seen in the bead fractions, which could be due to a non-specific interaction. The cleavage pattern indicates that IpaB-TEV-Knot purified with NCs is protected from enzymatic cleavage and digestion of purified IpaB-TEV-Knot demonstrates an accessible TEV recognition site for the fusion protein in the absence of NCs.

2.12.2 Chemical modification is limited by the presence of the NC

To gain better insights into the protective effect by the NC, the extent to which IpaB-Knot can be modified by treatment with crosslinking polyethylene glycol molecules (PEGylation) was assessed. Each PEG increases the molecular weight by 1.1 kDa and has a defined arm length of 8.8 nm. Consequently, PEGylation molecules cannot penetrate or diffuse into the NC channel for sterical reasons. Proteins can be PEGylated by crosslinking of primary amines (lysine residues and protein N-terminus) to the NHS-group of PEG. In IpaB-Knot, 58 PEGylation sites are evenly distributed across the protein. Analog to the TEV protease assay, Strep-Tactin beads were saturated with either purified IpaB-Knot or isolated NCs containing IpaB-Knot. The beads were treated with PEGylation agent and subsequently analyzed using a Strep-tag antibody. The Step-tag at the C-terminus of IpaB-Knot has no PEGylation sites and therefore the antibody epitope should not be modified. PEGylated IpaB-Knot shifted to about 110 kDa compared to 93 kDa for unmodified protein, which corresponds to PEGylation at 20-30 amines (Fig. 2.26, left panel).

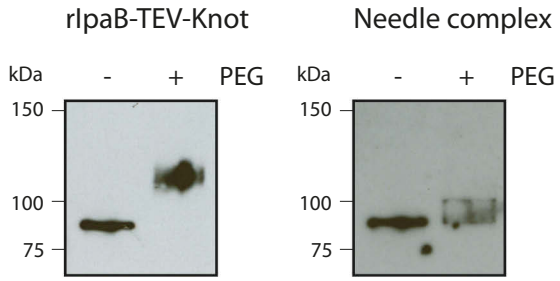

Figure 2.26: PEGylation of isolated NCs and purified IpaB-TEV-Knot. Purified IpaB-TEV-Knot (left panel) and isolated NCs (right panel) were either left untreated (-) or treated with 0.5 mM PEGylation reagent (+). Western blot analysis was performed with anti-Strep tag mAB.

In comparison, IpaB-Knot isolated together with NCs showed much lesser PEGylation and the protein size shifted not more than 10 kDa (Fig. 2.26, right panel). The difference in PEGylation accessibility is most likely caused by the NC channel which confers protection by surrounding IpaB-TEV-Knot, thereby partially covering the protein and shielding it against proteases and chemical modifications.

2.13 Initial single particle analysis of NCs with IpaB-Knot

cryo-EM images of NCs isolated from Δ*ipaD*::*ipaBknot* were recorded from 3 different preparations and images suitable for single particle analysis were manually selected based on image quality according to visibility of Thon rings, astigmatism, visible image drift and contamination.

In total, 958 pictures were selected, yielding 2086 manually boxed single particles that were further processed. An iterative rotational alignment based on cross-correlation scores of all particles collected is depicted in Fig. 2.27*A*, where the first image (0) shows overlay of centered particles. After the initial rotational adjustment of single particles, further refinement was performed with additional shifting of particles (Fig. 2.27*B*) Subsequently, particles were classified into 12 different classes by k-means clustering based on needle length (Fig 2.28).

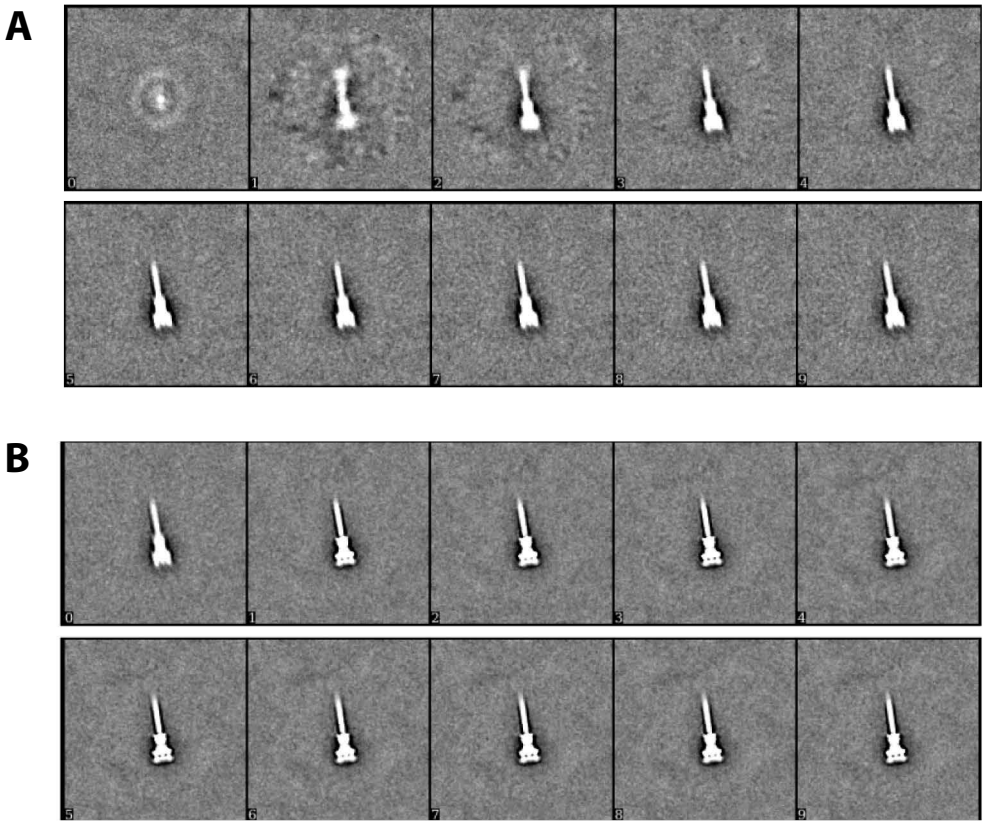

Figure 2.27: Rotational alignment of NCs. Computational iteration of particle alignment from left (no alignment) to refined alignment (right).

For some classes, an additional density was seen at the needle tip. However, in order to substantiate this observation, more particles are required. Also comparison to control particles (NC from Δ*ipaD*) without the fusion protein would be supportive to distinguishing empty from obstructed NC. The preliminary data demonstrate that alignment of these par-

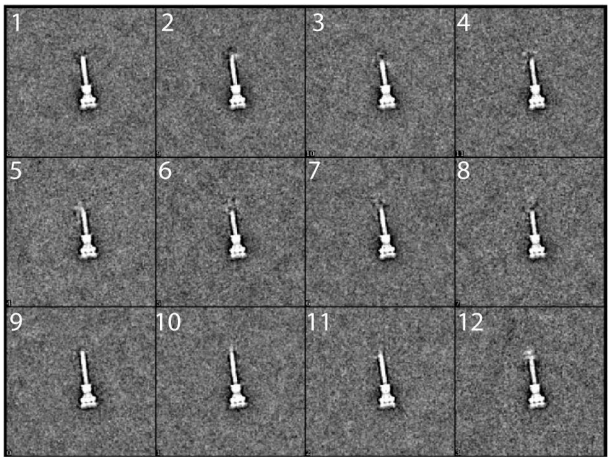

Figure 2.28: Single particle-analysis of isolated NCs. (*A*) Particle classes based on k-means clustering. (*B*) Iterative alignment of all particles from 0 (manual alignment) to 9 (refined alignment).

ticles works with the approach taken, however, more data is required to obtain structural information about the NC occupied with IpaB-Knot.

3 Discussion & Perspectives

The T3SS is an intricate bacterial secretion system with more than 25 structural proteins constituting the machinery for protein transport across the membranes and the periplasm. Many questions regarding the mechanism of secretion remain unanswered. Despite the extensive research on the driving force and substrate translocation, many details of effector secretion are not known. A general assumption in the field is that effector proteins are unfolded and secreted through a central channel in the structural part of the T3SS, the needle complex. However, a formal experimental basis for this assumption has not been provided. No experiments have addressed the localization of effectors during secretion using a direct approach or visualized the effector inside the channel. This work aimed to gain experimental insights into the secretion process by trapping an effector inside the needle during secretion. Therefore, fusion proteins consisting of endogenous T3SS substrates and a knotted protein domain were generated and studied in the context of the T3SS.

3.1 IpaB-Knot is a functional fusion protein

Obstruction of the channel by a knotted protein would occur if the Knot were inserted into the channel and arrested during transport as it exceeds the channel dimensions. *In silico* studies investigated translocation of knotted proteins in other protein transport systems (Huang & Makarov, 2008; Dzubiella, 2009). Modeling of complex knots and a 6.5 Å channel lead to the conclusion that a knot can be translocated. It was shown that distinct levels of tightening occur over relative chain slippage in the entangled peptide and water molecules leaving the knotted domain under higher forces applied on the peptide. It was also proposed that the trefoil-knot motif has a radius of 6 to 11 Å under a maximal force of 1.5 nN (Dzubiella, 2009). A recent study focused on blocking mitochondrial import by a knotted protein (Szymczak, 2013). Here, the modeling of a knotted protein being tightened by mitochondrial

import lead to a gyration radius of the knot of 7 to 8 Å with the mitochondrial pore having an inner diameter of 16 Å. As the inner diameter of the T3SS needle is 25 Å, this conformation might even allow translocation of a trefoil-knot motif through the NC channel.

This implies that, in theory, the trefoil knot would be able to pass the channel of the T3SS, assuming it has a maximal tightened conformation. However, the force acting on the peptide during secretion largely influences the conformation of the Knot and thereby the diameter of the trefoil-knot motif. It is not clear which force the T3SS applies to substrates during transport, if it is a push or a pull mechanism by ATPase and proton motif force or the needle channel itself, or how much it would squeeze the Knot within the fusion during secretion. The *in silico* modeling approaches used high-force for translocation studies (70-400 pN). In comparison, the estimated translocase force is about 10 to 30 pN for ATP-dependent processes in mitochondrial import or Sec-secretion in bacteria (Alder & Theg, 2003). Low-force studies are difficult to model because of the longer simulation times required (Szymczak, 2013). Suggesting that the force of T3SS is significantly lower than forces used in these simulations, the Knot would stay partially relaxed, most likely with a diameter that exceeds the the channel restrictions.

The trefoil-knot motifs in the chosen proteins are deep knots, which refers to knots that are formed by a central peptide of the protein and thus, are unlikely to slide off the peptide (Nureki *et al.*, 2002; Virnau *et al.*, 2011). This implies that the T3SS is unlikely to unwind the knotted peptide during secretion. Hence, a knot protein fused to a native T3SS substrate might have the capability to obstruct the T3SS.

Based on an initial analysis, the methyltransferase RrmA was chosen as an appropriate knotted protein with a simple trefoil knot in its C-terminus. Expression of *rrmA* did not affect secretion of T3SS effectors (Fig. 2.3). RrmA was fused to IpaB which resulted in the fusion protein IpaB-Knot. It was possible that fusing IpaB to the Knot could destroy the functionality of either domain. Therefore, assays were designed to probe the structure and function of IpaB-Knot using purified protein.

It was shown previously that purified IpaB can recreate many aspects of *Shigella* interactions with macrophages, including induced pyroptosis. This is an ideal assay to probe

whether IpaB-Knot folds correctly, since the protein can be purified from the bacterium and applied to host cells, bypassing the requirement for translocation through the T3SS (Fig. 2.4). IpaB-Knot was applied to murine bone marrow macrophages and induction of pyroptosis was quantified in a colorimetric assay (Fig. 2.5). Compared to previous studies, IpaB-Knot showed a similar capacity to induce cell death (Senerovic *et al.*, 2012), demonstrating that IpaB is still functional in the fusion protein.

Folding status of the trefoil knot within the fusion was investigated using two complementary approaches. First, unfolding properties of IpaB-Knot were compared to native Knot. Fluorescence spectroscopy assesses the molecular environment of tryptophans which changes during unfolding. Since IpaB contains only one tryptophan compared to four tryptophans of Knot (of which three directly localize in the trefoil-knot motif), the major signal results from the intrinsic fluorescence of the Knot domain. The spectrum of IpaB-Knot resembles the native Knot spectrum and both curves overlay when proteins were completely unfolded by adding chaotropic salt (Fig. 2.6). The similarity of fluorescence in the native state indicates that the Knot folds properly in the fusion protein.

In a different approach, Knot folding was analyzed by limited proteolysis. Digestion of native IpaB-Knot and Knot alone resulted in a fragment which was further cleaved, indicating that both proteins contained stably folded core domains that were inaccessible to Proteinase K (Fig. 2.7 and Fig. 2.8). This domain includes the trefoil-knot motif (Fig. 2.10). Since IpaB-Knot and Knot provided comparable results in terms of unfolding and limited proteolysis, the Knot folds into its native state when fused to IpaB.

With the characterization of the fusion protein, functionality of both domains within IpaB-Knot was confirmed. Therefore, IpaB-Knot was the tool to investigate if a fusion protein with a trefoil-knot domain could block the T3SS.

3.2 T3 secretion is attenuated by IpaB-Knot

In *S. flexneri*, the T3SS is regulated IpaB and IpaD. Wildtype bacteria do not secrete effector proteins *in vitro* but the T3SS can be artificially activated with Congo Red. It was first addressed, if IpaB-Knot can block Congo Red-induced effector secretion in the Δ*ipaB* strain.

The Δ*ipaB* mutant was complemented with either p*ipaB* (plasmid-encoded wildtype IpaB) or p*ipaBknot* and secretion was compared under Congo Red-induced conditions. In contrast to the Δ*ipaB* + p*ipaB* strain, the strain carrying p*ipaBknot* did not respond to Congo Red induction (Fig. 2.11). Consistent with the idea that IpaB-Knot cannot pass through the T3SS, IpaB-Knot was only found in bacterial lysates and was not secreted into culture supernatants.

Next, expression of p*ipaBknot* was tested in the Δ*ipaD* mutant, which hypersecretes effectors including IpaB without induction by Congo Red. This bypassed the requirement for Congo Red-induction and the effect of IpaB-Knot on T3 secretion was investigated in a strain that constantly secretes effectors by default. p*ipaBknot* or p*ipaB* were expressed in addition to endogenous *ipaB* (Fig. 2.12). While the expression of p*ipaB* did not influence secretion of other effectors, expression of p*ipaBknot* completely eradicated effector proteins from the supernatants and was not secreted itself. The secretion deficiency was at least partially because of reduced expression of other effectors. Even more so, IpaB-Knot reduced levels of endogenous IpaB. This suggests that reduced effector expression is due to a feedback mechanism of IpaB as its cognate chaperone IpgC plays a crucial role in the regulatory cascade of late effector expression (Schroeder & Hilbi, 2008). As long as IpgC is bound to IpaB and IpaC in the bacterial cytosol, expression of late effectors, including the IpaH family, is downregulated. Upon secretion of IpaB and IpaC, free IpgC activates the expression of late effectors *via* MxiE. As IpaB-Knot is not secreted and remains bound to IpgC in the cytoplasm, the fusion may completely deplete the IpgC pool and endogenous IpaB and IpaC are degraded, which has been observed in the absence of IpgC (Menard *et al.*, 1994b). Whether this phenotype depends on IpgC only and might be circumvented by co-expression of *ipgC* remains to be investigated.

In order to express *ipaBknot* under physiological conditions, the fusion allele was expressed under the native promoter of *ipaB* as it was intended to perturb the tightly regulated effector cascade as little as possible. The fusion allele was inserted into the virulence plasmid in the Δ*ipaD* strain so expression did not require artificial induction but relied on the endogenous promoter. Secretion of Δ*ipaD*::*ipaBknot* was compared to hypersecretion of Δ*ipaD*. Genomic expression of *ipaBknot* dramatically reduced effector secretion (Fig. 2.16). Using the approach of genomic expression, synthesis of other early effectors like IpaC was

not influenced. IpaC was expressed in similar amounts in all strains tested but was only secreted by the Δ*ipaD* strain. For Δ*ipaD*::*ipaBknot*, supernatants contained less IpaC. Again, the regulatory effect of IpgC constantly bound to IpaB-Knot on late effector genes adds to the phenotype of reduced effector secretion. Levels of the late effector IpaH were low in the supernatant as well as in the lysate. The T3SS-independent extracellular protein SepA was still secreted in the background of the Δ*ipaD*::*ipaBknot* strain, demonstrating that the effect of IpaB-Knot is limited to the T3SS pathway.

Furthermore, invasiveness of the wildtype carrying *ipaBknot* (M90T::*ipaBknot*) was quantified in comparison to wildtype M90T. Also levels of IpaB-Knot and the basal body protein MxiG were compared to IpaB and MxiG levels in M90T (Fig. 2.14). *ipaBknot* rendered M90T non-invasive to the extent of an *ipaB*-deficient strain. However, IpaB-Knot and IpaB levels were equal in both strains as was the level of the basal body protein MxiG. This suggests similar amounts of T3SS NCs and excluded that M90T::*ipaBknot* is attenuated in invasiveness due to a lower expression of T3SS. Analysis of the secretion phenotype showed a deregulated secretion compared to the wildtype, although M90T::*ipaBknot* partially responded to Congo Red (Fig. 2.15), which implies that M90T::*ipaBknot* might not be able to form a proper tip complex that regulates effector secretion.

In summary, IpaB-Knot is not secreted by *S. flexneri* but attenuates effector secretion and also expression of late effectors. The reduction of effectors from the supernatant is most likely a mixed phenotype resulting from impairment of the secretion pathway and limited expression. This impairment is caused by IpaB fused to the Knot, as the expression of *knot* independently from *ipaB* had no effect (Fig. 2.3 and Fig. 2.17).

Earlier studies concluded that fusion proteins impeding the T3SS arrest secretion by interacting with the NC and obstruction of the channel (Feldman *et al.*, 2002; Ghosh, 2004). Either these fusion proteins directly block the channel (Feldman *et al.*, 2002) or attenuated secretion results from constant occupation of the ATPase which co-purified in pulldown assays and is an essential component for T3SS (Sorg *et al.*, 2006). Since the understanding of the secretion mechanism is limited, it is possible that not the channel but essential components like the ATPase were blocked by IpaB-Knot which would also inhibit secretion of effectors. The next step was therefore to elucidate the mechanism by which IpaB-Knot interferes with secretion.

3.3 IpaB-Knot stably interacts with the NC

Analysis of effects on T3SS was continued by investigating whether or not decreased secretion results from a direct interaction between the T3SS channel and IpaB-Knot. Separation of proteins by zonal gradient centrifugation has been used to isolate intact T3SS from *S. typhimurium* SPI-1 from soluble protein impurities (Schraidt & Marlovits, 2011). This strategy was adopted to analyze interactions between IpaB-Knot and the NC. In isolates from Δ*ipaD*, IpaB does not interact with the NC as IpaD provides the binding site for IpaB. Consequently, soluble IpaB remained in the low density-fraction whereas high molecular weight complexes like the NC migrated to high density-fractions (Fig. 2.18). In contrast to Δ*ipaD*, isolated NCs from Δ*ipaD*::*ipaBknot* showed a clear co-localization with IpaB-Knot in high-density fractions. This was not observed for purified IpaB-Knot added to isolated NCs from *ipaD*, where IpaB-Knot remained in low- to medium-density fractions with the latter possibly containing aggregated IpaB-Knot (Fig. 2.18*C* and *D*, CsCl fraction 3).

Two conclusions regarding the interaction between IpaB-Knot and the NC can be drawn from this experiment. First, IpaB-Knot interacts with components of the NC as IpaB-Knot and MxiG co-migrate to high-density fractions. Second, this interaction is mediated by a mechanism depending on the bacterium as it cannot be restored by adding purified IpaB-Knot to isolated NCs from Δ*ipaD*.

It is possible that the mechanism that mediates IpaB-Knot interaction with the NC is attempted secretion by the T3SS. If IpaB-Knot is secreted with the N-terminus first and secretion occurs through the NC channel, this terminus would protrude from the needle and thus could be antibody-labeled. The T3SS needle dimensions require effectors to be unfolded prior to secretion as no globular domains could pass through the 2.5 nm channel. After being released from the channel, the effector domain might fold back into its native conformation, as it was shown that IpaB spontaneously forms oligomers when released from the chaperone IpgC (Senerovic *et al.*, 2012). The total length of 580 amino acids and a tendency to adopt a helical conformation (which complies with the inner diameter of the NC) restrict IpaB to 87 nm from N- to C-terminus. The prediction of a helical structure is based on a partial x-ray structure analysis (Adam *et al.*, 2012), which showed IpaB forming helical bundles, and is in agreement with *in silico* analyses using a protein structure prediction tool (Fig. 3.1). Together

with the Knot domain being to some extent engaged into the channel, it is most likely that the IpaB mAB epitope, which localizes between residues 118 and 179 (Barzu *et al.*, 1993), protrudes from the needle and is accessible to antibody-labeling.

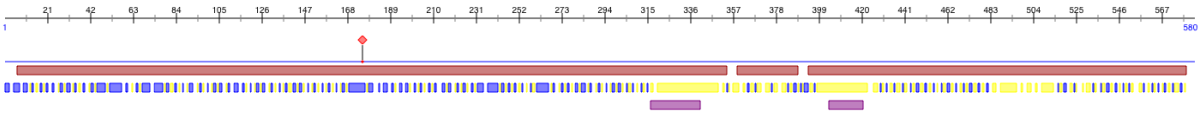

Figure 3.1: ProteinPredict analysis of IpaB amino acid sequence. Yellow/blue fragments correspond to exposed and buried stretches, respectively. Red bars indicate helical stretches, pink bars refer to transmembrane domains.

Considering that the first 150 amino acids (which contain the IpaB epitope) need to be outside the NC, the length of the remaining unfolded IpaB is limited to 64,5 nm. This stretch is extended by partial insertion of the Knot fused to IpaB C-terminus. The length of the NC in *S. flexneri* usually ranges from 70 to 80 nm in total (Tamano *et al.*, 2000; Magdalena *et al.*, 2002; Tamano *et al.*, 2002). This implies that IpaB N-terminus and the C-terminal Strep-tag should be accessible to antibody-labeling.

In agreement with this initial theoretical approach was the observation that labeling of IpaB occurred either close to the tip or the base of the NC (Fig. 2.19). As there were no gold particles seen in the negative control, isolated NCs from Δ*ipaD* (data not shown), specificity of gold particle labeling on NCs was determined by a nearest-neighbor analysis (Fig. 2.20). Comparing random distributions of gold particles to the distribution observed in labeling experiments, distances between gold and the nearest NC were quantified. The outer membrane ring was chosen as an NC coordinate as it lies in the middle of the NC. For distances between the outer membrane ring and gold particles, values around 30 to 50 nm were observed. This corresponds to half the NC length including variation by antibodies and gold particle radius (up to 16 nm (Amiry-Moghaddam & Ottersen, 2013)).

Labeling of IpaB occurred at both the distal and the basal side of the NC. The IpaB N-terminus being detected at needle tips supports the linear model of secretion with the N-terminus mediating secretion and being released from the NC first. For localization of IpaB N-terminus at the basal body side, one might speculate that IpaB-Knot is kept at the C-ring or the sorting platform, potentially by the ATPase. As the N-terminus is accessible to gold-labeling, it is not clear which part of the effector interacts with the NC in this state. This

might indicate an additional secretion signal downstream of the primary N-terminal signal sequence which interacts with the channel in a looped conformation while the N-terminus remains at the base until a stable interaction between this loop and NC is established. A more complex motif has been suggested for a recognition signal in earlier studies, where the secretion signal fused to a reporter was not sufficient for secretion but an additional stretch including the chaperone binding domain was required (Wilharm *et al.*, 2004a; Riordan *et al.*, 2008). Further experiments are necessary to understand the way effectors are engaged into the channel and which part is ultimately recognized by the T3SS prior to secretion.

Only 20 to 25 % of the overall NC population isolated from the bacterial membrane were labeled with gold. It is not clear whether this was due to technical limitations or if only a subpopulation of the isolated NCs occupy IpaB-Knot. Therefore, NCs interacting with IpaB-Knot were selectively enriched by additional affinity purification *via* the C-terminal Strep-tag of the fusion protein. This lead to isolation of NCs that lacked parts of the basal body and merely consisted of the central channel (Fig. 2.21). It is noteworthy that the fusion protein was still localized at these NCs. This suggests that the intrinsic interaction between IpaB-Knot and the channel is stronger than the interactions between basal body components of the NC. Still, frequent gold-labeling occurred, indicating that the low number of gold-positive NCs was rather due to technical reasons as these NCs were isolated based on their interaction with IpaB-Knot. Opposing the altering localization of the IpaB N-terminus at needle tips or bases, localization of IpaB-Knot C-terminal Strep-tag occurred only at the basal side of NCs or isolated channels (Fig. 2.22). This suggests that, in comparison to the N-terminus of the fusion, the C-terminus is less flexible during the process of secretion, perhaps because the Knot domain blocks the T3SS and thereby keeps the C-terminus of the fusion localized at the entry port of the channel.

To elucidate the orientation of IpaB-Knot interacting with the NC, simultaneous detection of both termini of the fusion was performed. As one cannot distinguish both primary antibodies generated in mouse in this approach, the IpaB antibody was transformed into a human IgG. The recombinant humanized monoclonal IpaB antibody was not recognized by an anti-mouse secondary antibody (Fig 2.23). Consequently, humanized anti-IpaB and mouse anti-Strep mABs can be labeled with species-specific secondary antibodies coupled to dif-

ferent gold particles. Dual localization of N- and C-terminus using both primary antibodies occurred reproducibly but was a rare event (Fig. 2.24). Immuno-labeling on single proteins using either IpaB or Strep mAB was not very efficient and therefore, labeling with two antibodies binding to each epitope on the same protein becomes technically unlikely. Further refinement of the labeling strategies is necessary in order to improve rates of labeling, for example with pre-conjugated primary/secondary antibody complexes or gold-conjugated primary antibodies, might help improving the rate of simultaneous N/C-terminus detection. Still, these experiments show the orientation of IpaB-Knot to be N-terminus at the NC tip and the C-terminus at the corresponding NC basal body.

3.4 IpaB-Knot is secreted through the NC channel

The observed gold localization at isolated NCs suggests secretion depending on the T3SS, but it does not necessarily imply secretion through the channel according to the model that the NC is a conduit for protein transport. An alternative model has been discussed in earlier studies where the needle guides the effectors towards the host cell in the plant pathogen *Pseudomonas syringae* pv. *tomato* along the T3SS Hrp pilus protruding from the bacterium (Jin & He, 2001) (Fig. 3.2).

These two models derived from the observation that the effector AvrPto was detected along the entire pilus as being stored on the pilus surface. The guiding-filament versus conduit function of the extracellular appendage was further analyzed by gold-labeling of effectors that accumulated at the tip of the pilus when their expression was uncoupled and delayed from pilus formation (Jin *et al.*, 2001; Li *et al.*, 2002). These analyses favor the conduit model but do not exclude the guiding-filament model which would also be in agreement with the recent studies where effectors were stored on the outer membrane of *Yersinia* (Ghosh, 2004; Akopyan *et al.*, 2011; Edgren *et al.*, 2012). In case the fusion localizes inside the NC channel, its access to modifications should be limited by the surrounding channel. In order to test this hypothesis, a TEV protease-recognition site was inserted between IpaB and Knot resulting in IpaB-TEV-Knot. If the site localizes inside the NC past insertion of the effector, the channel would protect it, whereas, if the recognition site is accessible, the protein should be digested. IpaB-TEV-Knot co-purified with NCs was not cleaved by an excess of TEV protease, whereas purified IpaB-TEV-Knot was digested already at low concentrations (Fig. 2.25). The

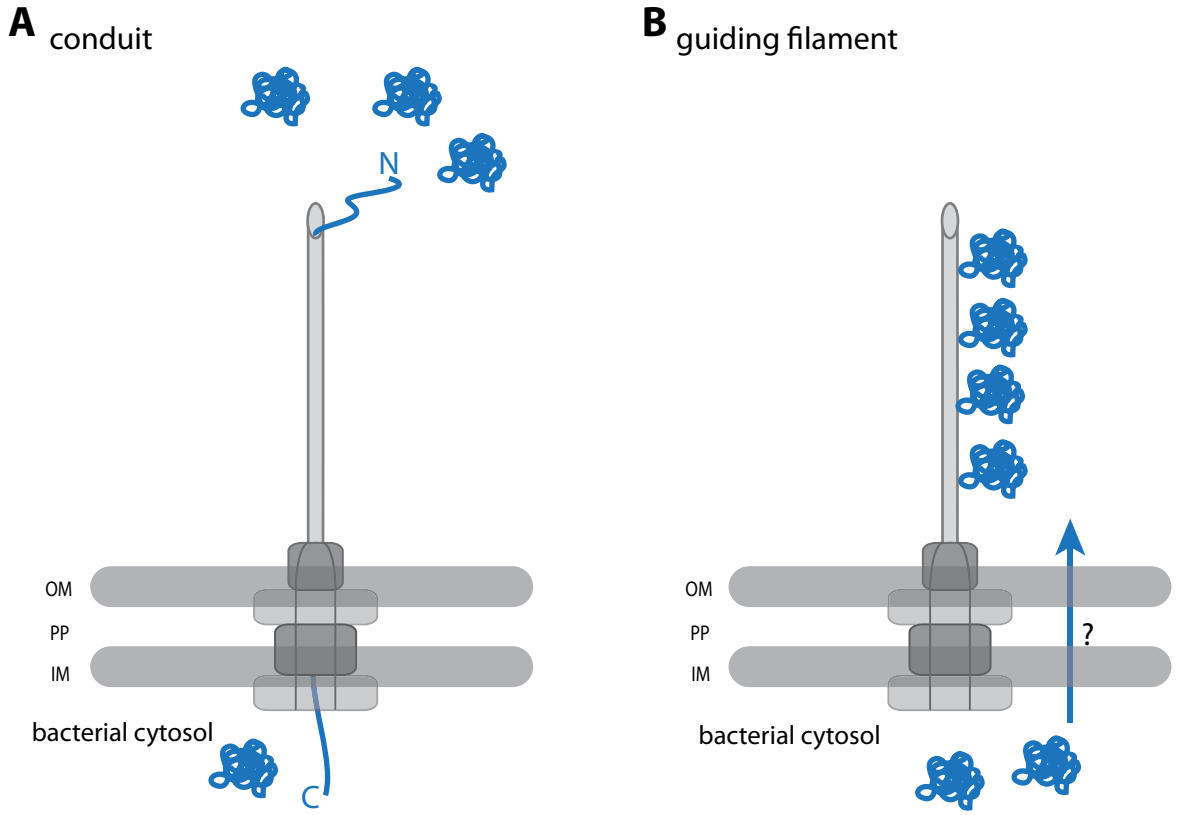

Figure 3.2: Models proposed for the T3SS mechanism. (*A*) The conduit model where effectors (blue) are unfolded and secreted through the NC channel. (*B*) The alternative guiding-filament model where effectors are translocated across the bacterial membrane by an unknown mechanism and guided along the needle of the NC. OM = outer membrane, PP = periplasm, IM = inner membrane.

limited proteolysis is most likely because of protection or sterical hindrance mediated by the channel interacting with and protecting the protein. However, it cannot be fully excluded that the fusion protein was arrested in a conformation that does not allow TEV cleavage but is still secreted outside the NC channel.

To further analyze exposure of IpaB-TEV-Knot, NCs occupied with IpaB-TEV-Knot were treated with $MS(PEG)_{24}$, a crosslinking reagent with an engineered PEG moiety. The PEGylation reagent adds PEG of discrete molecular weight and length (1.1 kDa/86.2 Å) to primary amines and diffusion into the needle channel is unlikely for sterical reasons. A difference in PEGylation of NCs compared to purified IpaB-TEV-Knot of approximately 15 to 30 PEGylation events was observed when treated with 0.5 mM $MS(PEG)_{24}$ (Fig. 2.26). At lower concentrations, no PEGylation was detectable whereas higher concentrations lead to maximal PEGylation of both samples, probably caused by the increased amount of solvent (DMSO) affecting the channel integrity (data not shown). The limited accessibility of the evenly distributed primary amines in IpaB-TEV-Knot to chemical modifications demonstrates protection of the

fusion protein conferred by the channel. At this point, it remains elusive which residues of the protein are exposed to PEGylation, however, this approach might help understanding which parts of the protein are protected by the channel if combined with for example mass spectrometric analyses in the future.

Together with data from immuno-labeling of IpaB-Knot at isolated NCs, the PEGylation experiments bespeak shielding of the fusion protein by the channel which physically encloses the substrate. Both termini of IpaB-Knot were detected at each side of isolated NCs and furthermore, IpaB-TEV-Knot is protected from site-specific proteolysis and less exposed to chemical modifications compared to purified fusion protein.

3.5 Towards structural data of active T3SS: Initial single particle analysis

Structural analysis using cryo-electron microscopy and single particle analysis revealed the conformation of the NC from *S. typhimurium* SPI-1 (Schraidt & Marlovits, 2011) and *S. flexneri* (Hodgkinson *et al.*, 2009). In addition to analyses of isolated complexes, a recent study investigated the conformation of NCs from *Yersinia* and *Shigella* in the bacterial envelope *in situ*. Interestingly, NCs inside the membrane were up to 40 % shorter compared to structural analysis of isolated particles (Kudryashev *et al.*, 2013). Such *in situ*-observations reveal important details on structural interactions inside the macromolecular complex.

However, for the isolated *S. typhimurium* SPI-1 and *S. flexneri* NC, both complexes were empty and therefore, these studies only addressed conformations of inactive channels. By investigating constantly occupied NCs, structural analysis of these particles has the potential to elucidate details of interactions between substrate and NC. This would include conformational changes of the channel components during secretion. Therefore, isolated particles from the Δ*ipaD*::*ipaBknot* strain were subjected to an initial single-particle analysis following cryo-EM imaging. Manually selected particles were grouped based on the needle length after k-means analysis. This resulted in 12 different classes of particles, of which some indicated additional densities at the needle tip (Fig. 2.27). However, as the particle number was too low to confirm this, it is not evident that the potential density is a protruding protein. More particle input is required for further analysis and validation of this initial study.

The standards for cryo-EM samples are high and criteria include a homogeneous distribution of particles, low background and ice of suitable quality and diameter. The samples were of poor quality for cryo-EM analysis as a granular, heterogeneous background was frequently observed. One possible source was the detergent included, as it forms micelles at certain concentrations which could affect the background. The purification of NCs without detergent leads to particle aggregation, therefore a strong detergent like Triton X-100 has proven to be indispensable for this process. Different detergents for purification were tested, which have a higher critical micelle concentration (CMC) but purification of NCs below the CMC was not successful yet. This process needs to be improved in order to obtain valid data based on sufficient single particles for either 2D or 3D structural analysis.

So far, these results show that the principle of single particle analysis works for isolated occupied NCs, as the iterative alignment based on cross-correlation values was applicable to isolated particles. With samples that are of better quality, this might lead to structural data on NCs arrested in the process of secretion in the future.

3.6 Conclusion

This work provides an experimental basis for the widely assumed mechanism of T3SS secretion. It was demonstrated that IpaB-Knot is partially secreted through the NC, albeit not released from the channel due to secretion arrest by the Knot domain, and that the channel surrounds and shields the fusion protein. Transport occurs with the N-terminus first as our constructs do not allow secretion by the C-terminus because of the C-terminal Knot fusion. The N-terminus could be detected at the distal end of the NC needle portion as it protrudes from the channel. Both termini of IpaB-Knot were detected on each side of isolated NCs. This is, as far as one can tell, the first visualization of an effector localized at isolated NCs and it implies that effector proteins are secreted through the T3SS channel. Regarding the localization of the N-terminus on either tip or basal side of the NC, the following model for effector secretion attempts to describe these observations. The effector is bound to the chaperone and presented to the T3SS basal side, where an interaction partner (for example the sorting platform including the ATPase) recognizes the effector/chaperone complex (Fig. 3.3).

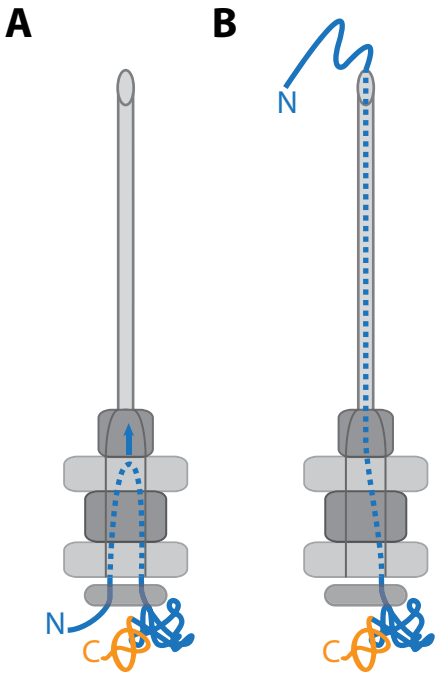

Figure 3.3: Model of effector insertion and secretion. (*A*) The effector fusion (blue and orange) interacts with a cytoplasmic component where a part of the effector is inserted into the NC but the Knot inhibits further secretion. (*B*) Secretion arrested at a later stage of insertion with the effector protruding from the channel.

An N-terminal stretch is inserted into the channel, however, the signal sequence remains outside and eventually, the Knot blocks further secretion. The N-terminus is secreted across the channel with the Knot remaining on the cytosolic side. This model is in line with the observation that the signal was in some cases not sufficient to mediate secretion of fusion constructs that in turn failed to obstruct the system (Lee & Schneewind, 2002; Riordan *et al.*, 2008).

Combined with structural analysis, this approach could lead to novel insights into the conformation of a T3SS channel during the process of secretion. This strategy is transferable onto other secretion or translocation systems which require unfolding of the substrate during secretion. As channels could be isolated based on the interacting substrate, other channels might be isolated and investigated using a similar approach.

4 Materials & Methods

4.1 Kits, Chemicals & Machinery

The commercially available kits, fine chemicals, reagents and machines used in the experiments during this study are listed below. Kits (table 4.1) were used according to manufacturers instructions. Fine chemicals were purchased in pro analysis (p.a.) quality, if available. Chemicals include ready-mixtures for bacterial and cell-culture media.

Table 4.1: Commercially available kits

Designation	Manufacturer
Zyppy DNA Plasmid prep	Zymo Research
Gel DNA Recovery	Zymo Research
DNA Clean & Concentrator	Zymo Research
RNeasy Mini Kit	QIAGEN
SuperSignal West Pico ECL enhancer	Thermo Scientific

Table 4.2: Machines used during the study

Device	Designation	Manufacturer
Centrifuge	Avanti J-20 XP/J-25	Beckman Coulter
Centrifuge	Heraeus Multifuge 3SR	Thermo Scientific
Centrifuge	Centrifuge 5415 /R	Eppendorf
Camera (TEM)	Soft Imaging System	Olympus
CO_2 incubator	ThermoForma Direct Heat CO2	Thermo Scientific

Device	Designation	Manufacturer
Coating System	MCS010/MED020	Bal-Tec
Electroporation System	Gene Pulser II	Bio-Rad Laboratories GmbH
Coffee Machine	SPIDEM Trevi Chiara	Saeco GmbH
FPLC	ÄKTA FPLC + P-920, UPC-900, Frac-920	GE Healthcare
Gel Imaging	AlphaImager™	fomerly Alpha Innotec
Fluorescence Spectrometer	LS-55	PerkinElmer
HPLC	ÄKTA Explorer + P-900, UV-900, PH/C-900, Frac-950	GE Healthcare
Incubator	Innova 44/R	New Brunswick Scientific/Eppendorf
PCR Cycler	C1000™	Bio-Rad Laboratories GmbH
Spectrophotometer	MDS SpectraMAX 190	Molecular Devices GmbH
Spectrophotometer	NanoDrop 2000	PEQLAB Biotechnologie GmbH
TEM	LEO 906E	Carl Zeiss
Thermomixer	Thermomixer compact	Eppendorf
Ultracentrifuge	Optima L-90K	Beckman Coulter
Ultracentrifuge	Optima MAX	Beckman Coulter
UV Table	UV Transilluminator 312nm	INTAS Science Imaging Instruments GmbH
ECL Detection	ImageQuant LAS 4000	GE Healthcare

Table 4.3: Chemicals used during the study

Designation	Manufacturer
Agarose for DNA electrophoresis	SERVA
Ampicillin	Sigma Aldrich
Anhydrotetracyclin (AHT)	Thermo Fisher
Chloramphenicol	Sigma Aldrich
Bromophenol Blue	Sigma Aldrich
Congo Red	Sigma Aldrich
Coomassie Brilliant Blue G-250	SERVA
Desthiobiotin	IBA
Dithiothreitol (DTT)	Enzo Life Sciences
Ethidium bromide (EtBr)	Sigma Aldrich

Designation	Manufacturer
Imidazole ultra-pure	Roth
Isopropyl-β-D-thiogalactopyranosid (IPTG)	Fermentas
Kanamycin	Sigma Aldrich
Lauryldimethylamine N-oxide (LDAO)	Sigma Aldrich
N-Lauroylsarcosine (Sarkosyl)	Sigma Aldrich
Lysogeny broth (LB) medium (Luria/Miller)	Roth
LB agar	Roth
n-Octyl-β-D-Glucopyranoside (OG), Anagrade	Affymetrix
NanoVan	Nanoprobes
Triton X-100	Sigma Aldrich
Tween20	Applichem
Tryptic soy broth (TSB) medium	Sigma Aldrich
Xylene Cyanol FF	SERVA

4.2 Buffer solutions

Buffers specific to experiments are included in the respective section in this chapter. Common buffer solutions and growth media are listed below. Standard buffer recipes are taken from Sambrook & Russel (2001).

Table 4.4: List of standard buffers

Designation	Ingredients
PBS	137 mM NaCl 2.7 mM KCl 4.3 mM Na_2HPO_4 1.47 mM KH_2PO_4
TAE	40 mM Tris acetate, pH 8.0 1 mM EDTA
DNA loading dye (6x, 10 ml)	25 mg Bromophenol Blue 25 mg Xylene Cyanol FF 3.3 ml Glycerol 6.7 ml ddH_2O
Towbin buffer	25 mM Tris base 192 mM Glycine

Designation	Ingredients
	20 % (v/v) Methanol
PBS-T	PBS 0.05 % (v/v) Tween20
Laemmli sample buffer	80 mM TrisHCl, pH 6.8 2 % (v/v) SDS 10 % (v/v) Glycerol 10 mM DTT 0.25 % (w/v) Bromophenol Blue
Coomassie stain	10 % (v/v) Isopropanol 13 % (v/v) Acetic acid 0.1 % (w/v) Coomassie Brilliant Blue G 250
Destain solution	10 % (v/v) Isopropanol 13 % Acetic acid
Tris-glycine SDS running buffer	25 mM Tris base 192 mM Glycine 3.5 mM SDS

4.3 Bacteria & DNA

All bacteria that were either used or generated during this study are listed below in table 4.5, DNA plasmids in table 4.6. Oligonucleotides used for qualitative DNA analysis, genetic modifications or generation of plasmid constructs were synthesized by MWG Eurofins and are listed in table 4.7. *E. coli* BL21 DE3 was used for protein purification following overexpression of the respective gene, *E. coli* GC10 was used for plasmid preparations and cloning of constructs listed in table 4.6.

Constructs with pASK-IBA3+ carry a 3' *strep*-tag, constructs with pASK-IBA33+ a 3' *6his*-tag and confer resistance to ampicillin. These constructs have a *tet*-promoter and are inducible with anhydrotetracyclin (AHT). pET28a has a kanamycin resistance cassette and attaches a 3' *6his*-tag to the inserted gene. Expression under the pET28a *lac*-promoter is induced by IPTG. The sequence of *knot1* is derived from "conserved protein MT0001" (here termed Akp1) from Methanobacterium thermoautotrophicum (PDB ID: 1K3R), the sequence of *knot2* or *knot*, respectively, is derived from RrmA from *Thermus thermophilus* (PDB ID: 1IPA). Plasmids and oligonucleotides that are designated "*rrmA*" thereby refer to *knot* and vice versa. For amplification of *knot1* and *knot2*, the protein sequences of Akp1 and RrmA

were reverse-translated *in silico* and codon-optimized for *E. coli* K12 by MWG Eurofins. The genes were synthesized with a 5' PstI site and a 3' NcoI site and TOPO-cloned into pCR2.1 by MWG Eurofins.

Table 4.5: Bacterial strains used in this study.

Bacterial strain	Genotype	Source
Shigella flexneri M90T	wildtype strain, serovar 5a isolate	Sansonetti *et al.* (1982)
S. flexneri Δ*ipaB*	M90T *ipaB*$^-$	Lab collection
S. flexneri Δ*ipaD*	M90T *ipaD*$^-$	Lab collection
S. flexneri Δ*mxiH*Δ*ipaD*	M90T *mxiH*$^-$,*ipaD*$^-$	Lab collection
S. flexneri M90T::*ipaBknot*	M90T with *ipaBknot* fusion allele	This study
S. flexneri Δ*ipaD*::*ipaBknot*	M90T *ipaD*$^-$, with *ipaBknot* fusion allele	This study
S. flexneri Δ*ipaD*::*ipaBTEVknot*	with *ipaBTEVknot* fusion allele	This study
Escherichia coli BL21 DE3	&F- *omp*T *hsd*SB(rB-, mB-) *gal dcm*	Invitrogen
E. coli GC10	F- *mcr*A Δ(*mrr-hsd*RMS-*mcr*BC) ϕ80d*lacZ*ΔM15. Δ*lac*X74 *end*A1 *dam* Δ(*ara*, *leu*)7697 *ara*D139 *gal*U *gal*K *nup*G *rps*L λ^- T1R	Sigma

The *Shigella* mutant strains Δ*ipaB*, Δ*ipaD* and Δ*mxiH*Δ*ipaD* have been kindly provided by Anna Brotcke, MPIIB, Department for Cellular Microbiology.

Table 4.6: Plasmid DNA used in this study.

Plasmid backbone	Insert
pCR2.1	*akp1* (henceforth: *knot1*)
pCR2.1	*rrmA* (henceforth: *knot* or *knot2*)
pASK-IBA33+	*knot1*
pASK-IBA33+	*knot2*
pASK-IBA3+	*ipaBknot*
pASK-IBA3+	*ipaB*
pASK-IBA3+	*ipaBTEVknot*
pET28a	*ipgC*
pKD3	chloramphenicol cassette for gene targeting

Plasmid backbone	Insert
pKM208	FLP recombinase for gene targeting
gamma1	IpaB mAB gamma chain
kappa1	IpaB mAB kappa chain

The plasmid pET28a-*ipgC* has been published before in Lunelli *et al.* (2009), as well as pKD3 and pKM208 in Datsenko & Wanner (2000). Plasmids backbones for recombinant IgG expression have been provided by the Wardemann lab, MPIIB, and are described in Tiller *et al.* (2008) and Tiller *et al.* (2009).

Table 4.7: Oligonucleotides used in this study.

Name	Sequence (5' to 3')	Description
BsaI-akp1-Fw	AGC AGA GGT CTC TA ATG AAT CGC GTT GAT CTT TCC CTG TTC	cloning *knot1* w *Bsa*I in pASK-IBA
BsaI-akp1-Rv	AGA CAC GGT CTC TGC GCT TTC GTC TTT CTC GTC G	cloning *knot1* w *Bsa*I in pASK-IBA
BsaI-rrmA-Fw	AGC AGA GGT CTC TA ATG CGC ATT ACC TCA ACG GCG AAT C	cloning *ipaB* w *Bsa*I in pASK-IBA
BsaI-ipaBrrmAST-Fw	AGC AGA GGT CTC TA ATG CAT AAT GTA AGC ACC ACA ACC T	cloning *ipaB* w *Bsa*I in pASK-IBA
BsaI-ipaBrrmAST-Rv	AGA CAC GGT CTC TGC GCT AAG CGT CGA ATG GGT	cloning *knot2* (*knot*) w *Bsa*I in pASK-IBA
ipaBPstIrrmA-Fw	TAC TGC TCT GCA GAT GCG CAT TAC CTC AA	forward fusion primer for *ipaB* & *knot*
ipaBPstIrrmA-Rv	GCG CAT CTG CAG AGC AGT AGT TTG TTG CA	reverse fusion primer for *ipaB* & *knot*
BsaI-rrmA-Fw	AGC AGA GGT CTC TA ATG CGC ATT ACC TCA ACG GCG AAT C	cloning *knot* w *Bsa*I in pASK-IBA
iBrrmA-Cm usF	AGC CTC AAT GTC CAA CTC TCA GGC TAA TAG AAC TGA TGT TGC AAA AGC AAT TTT GCA ACA AAC TAC TGC TAT GCG CAT TAC CTC AAC GGC G	upstream flanking primer for *knot* fusion to *ipaB* in pWR100
iBrrmA-Cm usR	GGA CCA TGG CTA ATT CCC ATT TAT TAT TTT TCG AAC TGC G	forward fusion of *knot* and *cam*
iBrrmA-Cm dsF	CGC AGT TCG AAA AAT AAT AAA TGG GAA TTA GCC ATG GTC C	reverse fusion of *knot* and *cam*
iBrrmA-Cm dsR	GGA TAT ATC TGT ATA TAA AGT CTG GGT TGG TTT TGT GTT TTG AAT TTC CAT AAC ATT CTC CTT ATT TGT AGT GTA GGC TGG AGC TGC TTC	downstream flanking primer for *knot* insertion in pWR100

Name	Sequence (5’ to 3’)	Description
iBTrrmA-Cm usF	AGG CTA ATA GAA CTG ATG TTG CAA AAG CAA TTT TGC AAC AAA CTA CTG CTG AAA ACC TTT ATT TTC AGT CTA TGC GCA TTA CCT CAA CGG CG	upstream flanking primer for *TEVknot* insertion in pWR100
ipaB TAA rrmA F	TCC AAC TCT CAG GCT AAT AGA ACT GAT GTT GCA AAA GCA ATT TTG CAA CAA ACT ACT GCT TAA TAC AAA TAA GGA GAA TGT TAT GCG CAT TAC CTC AAC GGC	upstream flanking primer for *knot* insertion with *ipaC*-RBS in pWR100
iBrAC short F	AGC CTC AAT GTC CAA CTC TCA GG	short forward primer for *knot-cam* and *TEVknot-cam* PCR
iBrAC short R	GGA TAT ATC TGT ATA TAA AGT CTG GGT TGG	short reverse primer for *knot-cam* and *TEVknot-cam* PCR
insert seq Fw	ATT CGG CCA ATT GCA GGA AG	insert check for *ipaB* fusions
insert seq Rv	AAT GTG GTT GTT AAT ACG GG	insert check for *ipaB* fusions
msVHE	GGG AAT TCG AGG TGC AGC TGC AGG AGT CTG G	universal murine gamma forward
mCh-g1-outer	GGA AGG TGT GCA CAC CGC TGG AC	murine Ig constant region (gamma chain), semi-nested outer primer, reverse
mCh-g1-inner	GCT CAG GGA AAT AGC CCT TGA C	murine Ig constant region (gamma chain), semi-nested inner primer, reverse
P-mVH02	CTG CAA CCG GTG TAC ATT CCC AGG TGC AGC TGC AGC AGT CTG G	specific gamma segment (with AgeI site), forward
mJh3-SalI-rev	TGC GAA GTC GAC GCT GCA GAG ACA GTG ACC AGA G	specific gamma segment
mVkappa	GAY ATT GTG MTS ACM CAR WCT MCA	universal murine kappa forward
mCkappa-outer	ACT GAG GCA CCT CCA GAT GTT	murine Ig constant region (kappa chain), semi-nested outer primer, reverse
mCkappa-inner	TGG GAA GAT GGA TAC AGT T	murine Ig constant region (kappa chain), semi-nested inner primer, reverse

Name	Sequence (5’ to 3’)	Description
P-mVk03	CTG CAA CCG GTG TAC ATT CCC AAA TTG TTC TCA CCC AGT CTC CA	specific kappa segment (with AgeI site), forward
mJk5-BsiWI-rev	GCC ACC GTA CGT TTC AGC TCC AGC TTG GTC	specific kappa segment
5’ Ab sense	GCT TCG TTA GAA CGC GGC TAC	sequencing subcloned murine Ig, forward
3’ IgG internal	GTT CGG GGA AGT AGT CCT TGA C	sequencing heavy chain, reverse
3’ Cκ 494	GTG CTG TCC TTG CTG TCC TGC T	sequencing kappa, reverse

4.4 Enzymes

All enzymes for DNA manipulation, including restriction enzymes, ligases and polymerases were obtained from New England Biolabs or Rapidozym and used according to manufacturers instructions. A list of enzymes for DNA and protein manipulation which were used in this study is given in table 4.8.

Table 4.8: Enzymes used in this study.

Name	Manufacturer
DNA-modifying enzymes	
Restriction endonucleases	New England Biolabs
T4 DNA Ligase	New England Biolabs
QuickLigase	New England Biolabs
Phusion Polymerase	New England Biolabs
Taq Polymerase	Rapidozym
Superscript III Reverse Transcriptase	Invitrogen
Protein-modifying enzymes	
Trypsin	Sigma
Proteinase K	Sigma
TEV protease	R&D Diagnostics
Lysozyme 10 mg/ml stock	Novagen

4.5 Cellular Methods

4.5.1 General cell culture

HeLa cells were obtained from the DSMZ (Acc. 57, lot 16). The cells were passaged at a confluescence of 75 % and maintained in Dulbecco medium (DMEM, Life Technologies)

supplemented with 10 % fetal calf serum (FCS), 100µg/ml Penicillin/Streptomycin (Pen/Strep), 1 % Pyruvate and 2 mM L-glutamine (DMEM complete).

Murine bone marrow macrophages were isolated from C57BL/6J mice (The Jackson Lab) and kept in liquid nitrogen. Before experimental work, cells were seeded into 96-well plates (Nunc).

HEK293T cells were grown in 150 mm petri dishes in DMEM complete. Medium was replaced by 25 ml of DMEM supplemented with 1 % Nutridoma-SP (Roche) prior to polyethyleneimine (PEI)-mediated transfection.

4.5.2 Cytotoxicity assay

IpaB cytotoxicity was quantified as described before (Senerovic *et al.*, 2012). Murine bone marrow macrophages (mBMM) from C57BL/6J mice (Jackson Lab) were seeded in 96-well plates (10^5 mBMM/well) in DMEM with 2 % FCS and incubated overnight. Medium was replaced with DMEM with reduced FCS (0.5 %). Different concentrations of recombinant IpaB-Knot or bovine serum albumin (BSA) were added to cells. The cells were then incubated for 2 h at 37 °C. Supernatants were collected and analyzed for the presence of lactate dehydrogenase (LDH) using a colorimetric assay (Cytotox96, Promega) according to the manufacturers instructions.

4.5.3 Gentamicin protection assay

Invasion of *Shigella* strains was quantified as described previously (Sansonetti *et al.*, 1986). 10^5 HeLa cells per well were seeded in 24-well plates and grown overnight in DMEM complete. Cell culture medium was exchanged the next day to 500 µl DMEM without Pen/Strep ($DMEM^{-P/S}$). HeLa cells were infected with 10^7 bacteria (log phase) in 100 µl PBS and centrifuged at 1.340 rcf for 10 min. Infection occurred for 30 min at 37 °C, 0.5 % CO_2. Medium was exchanged to $DMEM^{-P/S}$ + 50 µg/ml gentamicin to avoid continuous reinfection and bacteria were allowed to replicate inside cells for 2 h at 37 °C. HeLa cells were then washed with PBS and lysed in the presence of 1 % (v/v) Triton X-100 in PBS and dilutions were plated on LB agar. Bacterial invasion was quantified by number of colony-forming units (CFU) per ml culture after overnight incubation at 37°C.

4.6 Molecular Methods

4.6.1 Polymerase Chain Reaction (PCR)

DNA was amplified with commercially available enzymes. All reactions for cloning were carried out using Phusion High-Fidelity DNA Polymerase (New England Biolabs) according to manufacturers instructions. For analytical PCRs, Taq polymerase (Rapidozym) was used. Primer were used at a concentration of 0.4 mM per reaction, template DNA was used at 10-100 ng per reaction. For amplification, DNA was initially denatured at 95 °C, followed by another short denaturation (15 sec), annealing (30 sec) and elongation (1 min/kb). The latter three steps were repeated for 25-35 cycles and finished with a final elongation of 7 min.

For site-directed mutagenesis, an initial program consisting of three cycles as mentioned above was run with the reverse and the forward primer in separate reactions. After the initial program, the forward and corresponding reverse reactions were mixed 1:1 and additional polymerase (2 units of Phusion polymerase) was added. The program was then continued for 35 cycles.

4.6.2 Gene Targeting with linear DNA products

According to the method described by Datsenko & Wanner (Datsenko & Wanner, 2000), genes can be efficiently targeted for a deletion or insertion using linear DNA products and recombinase-mediated insertion. The DNA product encodes for flanking regions of the gene of interest, or an insertion product flanked by upstream and downstream sequences of the insertion site. Both products are fused by PCR to an antibiotic cassette. Bacteria were initially transformed with the pKM208 plasmid which encodes for a FLP recombinase. In a subculture, expression of the FLP recombinase was induced with 2 mM IPTG at an OD_{600} of 0.1-0.15/ml. After one hour, bacteria were harvested and washed once with ice-cold ddH_2O and once with 20 % glycerol. The bacteria were transformed with up to 1 µg purified PCR product and recovered in 1 ml TSB medium after electroporation for 1.5-2 h at 37 °C. Growing at 37 °C cures bacteria from the pKM208 plasmid. Subsequently, bacteria were plated on TSB with the respective antibiotics. Positive clones were checked by analytical PCR using a subculture as direct template.

4.6.3 Conventional agarose gel electrophoresis

Linear DNA products between 200 bp and 8 kb were analyzed by constant field electrophoresis using 1-1.2 % agarose gels in TAE buffer. Agarose (SERVA) was molten in TAE buffer using a microwave (600 W, 2-3 min). The mix was supplied with EtBr (3 µl/ml), poured into gelcasts and allowed to cool down for 30-60 min at RT. Preparative and analytic electrophoresis were performed at 100-140 V. Bands were visualized using a UV cabinet (AlphaImager) or a UV table (BalTec) for excision. Eurogentec SmartLadder was used as a standard with 5 µl per lane.

4.6.4 Standard cloning of plasmid constructs

Plasmid constructs were generated by ligation of PCR-generated inserts into plasmid backbones. PCR amplicons were purified from the reaction by preparative agarose gel electrophoresis and Zyppy Gel DNA recovery kit. The amplicon as well as 1 µg of the plasmid backbone were digested with restriction enzymes according to manufacturers recommendations. For standard DNA digestion, 20 units per 50 µl reaction were incubated for 1 h at 37 °C. Amplicons were purified with Zyppy Clean & Concentrator kit, plasmid backbones were separated from the digestion product by preparative agarose gel electrophoresis. Ligation was performed using either T4 DNA Ligase or the QuickLigation kit (both New England Biolabs).

4.6.5 Cloning and expression of murine Ig genes

Cloning and expression of recombinant murine Ig genes was performed in collaboration with the Wardemann lab, MPIIB Berlin, according to the procedure described by Tiller *et al.* (Tiller *et al.*, 2008, 2009). The protocol consists of two steps, reverse transcriptase-PCR (RT-PCR) and subsequent cloning of the respective heavy and light chain gene segments followed by *in vitro* expression in HEK293 cells.

RT-PCR and subcloning

Total RNA from 10^6 H16 hybridoma cells producing IpaB monoclonal antibody (mAB) was prepared using the RNeasy kit (QIAGEN). RNA was reverse-transcribed into cDNA using RT Superscript III under the following conditions: 27 µl bulk RNA were incubated with 1 µl random hexameric primers (300 ng/µl) and 0.5 µl dNTPs (25 nmol each) at 65 °C for 5 min and at 4 °C

for 2 min. 8 µl 5x buffer were added together with 2 µl 100 mM DTT, 1 µl RNAsin (400 U/µl) and 1 µl Superscript III enzyme. The reaction was performed by incubating the mix 5 min at 25 °C followed by 1 h at 50 °C and 15 min at 70 °C. cDNA was stored at 4 °C. Variable Ig regions were amplified in a semi-nested PCR using cDNA as templates. After sequence identification of the respective murine heavy (gamma) and light (kappa) chain variable region gene segments (standard sequencing of PCR products, MWG), these segments were subcloned into plasmids containing leader peptides and human constant regions for kappa and gamma1. This way, full Ig heavy and light chains are expressed containing the murine epitope-specific region joined to a human constant region. Assembly of both chains into a functional IgG1 takes place during co-expression *in vitro* in HEK293T cells.

Transfection of HEK293 cells

8.5 µg of plasmid DNA (each kappa and gamma1 plasmids) per dish were used together with a pAdvantage plasmid in 2 ml 150 mM NaCl solution with 3 µg of PEI per µg of DNA. The mix was stirred for 10 sec, incubated for 10 min at RT and distributed evenly on the cells. Cells were incubated for 3 days, supernatants were harvested and new DMEM + 1 % Nutridoma-SP was added for a second harvest after additional 3 days. Secreted IgG1 was purified as described below.

4.7 Microbiological & Biochemical Methods

4.7.1 Bacterial Lifestyle

S. flexneri strains were grown in TSB medium or on TSB agar plates supplemented with 0.2 % Congo Red. Antibiotics were used at concentrations given in table 4.9. *E. coli* were grown in LB medium or on LB agar plates. Antibiotics were used as listed in table 4.9.

Table 4.9: Antibiotics and their concentrations.

Antibiotic	Final concentration
Ampicillin	50 µg/ml
Carbenicillin	50 µg/ml
Chloramphenicol (*E. coli*)	34 µg/ml
Chloramphenicol (*S. flexneri*)	6 µg /ml
Kanamycin	50 µg/ml

4.7.2 Electrocompetent cells

E. coli GC10 or BL21 were subcultured to mid-log phase and optical density (OD) of the culture was measured by absorption at 600 nm (OD_{600} = 0.4-0.6) in LB medium and harvested by centrifugation at 10.000 rcf for 10 min at 4 °C. All subsequent steps were carried out maintaining the bacteria on ice. The bacteria were washed twice with ice-cold ddH_2O and once with 10 % (v/v) glycerol (sterile filtered). The final pellet was resuspended in 1-2 ml of 10 % (v/v) glycerol, aliquoted in 40 µl and immediately flash-frozen in liquid N_2. Aliquots were stored at -80 °C.

4.7.3 Transformation of bacteria

After thawing on ice, electrocompetent cells were transformed with either 50-100 ng of plasmid DNA or 10 µl ligation reaction which has been dialysed against ddH_2O for 10 min using PVDF membrane floats with 0.22 µm pore size (Millipore). 40 µl of competent cells were mixed with the DNA in a pre-cooled electroporation cuvette (Bio-Rad) and pulsed for 1 sec (200 Ω pulse-controller, 25 mF, 2.5 kV). Cells were immediately resuspended in 200 µl LB medium and incubated at 37 °C under agitation. For re-transformation, 50 µl were plated on LB agar plates with selective antibiotics. For ligations, the complete mix was plated on LB agar plates with selection markers.

4.7.4 Secretion assay

Bacteria were grown over night and culture aliquots corresponding to an OD_{600} of 2/ml (about 10^9 bacteria) were harvested and the supernatant was saved. Bacteria were washed once with PBS and resuspended in 100 µl SDS sample buffer. The supernatant was filtered (0.22 µm) and proteins were precipitated with 10 % (v/v) Trichloroacetic acid (TCA) for 5 min at -20 °C and harvested subsequently by centrifugation at 16.100 rcf for 30 min at 4 °C. Pellets were washed once with 1 ml ice-cold acetone and centrifuged again for 30 min. Acetone was discarded directly after centrifugation and the pellets dried at room temperature and resuspended in 10 µl 3 M TrisHCl, pH 8.5, plus 90 µl SDS sample buffer. Supernatants and 10 % of the equivalent bacterial lysates were analyzed by SDS PAGE and Western blotting.

4.7.5 Induction of T3SS with Congo Red

Bacteria were grown in 25 ml TSB to mid-log phase (OD_{600} = 0.4-0.6) and harvested at 4.500 rcf for 10 min. Cells were washed with PBS and concentrated in 1 ml PBS supplemented with 20 µg/ml Congo Red or just PBS in eppendorf tubes. The suspension was incubated under agitation at 400 rpm for 1 h at 37 °Cand supernatants were filtered and precipitated with TCA as described before.

4.7.6 SDS PAGE and Western blot

All SDS PAGE (except 2D-electrophoresis) were performed using TrisHCl gradient gels (Criterion AnykD or 4-20 %, Bio-Rad) according to manufacturers instructions, or manually cast 12 % gels as previously described (Laemmli, 1970). Proteins were transferred on nitrocellulose membrane (Amersham Hybond ECL, GE Healthcare) as previously described (Towbin *et al.*, 1979) with 2 mA/cm^2 for 1 h and blocked with 5 % (w/v) milk powder in PBS-T for 30-60 min. Proteins were detected using monoclonal antibodies (mABs) or polyclonal antibodies (pABs) listed in table 4.10. Primary antibodies were incubated 1-16 h (1 h at RT or over night at 12 °C), membranes were washed 3-4 times with PBS-T and secondary antibodies coupled to horse radish-peroxidase were incubated for 30-60 min at RT. Visualization was performed with enhanced chemiluminescence using ECL substrate (SuperSignal West, Thermo Scientific) with a chemiluminescence detector cabinet or on film (Amersham Hyperfilm, GE Healthcare). The IpaB mAB was purified from the H16 hybridoma cell line (Barzu *et al.*, 1993).

Table 4.10: Antibodies used in this study

Name	Source
IpaB mouse IgG1 monoclonal H16	Armelle Phalipon
IpaB IgG1 human Fc monoclonal	This study
IpaC rabbit polyclonal	Institut Pasteur
DnaK mouse monoclonal	Stressgen
MxiG mouse monoclonal 7G1	Lab collection
Strep-tag mouse monoclonal	QIAGEN
anti-mouse goat HRP conjugate	Dianova

Name	Source
anti-human goat HRP conjugate	Dianova
anti-mouse goat Au conjugate 5 nm	BBInternational
anti-mouse goat Au conjugate 12 nm	BBInternational
anti-human goat Au conjugate 5 nm	BBInternational

4.7.7 In-gel visualization of SDS PAGE

For regular staining, Coomassie stain or a commercial Coomassie Brilliant Blue G250-based staining solution was used (Instant blue, Biozol). For silver staining, a rapid protocol by Nesterenko et al. (Nesterenko *et al.*, 1994) was adopted. The procedure is described below in table 4.11.

Table 4.11: Rapid silver staining protocol.

Step	Solutions used	Duration
Fixing	60 ml acetone stock, 1.5 ml TCA stock, 25 µl 37 % (v/v) HCHO	5 min
Rinse	3 x 50 ml ddH_2O	10 sec
Wash	50 ml ddH_2O	5 min
Rinse	3 x 50 ml ddH_2O	10 sec
Pretreat I	60 ml acetone stock	5 min
Pretreat II	100 µl $Na_2S_2O_3 \cdot 5\,H_2O$ stock in 60 ml ddH_2O	1 min
Impregnate	800 µl $AgNO_3$ stock, 600 µl 37 % (v/v) HCHO	8 min
Rinse	3 x 50 ml ddH_2O	10 sec
Develop	0.6 g Na_2CO_3 ddH_2O, 25 µl 37 % (v/v) HCHO, 25 µl $Na_2S_2O_3 \cdot 5\,H_2O$ stock in 60 ml ddH_2O	10-60 sec
Stop	1 % (v/v) glacial acetic acid in 60 ml ddH_2O	30-60 sec

Stock solutions:

Acetone stock (50 % (v/v) acetone in ddH_2O); TCA stock: (50 % (v/v) TCA in ddH_2O), 20 % (w/v) $AgNO_3$ (fresh each time, kept at RT in dark for short-term storage), 10 % $Na_2S_2O_3 \cdot 5\,H_2O$ in ddH_2O.

4.7.8 Protein expression in *E. coli* BL21

Bacteria carrying the plasmid encoding the protein of interest were subcultured in 2-4 l of LB medium to mid-log phase (OD_{600} = 0.4-0.6) and induced with either 0.5-1 mM IPTG (for pET-vectors) or 0.5-1 µg/ml AHT for 2-3 h at 37 °C. Bacteria were harvested by centrifugation at 10.000 rcf for 10 min and pellets were flash-frozen in in liquid N_2. Pellets were stored at -80 °C.

4.7.9 Purifying proteins from heterologous expression

Protein purification from bacteria

IpaB-Knot or IpaB-Knot in complex with IpgC were purified as previously described (Lunelli *et al.*, 2009; Senerovic *et al.*, 2012). *E. coli* BL21 co-transformed with pET28a::*ipgC* (with a 3' *6his*-tag) and pASK-IBA3+::*ipaBknot* (with a 3' *strep*-tag) were grown to early log-phase and expression of *ipgC* was induced with 0.5 mM IPTG for 30 min. Then, expression of *ipaBknot* or *ipaB* was induced with 0.7 µg/ml (w/v) AHT. Bacteria were opened using a French Pressure Cell, 3 cycles with 10.000 psig and the lysate was collected on ice. Debris was removed by centrifugation at 45.000 rcf for 20 min at 4 °C. IpgC and IpaB-Knot were co-purified using 5 ml HisTrap HP cartridges (GE Healthcare) according to manufacturers instructions. The complex binds to the resin via IpgC and IpaB-Knot is eluted with 0.1 % (w/v) LDAO. For fluorescence spectrometry and Proteinase K digestion, full complex of IpgC/IpaB-Knot was eluted with 0.5 M imidazole. Additional affinity chromatography in the presence of 0.05 % LDAO using 5 ml Strep-Tactin columns (IBA) was performed to separate full length IpaB-Knot from IpaB contaminants which might occur because of instability of the fusion protein. Native protein was separated from aggregates by size exclusion chromatography using a Superdex 200 16/60 column (GE Healthcare) with 20 mM 4-(2-hydroxyethyl)-1-piperazineethanesulfonic acid (HEPES), pH 7.4, and 150 mM NaCl. The *knot* was expressed with a C-terminal His-tag (pASK-IBA33+::*knot*) in *E. coli* BL21 and purified via a 5 ml HisTrap HP column in 20 mM TrisHCl, pH 7.4, 300 mM NaCl, 1 mM DTT, 40 mM Imidazole and eluted with 400 mM Imidazole under same buffer conditions. Proteins were concentrated to 1-2 mg/ml using Amicon spin-filters with appropriate molecular weight cut-off.

IgG purification from HEK293 cells

Supernatants from HEK293 cells (25 ml each dish) were collected and incubated over night with 50 µl Protein G sepharose with gentle rotation at 12 °C. The mixture was passed over an empty Poly-Prep column (Bio-Rad) and washed with 3 x 1 ml PBS. Residual PBS was removed with gentle air pressure. IgG1 was eluted under acidic conditions with 225 µl 100 mM Glycine pH 3.0 incubated for 5 min on the column bed and elution volume was collected in eppendorf cups with 25 µl 1 M Tris pH 8.0, 0.1 % (w/v) sodium azide. Elution of IgG1 was repeated three times and the protein concentration was measured using the NanoDrop 2000

IgG analysis program. The antibody was concentrated to 2 mg/ml.

4.7.10 Fluorescence spectroscopy

Purified protein (either IpaB-Knot in complex with IpgC or Knot) was used at 2.5 µM concentrations at 25 °C in quartz cuvettes (Helma). Samples were excited with 295 nm monochromatic light using 2.5 nm or 5 nm slit-width. Detector voltage was set to 650 V. Emission spectra were recorded ranging from 300 to 400 nm at a slit-width of 5 nm or 10 nm. Control emission spectra (buffer with IpgC as a control for IpaB-Knot in complex with IpgC) were subtracted from sample protein spectra. Emissions were normalized to their respective maximum.

4.7.11 Limited proteolysis and mass spectrometry (MS)

Mass spectrometry and 2D-electrophoresis (2D-E) were performed by the Protein analysis core facility, MPIIB Berlin. Purified IpaB-Knot in complex with IpgC or Knot were treated with Proteinase K at a molar ratio of 1:100 (enzyme to substrate) for 1 h at room temperature. The reaction was stopped by adding complete EDTA-free protease inhibitor cocktail (Roche) and the cleavage products were separated by 2D-E (Jungblut & Seifert, 1990). Respective protein cleavage products were trypsinated and analyzed by MS, whereas fragments of specific interest were confirmed by MS/MS.

4.7.12 Isolation of needle complexes

Needle complexes were isolated from bacteria as described previously (Blocker *et al.*, 2001). 2 L of bacterial culture were inoculated 1:50 and grown to an OD_{600} of 1.2-1.6/ml and washed once with PBS. Cells were osmotically shocked by resuspension in 0.5 M sucrose. 0.1 M TrisHCl, pH 8.0 and 5 mM EDTA were added. Bacteria were incubated in the presence of 1-2 mg lysozyme (Novagen) for 30-60 min and lysed with 2 % (v/v) Triton X-100. Debris was removed by centrifugation for 20 min at 45.000 rcf and needle complexes were harvested by pelleting the supernatant at 110.000 rcf for 1 h. The pellet was washed in 10 mM TrisHCl pH 8.0, 150 mM KCl, 5 mM EDTA, 1 % (v/v) Triton X-100 and 0.3 % (w/v) Sarkosyl. Centrifugation steps were repeated and pelleted needle complexes were resuspended in 1-2 ml 50 mM TrisHCl, pH 8.0, 50 mM EDTA, 0.1 % Triton X-100 (TET buffer).

Cesium chloride density fractionation

Needle complexes were further separated by CsCl gradient centrifugation (27.5 % (w/v) CsCl in TET) and size exclusion chromatography (Superose 6 16/60, GE Healthcare, in TE buffer). The solubilized needle complexes in TET were supplemented with 27.5 % (w/v) CsCl and the volume adjusted to 6 ml. The sample was centrifuged in a MLS-50 swing-out rotor at 50.000 rpm (Beckman Optima MAX) overnight (14 h). Aliquots of 500 µl each were carefully removed from top to bottom and diluted in 2.5 ml TE buffer. Needle complexes were concentrated by ultracentrifugation (100.000 g, 1 h, 4 °C), the pellet resuspended in 100 µl TET and subjected to size-exclusion chromatography on a Superose 6 10/300 column (GE Healthcare). Needle complexes eluted in the void volume of the column (7-8 ml) and 1 ml fractions were concentrated by ultracentrifugation at 100.000 g for 1 h at 4 °C. Sample volume was adjusted to 3 ml with TET buffer prior to centrifugation. After pelleting, supernatants were discarded and the needle complexes carefully resuspended using a cut yellow tip in 20-40 µl TET buffer avoiding foam formation.

Affinity purification

Affinity purification of needle complexes via Strep-Tactin sepharose (IBA) in TET was performed by interaction of the C-terminal Strep-tag of IpaB-Knot. Strep-Tactin resin was used for batch purification of needle complexes interacting with IpaB-Knot. Needle complexes solubilized in TET buffer were added to 100-150 µl Strep-Tactin 50 % suspension and incubated with gentle rotation at 12 °C for 1 h. The saturated beads were washed 3 times (centrifugation at 2000 rcf for 2 min and careful removal of the supernatant using a pipet) with 1 ml TET buffer and collected on a Pierce centrifuge column by gravity flow. Subsequently, the beads were treated with 50 µl TET + 10 mM desthiobiotin and incubated for 10 min prior to elution. Needle complexes were eluted by centrifugation at 2000 rcf for 2 min and the elution step was repeated with additional 50 µl TET + desthiobiotin.

4.7.13 TEV protease protection assay

Isolated needle complexes or recombinant IpaB-TEV-Knot in complex with IpgC was added to 100 µl Strep-Tactin beads (IBA) and incubated for 1-2 h at 4 °C with gentle rotation (12-15 rpm). Beads were washed twice with 500 µl TET buffer and subsequently washed twice

with 1 ml 50 mM Tris, pH 8.0, 0.5 mM EDTA, 1 mM DTT (TEV assay buffer) and finally resuspended with 100 µl TEV assay buffer. 4 aliquots of 40 µl bead slurry were adjusted to room temperature and subsequently incubated with either 10 µl TEV assay buffer (negative control), 0.1 µg, 1 µg or 10 µg TEV protease at 400 rpm at 26 °C. The beads were collected by centrifuging at 2000 rcf for 2 min. 30 µl aliquots of supernatant were collected and supplemented with SDS sample buffer. The bead fraction was washed 2 times with 1 ml TEV assay buffer and the beads resuspended in 30 µl TEV assay buffer and supplemented with SDS sample buffer. Samples were analyzed by SDS PAGE and Western blotting.

4.7.14 Addition of PEG moieties by crosslinking (PEGylation)

Engineered PEG molecules that contain an N-hydroxysuccinimide (NHS) ester group can be linked to free primary amines in proteins by a spontaneous formation of an amide bond and releasing the NHS. For PEGylation of IpaB-TEV-Knot, isolated needle complexes (with IpaB-TEV-Knot) or purified IpaB-TEV-Knot were added to 100 µl Strep-Tactin resin (IBA) and incubated for 1-2 h at 4 °C with gentle rotation (12-15 rpm). Beads were washed twice with 500 µl TET buffer and subsequently washed twice with PBS and finally resuspended with 50 µl PBS. 2 aliquots of 40 µl bead slurry were adjusted to room temperature and subsequently incubated with 0.5 mM PEGylation reagent $MS(PEG)_{24}$ (Thermo Scientific) for 1 h at room temperature. The reaction was quenched by addition of 100 mM TrisHCl for 5 min at room temperature and the reaction was directly incubated with SDS sample buffer and analyzed by SDS PAGE and Western blotting.

4.8 Imaging & Bioinformatics

4.8.1 Immuno-electron Microscopy (iEM)

Staining of samples and image acquisition were performed by Christian Goosmann at the Microscopy core facility, MPIIB Berlin.

10 µl aliquots of the needle complex preparations were applied to freshly glow-discharged carbon- and pioloform-film-coated copper grids and allowed to adsorb for 10 min. The grids were then washed with PBS, blocked for 15 min and then incubated with human or mouse antibody against IpaB for 2-3 h at RT. After washing with PBS the samples were incubated with goat anti-mouse antibody adsorbed to 12 nm gold particles or goat anti-human antibody ad-

sorbed to 6 nm gold for 30 min and washed with PBS. Strep-tag labeling was done in a similar manner but using mouse anti-Strep-tag antibody and goat anti-mouse antibody adsorbed to 12 nm gold. For double-labeling of both IpaB and Strep-tag, IpaB was labeled first with human anti-IpaB and the matching secondary antibody followed by labeling of the Strep-tag. In this case, the Strep-tag antibody was incubated over night followed by secondary antibody incubation.

After three washes with distilled water, the grids were contrasted with 4 % phosphotungstic-acid (PTA), 1 % Trehalose, pH 7.0, or NanVan, touched onto filter paper and air-dried. The grids were examined in a LEO 906 transmission electron microscope (Zeiss AG) operated at 100 kV and images were recorded with a Morada (SIS-Olympus) digital camera.

4.8.2 Nearest-neighbor analysis

Coordinates (X and Y) for gold labels and needle complex centers from 50 iEM images (2048x2048 px^2) were manually obtained using the ImageJ analysis package (Abramoff *et al.*, 2004). The values were processed in R (R Development Core Team (2003)) and subjected to a nearest-neighbor analysis with the Biobase package (Gentleman *et al.*, 2004). Coordinates of needle complex centers were matched with coordinates of the closest gold particle coordinates. As a control, random coordinates of needle complexes and gold particles were generated and used in comparison to the manually obtained coordinates. This way, exact counts per image were maintained.

4.8.3 cryo-electron microscopy (cryo-EM)

The procedures described below were performed in close collaboration with Jörg Bürger and Thorsten Mielke, MPI for Molecular Genetics, Berlin. Electron microscopy at near-liquid nitrogen temperatures was performed on vitrified isolated needle complexes in TE buffer with 0.02 % Triton-X100 or 0.4 % OG.

Sample preparation for cryo-EM

Holey carbon grids (300 mesh R3/3 Quantifoil® Cu grids, Quantifoil Micro Tools GmbH) layered with 2 nm of carbon film were glow-discharged for 30 sec and used directly after the discharging procedure. 3.5 µl of sample were loaded on holey film grids and adsorbed for 45 sec in a Vitrobot Mark II device (FEI) at 4 °C and 100 % humidity. The grid was blotted for

4 sec and plunge-frozen in liquid ethane at 77 K. Grids were kept at ultra-low temperatures at all times after freezing.

cryo-EM imaging

Grids were analyzed with a Tecnai™ G^2 Spirit transmission electron microscope together with a 2 k Eagle 4 Mpx CCD™ camera (both FEI) operated at 120 kV (LaB_6 cathode). Objective and C2 apertures were set to 100 µm. Images have a final resolution of 2048px x 2048px at a nominal magnification of 30,000-fold, resulting at a pixel size of 7 Å relative to the specimen scale. The Leginon system (Suloway *et al.*, 2005) was used for automated image collection.

4.8.4 Single particle-analysis

Single particle-analysis was performed with Elmar Behrmann, Institut für medizinische Biophysik, Charité Berlin. Particles were selected semi-automatically using EMAN2 (Tang *et al.*, 2007) after evaluation of the contrast transfer function using CTFFIND3 (Mindell & Grigorieff, 2003). From projection images of the selected particles, 2D class averages were calculated using the SPARX software package (Hohn *et al.*, 2007).

5 References and Tables

Bibliography

Abramoff, M. D., J., M. P., & S.J., R. (2004): Image Processing with ImageJ. *Biophotonics International*, 11 (7), 36–42.

Adam, P. R., Patil, M. K., Dickenson, N. E., Choudhari, S., Barta, M., Geisbrecht, B. V., Picking, W. L., & Picking, W. D. (2012): Binding Affects the Tertiary and Quaternary Structures of the Shigella Translocator Protein IpaB and Its Chaperone IpgC. *Biochemistry*, 51 (19), 4062–4071.

Akeda, Y. & Galan, J. E. (2005): Chaperone release and unfolding of substrates in type III secretion. *Nature*, 437 (7060), 911–5.

Akopyan, K., Edgren, T., Wang-Edgren, H., Rosqvist, R., Fahlgren, A., Wolf-Watz, H., & Fallman, M. (2011): Translocation of surface-localized effectors in type III secretion. *Proceedings of the National Academy of Sciences of the United States of America*, 108 (4), 1639–44.

Alder, N. N. & Theg, S. M. (2003): Energy use by biological protein transport pathways. *Trends in Biochemical Sciences*, 28 (8), 442–451.

Amiry-Moghaddam, M. & Ottersen, O. P. (2013): Immunogold cytochemistry in neuroscience. *Nature Neuroscience*, 16 (7), 798–804.

Arnold, R., Brandmaier, S., Kleine, F., Tischler, P., Heinz, E., Behrens, S., Niinikoski, A., Mewes, H. W., Horn, M., & Rattei, T. (2009): Sequence-based prediction of type III secreted proteins. *PLoS Pathogens*, 5 (4), e1000376.

Bahrani, F. K., Sansonetti, P. J., & Parsot, C. (1997): Secretion of Ipa proteins by Shigella flexneri: inducer molecules and kinetics of activation. *Infection and Immunity*, 65 (10), 4005–10.

Barison, N., Cendron, L., Loconte, V., Proctor, E. A., Dokholyan, N. V., & Zanotti, G. (2013): Protein HP1028 from the human pathogen Helicobacter pylori belongs to the lipocalin family. *Acta Crystallographica Section D-Biological Crystallography*, 69, 1387–1394.

Barzu, S., Nato, F., Rouyre, S., Mazie, J. C., Sansonetti, P., & Phalipon, A. (1993): Characterization of B-cell epitopes on Ipab, an invasion-associated antigen of Shigella flexneri: identification of an immunodominant domain recognized during natural infection. *Infection and Immunity*, 61 (9), 3825–31.

Bateman, A., Coin, L., Durbin, R., Finn, R. D., Hollich, V., Griffiths-Jones, S., Khanna, A., Marshall, M., Moxon, S., Sonnhammer, E. L., Studholme, D. J., Yeats, C., & Eddy, S. R. (2004): The Pfam protein families database. *Nucleic Acids Research*, 32 (Database issue), D138–41.

Bayan, N., Guilvout, I., & Pugsley, A. P. (2006): Secretins take shape. *Molecular microbiology*, 60 (1), 1–4.

Birket, S. E., Harrington, A. T., Espina, M., Smith, N. D., Terry, C. M., Darboe, N., Markham, A. P., Middaugh, C. R., Picking, W. L., & Picking, W. D. (2007): Preparation and characterization of translocator/chaperone complexes and their component proteins from Shigella flexneri. *Biochemistry*, 46 (27), 8128–37.

Blocker, A., Gounon, P., Larquet, E., Niebuhr, K., Cabiaux, V., Parsot, C., & Sansonetti, P. (1999): The tripartite type III secreton of Shigella flexneri inserts Ipab and Ipac into host membranes. *The Journal of Cell Biology*, 147 (3), 683–93.

Blocker, A., Jouihri, N., Larquet, E., Gounon, P., Ebel, F., Parsot, C., Sansonetti, P., & Allaoui, A. (2001): Structure and composition of the Shigella flexneri "needle complex", a part of its type III secreton. *Molecular Microbiology*, 39 (3), 652–63.

Botteaux, A., Sory, M. P., Biskri, L., Parsot, C., & Allaoui, A. (2009): Mxic is secreted by and controls the substrate specificity of the Shigella flexneri type III secretion apparatus. *Molecular Microbiology*, 71 (2), 449–60.

Buchrieser, C., Glaser, P., Rusniok, C., Nedjari, H., D'Hauteville, H., Kunst, F., Sansonetti, P., & Parsot, C. (2000): The virulence plasmid pWR100 and the repertoire of proteins secreted by the type III secretion apparatus of Shigella flexneri. *Molecular Microbiology*, 38 (4), 760–71.

Büttner, D. & He, S. Y. (2009): Type III protein secretion in plant pathogenic bacteria. *Plant Physiology*, 150 (4), 1656–64.

Chatterjee, S., Chaudhury, S., McShan, A. C., Kaur, K., & De Guzman, R. N. (2013): Structure and biophysics of type III secretion in bacteria. *Biochemistry*, 52 (15), 2508–17.

Clatworthy, A. E., Pierson, E., & Hung, D. T. (2007): Targeting virulence: a new paradigm for antimicrobial therapy. *Nature Chemical Biology*, 3 (9), 541–8.

Cornelis, G. R. (2006): The type III secretion injectisome. *Nature reviews Microbiology*, 4 (11), 811–25.

Datsenko, K. A. & Wanner, B. L. (2000): One-step inactivation of chromosomal genes in Escherichia coli K-12 using PCR products. *Proceedings of the National Academy of Sciences of the United States of America*, 97 (12), 6640–5.

Dean, P. (2011): Functional domains and motifs of bacterial type III effector proteins and their roles in infection. *FEMS Microbiology reviews*, 35 (6), 1100–25.

Demers, J. P., Sgourakis, N. G., Gupta, R., Loquet, A., Giller, K., Riedel, D., Laube, B., Kolbe, M., Baker, D., Becker, S., & Lange, A. (2013): The common structural architecture of Shigella flexneri and Salmonella typhimurium type three secretion needles. *PLoS Pathogens*, 9 (3), e1003245.

DuPont, H. L., Levine, M. M., Hornick, R. B., & Formal, S. B. (1989): Inoculum Size in Shigellosis and Implications for Expected Mode of Transmission. *Journal of Infectious Diseases*, 159 (6), 1126–1128.

Dzubiella, J. (2009): Sequence-Specific Size, Structure, and Stability of Tight Protein Knots. *Biophysical Journal*, 96 (3), 831–839.

Edgren, T., Forsberg, A., Rosqvist, R., & Wolf-Watz, H. (2012): Type III secretion in Yersinia: injectisome or not? *PLoS Pathogens*, 8 (5), e1002669.

Eilers, M. & Schatz, G. (1986): Binding of a specific ligand inhibits import of a purified precursor protein into mitochondria. *Nature*, 322 (6076), 228–32.

Enninga, J., Mounier, J., Sansonetti, P., & Tran Van Nhieu, G. (2005): Secretion of type III effectors into host cells in real time. *Nature Methods*, 2 (12), 959–65.

Epler, C. R., Dickenson, N. E., Bullitt, E., & Picking, W. L. (2012): Ultrastructural analysis of IpaD at the tip of the nascent MxiH type III secretion apparatus of Shigella flexneri. *Journal of Molecular Biology*, 420 (1-2), 29–39.

Erhardt, M., Namba, K., & Hughes, K. T. (2010): Bacterial nanomachines: the flagellum and type III injectisome. *Cold Spring Harbor perspectives in biology*, 2 (11), a000299.

Espina, M., Olive, A. J., Kenjale, R., Moore, D. S., Ausar, S. F., Kaminski, R. W., Oaks, E. V., Middaugh, C. R., Picking, W. D., & Picking, W. L. (2006): IpaD localizes to the tip of the type III secretion system needle of Shigella flexneri. *Infection and Immunity*, 74 (8), 4391–400.

Feldman, M. F., Muller, S., Wuest, E., & Cornelis, G. R. (2002): SycE allows secretion of YopE-DHFR hybrids by the Yersinia enterocolitica type III Ysc system. *Molecular Microbiology*, 46 (4), 1183–97.

Galan, J. E. (2009): Common themes in the design and function of bacterial effectors. *Cell Host & Microbe*, 5 (6), 571–9.

Galan, J. E. & Collmer, A. (1999): Type III secretion machines: bacterial devices for protein delivery into host cells. *Science*, 284 (5418), 1322–8.

Galan, J. E. & Wolf-Watz, H. (2006): Protein delivery into eukaryotic cells by type III secretion machines. *Nature*, 444 (7119), 567–73.

Gentleman, R. C., Carey, V. J., Bates, D. M., Bolstad, B., Dettling, M., Dudoit, S., Ellis, B., Gautier, L., Ge, Y., Gentry, J., Hornik, K., Hothorn, T., Huber, W., Iacus, S., Irizarry, R., Leisch, F., Li, C., Maechler, M., Rossini, A. J., Sawitzki, G., Smith, C., Smyth, G., Tierney, L., Yang, J. Y., & Zhang, J. (2004): Bioconductor: open software development for computational biology and bioinformatics. *Genome Biology*, 5 (10), R80.

Ghosh, P. (2004): Process of protein transport by the type III secretion system. *Microbiology and Molecular Biology Reviews : MMBR*, 68 (4), 771–95.

Gorden, J. & Small, P. L. (1993): Acid resistance in enteric bacteria. *Infection and Immunity*, 61 (1), 364–7.

Henderson, I. R., Navarro-Garcia, F., Desvaux, M., Fernandez, R. C., & Ala'Aldeen, D. (2004): Type V protein secretion pathway: the autotransporter story. *Microbiology and Molecular Biology Reviews : MMBR*, 68 (4), 692–744.

High, N., Mounier, J., Prevost, M. C., & Sansonetti, P. J. (1992): IpaB of Shigella flexneri causes entry into epithelial cells and escape from the phagocytic vacuole. *The EMBO journal*, 11 (5), 1991–9.

Hilbi, H., Moss, J. E., Hersh, D., Chen, Y., Arondel, J., Banerjee, S., Flavell, R. A., Yuan, J., Sansonetti, P. J., & Zychlinsky, A. (1998): Shigella-induced apoptosis is dependent on caspase-1 which binds to IpaB. *The Journal of Biological Chemistry*, 273 (49), 32895–900.

Hilz, H., Wiegers, U., & Adamietz, P. (1975): Stimulation of proteinase K action by denaturing agents: application to the isolation of nucleic acids and the degradation of 'masked' proteins. *European Journal of Biochemistry / FEBS*, 56 (1), 103–8.

Hodgkinson, J. L., Horsley, A., Stabat, D., Simon, M., Johnson, S., da Fonseca, P. C., Morris, E. P., Wall, J. S., Lea, S. M., & Blocker, A. J. (2009): Three-dimensional reconstruction of the Shigella T3SS transmembrane regions reveals 12-fold symmetry and novel features throughout. *Nature Structural & Molecular Biology*, 16 (5), 477–85.

Hohn, M., Tang, G., Goodyear, G., Baldwin, P. R., Huang, Z., Penczek, P. A., Yang, C., Glaeser, R. M., Adams, P. D., & Ludtke, S. J. (2007): SPARX, a new environment for Cryo-EM image processing. *Journal of Structural Biology*, 157 (1), 47–55.

Huang, L. & Makarov, D. E. (2008): Translocation of a knotted polypeptide through a pore. *Journal of Chemical Physics*, 129 (12).

Hueck, C. J. (1998): Type III protein secretion systems in bacterial pathogens of animals and plants. *Microbiology and Molecular Biology Reviews : MMBR*, 62 (2), 379–433.

Hurt, E. C., Pesold-Hurt, B., & Schatz, G. (1984): The amino-terminal region of an imported mitochondrial precursor polypeptide can direct cytoplasmic dihydrofolate reductase into the mitochondrial matrix. *The EMBO journal*, 3 (13), 3149–56.

Iwai, H., Kim, M., Yoshikawa, Y., Ashida, H., Ogawa, M., Fujita, Y., Muller, D., Kirikae, T., Jackson, P. K., Kotani, S., & Sasakawa, C. (2007): A bacterial effector targets Mad2L2, an APC inhibitor, to modulate host cell cycling. *Cell*, 130 (4), 611–23.

Jennison, A. V. & Verma, N. K. (2007): The acid-resistance pathways of Shigella flexneri 2457T. *Microbiology*, 153 (Pt 8), 2593–602.

Jin, Q. L. & He, S. Y. (2001): Role of the Hrp pilus in type III protein secretion in Pseudomonas syringae. *Science*, 294 (5551), 2556–2558.

Jin, Q. L., Hu, W. Q., Brown, I., McGhee, G., Hart, P., Jones, A. L., & He, S. Y. (2001): Visualization of secreted Hrp and Avr proteins along the Hrp pilus during type III secretion in Erwinia amylovora and Pseudomonas syringae. *Molecular Microbiology*, 40 (5), 1129–1139.

Johnson, S., Roversi, P., Espina, M., Olive, A., Deane, J. E., Birket, S., Field, T., Picking, W. D., Blocker, A. J., Galyov, E. E., Picking, W. L., & Lea, S. M. (2007): Self-chaperoning of the type III secretion system needle tip proteins IpaD and BipD. *The Journal of Biological Chemistry*, 282 (6), 4035–44.

Jouihri, N., Sory, M. P., Page, A. L., Gounon, P., Parsot, C., & Allaoui, A. (2003): MxiK and MxiN interact with the Spa47 ATPase and are required for transit of the needle components MxiH and MxiI, but not of Ipa proteins, through the type III secretion apparatus of Shigella flexneri. *Molecular Microbiology*, 49 (3), 755–67.

Jungblut, P. R. & Seifert, R. (1990): Analysis by high-resolution two-dimensional electrophoresis of differentiation-dependent alterations in cytosolic protein pattern of HL-60 leukemic cells. *Journal of Biochemical and Biophysical Methods*, 21 (1), 47–58.

Kubori, T., Matsushima, Y., Nakamura, D., Uralil, J., Lara-Tejero, M., Sukhan, A., Galan, J. E., & Aizawa, S. I. (1998): Supramolecular structure of the Salmonella typhimurium type III protein secretion system. *Science*, 280 (5363), 602–5.

Kudryashev, M., Stenta, M., Schmelz, S., Amstutz, M., Wiesand, U., Castano-Diez, D., Degiacomi, M. T., Munnich, S., Bleck, C. K., Kowal, J., Diepold, A., Heinz, D. W., Dal Peraro, M., Cornelis, G. R., & Stahlberg, H. (2013): In situ structural analysis of the Yersinia enterocolitica injectisome. *eLife*, 2, e00792.

Laemmli, U. K. (1970): Cleavage of structural proteins during the assembly of the head of bacteriophage T4. *Nature*, 227 (5259), 680–5.

Lafont, F., Tran Van Nhieu, G., Hanada, K., Sansonetti, P., & van der Goot, F. G. (2002): Initial steps of Shigella infection depend on the cholesterol/sphingolipid raft-mediated CD44-IpaB interaction. *The EMBO journal*, 21 (17), 4449–57.

Lan, R. & Reeves, P. R. (2002): Escherichia coli in disguise: molecular origins of Shigella. *Microbes and Infection / Institut Pasteur*, 4 (11), 1125–32.

Lara-Tejero, M., Kato, J., Wagner, S., Liu, X., & Galan, J. E. (2011): A sorting platform determines the order of protein secretion in bacterial type III systems. *Science*, 331 (6021), 1188–91.

Lee, V. T. & Schneewind, O. (2002): Yop fusions to tightly folded protein domains and their effects on Yersinia enterocolitica type III secretion. *Journal of Bacteriology*, 184 (13), 3740–5.

Li, C. M., Brown, I., Mansfield, J., Stevens, C., Boureau, T., Romantschuk, M., & Taira, S. (2002): The Hrp pilus of Pseudomonas syringae elongates from its tip and acts as a conduit for translocation of the effector protein HrpZ. *The EMBO Journal*, 21 (8), 1909–1915.

Lokareddy, R. K., Lunelli, M., Eilers, B., Wolter, V., & Kolbe, M. (2010): Combination of Two Separate Binding Domains Defines Stoichiometry between Type III Secretion System Chaperone IpgC and Translocator Protein IpaB. *Journal of Biological Chemistry*, 285 (51), 39965–39975.

Loquet, A., Sgourakis, N. G., Gupta, R., Giller, K., Riedel, D., Goosmann, C., Griesinger, C., Kolbe, M., Baker, D., Becker, S., & Lange, A. (2012): Atomic model of the type III secretion system needle. *Nature*, 486 (7402), 276–9.

Lower, M. & Schneider, G. (2009): Prediction of type III secretion signals in genomes of gram-negative bacteria. *PloS One*, 4 (6), e5917.

Lunelli, M., Lokareddy, R. K., Zychlinsky, A., & Kolbe, M. (2009): IpaB-IpgC interaction defines binding motif for type III secretion translocator. *Proceedings of the National Academy of Sciences of the United States of America*, 106 (24), 9661–6.

Magdalena, J., Hachani, A., Chamekh, M., Jouihri, N., Gounon, P., Blocker, A., & Allaoui, A. (2002): Spa32 regulates a switch in substrate specificity of the type III secreton of Shigella flexneri from needle components to Ipa proteins. *Journal of Bacteriology*, 184 (13), 3433–41.

Mallam, A. L. & Jackson, S. E. (2007a): A comparison of the folding of two knotted proteins: Ybea and yibk. *Journal of Molecular Biology*, 366 (2), 650–65.

Mallam, A. L. & Jackson, S. E. (2007b): The dimerization of an alpha/beta-knotted protein is essential for structure and function. *Structure*, 15 (1), 111–22.

Mallam, A. L., Onuoha, S. C., Grossmann, J. G., & Jackson, S. E. (2008): Knotted fusion proteins reveal unexpected possibilities in protein folding. *Molecular Cell*, 30 (5), 642–648.

Mansfield, M. L. (1994): Are there knots in proteins? *Nature Structural Biology*, 1 (4), 213–4.

Martinez-Argudo, I. & Blocker, A. J. (2010): The Shigella T3SS needle transmits a signal for MxiC release, which controls secretion of effectors. *Molecular Microbiology*, 78 (6), 1365–78.

Maurelli, A. T., Baudry, B., d'Hauteville, H., Hale, T. L., & Sansonetti, P. J. (1985): Cloning of plasmid DNA sequences involved in invasion of HeLa cells by Shigella flexneri. *Infection and Immunity*, 49 (1), 164–71.

Menard, R., Sansonetti, P., & Parsot, C. (1994a): The secretion of the Shigella flexneri Ipa invasins is activated by epithelial cells and controlled by IpaB and IpaD. *The EMBO journal*, 13 (22), 5293–302.

Menard, R., Sansonetti, P., Parsot, C., & Vasselon, T. (1994b): Extracellular association and cytoplasmic partitioning of the IpaB and IpaC invasins of S. flexneri. *Cell*, 79 (3), 515–25.

Menard, R., Sansonetti, P. J., & Parsot, C. (1993): Nonpolar mutagenesis of the ipa genes defines IpaB, IpaC, and IpaD as effectors of Shigella flexneri entry into epithelial cells. *Journal of Bacteriology*, 175 (18), 5899–906.

Michiels, T. & Cornelis, G. R. (1991): Secretion of hybrid proteins by the Yersinia Yop export system. *Journal of Bacteriology*, 173 (5), 1677–85.

Mindell, J. A. & Grigorieff, N. (2003): Accurate determination of local defocus and specimen tilt in electron microscopy. *Journal of Structural Biology*, 142 (3), 334–47.

Morita-Ishihara, T., Ogawa, M., Sagara, H., Yoshida, M., Katayama, E., & Sasakawa, C. (2006): Shigella Spa33 is an essential C-ring component of type III secretion machinery. *The Journal of Biological Chemistry*, 281 (1), 599–607.

Mounier, J., Boncompain, G., Senerovic, L., Lagache, T., Chretien, F., Perez, F., Kolbe, M., Olivo-Marin, J. C., Sansonetti, P. J., & Sauvonnet, N. (2012): Shigella effector IpaB-induced cholesterol relocation disrupts the Golgi complex and recycling network to inhibit host cell secretion. *Cell Host & Microbe*, 12 (3), 381–9.

Mounier, J., Vasselon, T., Hellio, R., Lesourd, M., & Sansonetti, P. J. (1992): Shigella flexneri enters human colonic Caco-2 epithelial cells through the basolateral pole. *Infection and Immunity*, 60 (1), 237–48.

Müller, C. A., Broz, P., & Cornelis, G. R. (2008): The type III secretion system tip complex and translocon. *Molecular Microbiology*, 68 (5), 1085–95.

Nesterenko, M. V., Tilley, M., & Upton, S. J. (1994): A simple modification of blum's silver stain method allows for 30 minute detection of proteins in polyacrylamide gels. *Journal of Biochemical and Biophysical Methods*, 28 (3), 239–42.

Nureki, O., Shirouzu, M., Hashimoto, K., Ishitani, R., Terada, T., Tamakoshi, M., Oshima, T., Chijimatsu, M., Takio, K., Vassylyev, D. G., Shibata, T., Inoue, Y., Kuramitsu, S., & Yokoyama, S. (2002): An enzyme with a deep trefoil knot for the active-site architecture. *Acta Crystallographica. Section D, Biological crystallography*, 58 (Pt 7), 1129–37.

Ohgita, T., Hayashi, N., Hama, S., Tsuchiya, H., Gotoh, N., & Kogure, K. (2013): A novel effector secretion mechanism based on proton-motive force-dependent type III secretion apparatus rotation. *FASEB journal : official publication of the Federation of American Societies for Experimental Biology*, 27 (7), 2862–72.

Osborne, S. E. & Coombes, B. K. (2011): Expression and secretion hierarchy in the nonflagellar type III secretion system. *Future Microbiology*, 6 (2), 193–202.

Page, A. L., Ohayon, H., Sansonetti, P. J., & Parsot, C. (1999): The secreted IpaB and IpaC invasins and their cytoplasmic chaperone IpgC are required for intercellular dissemination of Shigella flexneri. *Cellular Microbiology*, 1 (2), 183–93.

Parsot, C. (2009): Shigella type III secretion effectors: how, where, when, for what purposes? *Current Opinion in Microbiology*, 12 (1), 110–6.

Parsot, C., Menard, R., Gounon, P., & Sansonetti, P. J. (1995): Enhanced secretion through the Shigella flexneri Mxi-Spa translocon leads to assembly of extracellular proteins into macromolecular structures. *Molecular Microbiology*, 16 (2), 291–300.

Peng, J., Yang, J., & Jin, Q. (2009): The molecular evolutionary history of Shigella spp. and enteroinvasive Escherichia coli. *Infection, Genetics and Evolution : Journal of molecular epidemiology and evolutionary genetics in infectious diseases*, 9 (1), 147–52.

Perdomo, J. J., Gounon, P., & Sansonetti, P. J. (1994): Polymorphonuclear leukocyte transmigration promotes invasion of colonic epithelial monolayer by Shigella flexneri. *The Journal of Clinical Investigation*, 93 (2), 633–43.

Phalipon, A., Mulard, L. A., & Sansonetti, P. J. (2008): Vaccination against shigellosis: is it the path that is difficult or is it the difficult that is the path? *Microbes and Infection / Institut Pasteur*, 10 (9), 1057–62.

Preston, G. M. (2007): Metropolitan microbes: type III secretion in multihost symbionts. *Cell Host & Microbe*, 2 (5), 291–4.

Prevost, M. C., Lesourd, M., Arpin, M., Vernel, F., Mounier, J., Hellio, R., & Sansonetti, P. J. (1992): Unipolar reorganization of F-actin layer at bacterial division and bundling of actin filaments by plastin correlate with movement of Shigella flexneri within HeLa cells. *Infection and Immunity*, 60 (10), 4088–99.

Ray, K., Marteyn, B., Sansonetti, P. J., & Tang, C. M. (2009): Life on the inside: the intracellular lifestyle of cytosolic bacteria. *Nature reviews. Microbiology*, 7 (5), 333–40.

Riordan, K. E., Sorg, J. A., Berube, B. J., & Schneewind, O. (2008): Impassable YscP substrates and their impact on the Yersinia enterocolitica type III secretion pathway. *Journal of Bacteriology*, 190 (18), 6204–16.

Roehrich, A. D., Martinez-Argudo, I., Johnson, S., Blocker, A. J., & Veenendaal, A. K. (2010): The extreme C-terminus of Shigella flexneri IpaB is required for regulation of type III secretion, needle tip composition, and binding. *Infection and Immunity*, 78 (4), 1682–91.

Rosqvist, R., Magnusson, K. E., & Wolf-Watz, H. (1994): Target cell contact triggers expression and polarized transfer of Yersinia YopE cytotoxin into mammalian cells. *The EMBO journal*, 13 (4), 964–72.

Salmond, G. P. & Reeves, P. J. (1993): Membrane traffic wardens and protein secretion in gram-negative bacteria. *Trends in Biochemical Sciences*, 18 (1), 7–12.

Sambrook, J. & Russel, D. (2001): Molecular cloning: A laboratory manual. *Cold Spring Harbor Laboratory press*, 3rd edition.

Samudrala, R., Heffron, F., & McDermott, J. (2009): Accurate Prediction of Secreted Substrates and Identification of a Conserved Putative Secretion Signal for Type III Secretion Systems. *PLoS Pathogens*, 5 (4), e1000375.

Sansonetti, P. J. (2006): Shigellosis: an old disease in new clothes? *PLoS Medicine*, 3 (9), e354.

Sansonetti, P. J., Kopecko, D. J., & Formal, S. B. (1982): Involvement of a plasmid in the invasive ability of Shigella flexneri. *Infection and Immunity*, 35 (3), 852–60.

Sansonetti, P. J., Ryter, A., Clerc, P., Maurelli, A. T., & Mounier, J. (1986): Multiplication of Shigella flexneri within HeLa cells: lysis of the phagocytic vacuole and plasmid-mediated contact hemolysis. *Infection and Immunity*, 51 (2), 461–9.

Sansonetti, P. J., Tran Van Nhieu, G., & Egile, C. (1999): Rupture of the intestinal epithelial barrier and mucosal invasion by Shigella flexneri. *Clinical Infectious Diseases : an official publication of the Infectious Diseases Society of America*, 28 (3), 466–75.

Schesser, K., Frithz-Lindsten, E., & Wolf-Watz, H. (1996): Delineation and mutational analysis of the Yersinia pseudotuberculosis YopE domains which mediate translocation across bacterial and eukaryotic cellular membranes. *Journal of Bacteriology*, 178 (24), 7227–33.

Schraidt, O. & Marlovits, T. C. (2011): Three-dimensional model of Salmonella's needle complex at subnanometer resolution. *Science*, 331 (6021), 1192–5.

Schroeder, G. N. & Hilbi, H. (2008): Molecular pathogenesis of Shigella spp.: controlling host cell signaling, invasion, and death by type III secretion. *Clinical Microbiology Reviews*, 21 (1), 134–56.

Schroeder, G. N., Jann, N. J., & Hilbi, H. (2007): Intracellular type III secretion by cytoplasmic Shigella flexneri promotes caspase-1-dependent macrophage cell death. *Microbiology*, 153 (Pt 9), 2862–76.

Schuch, R. & Maurelli, A. T. (2001): MxiM and MxiJ, base elements of the Mxi-Spa type III secretion system of Shigella, interact with and stabilize the MxiD secretin in the cell envelope. *Journal of Bacteriology*, 183 (24), 6991–8.

Senerovic, L., Tsunoda, S. P., Goosmann, C., Brinkmann, V., Zychlinsky, A., Meissner, F., & Kolbe, M. (2012): Spontaneous formation of IpaB ion channels in host cell membranes reveals how Shigella induces pyroptosis in macrophages. *Cell Death & Disease*, 3, e384.

Shiferaw, B., Solghan, S., Palmer, A., Joyce, K., Barzilay, E. J., Krueger, A., & Cieslak, P. (2012): Antimicrobial susceptibility patterns of Shigella isolates in Foodborne Diseases Active Surveillance Network (FoodNet) sites, 2000-2010. *Clinical infectious diseases : an official publication of the Infectious Diseases Society of America*, 54 Suppl 5, S458–63.

Skoudy, A., Mounier, J., Aruffo, A., Ohayon, H., Gounon, P., Sansonetti, P., & Tran Van Nhieu, G. (2000): CD44 binds to the Shigella IpaB protein and participates in bacterial invasion of epithelial cells. *Cellular Microbiology*, 2 (1), 19–33.

Sorg, J. A., Blaylock, B., & Schneewind, O. (2006): Secretion signal recognition by YscN, the Yersinia type III secretion ATPase. *Proceedings of the National Academy of Sciences of the United States of America*, 103 (44), 16490–5.

Sory, M. P. & Cornelis, G. R. (1994): Translocation of a hybrid YopE-adenylate cyclase from Yersinia enterocolitica into HeLa cells. *Molecular Microbiology*, 14 (3), 583–94.

Soto, M. J., Sanjuan, J., & Olivares, J. (2006): Rhizobia and plant-pathogenic bacteria: common infection weapons. *Microbiology*, 152 (Pt 11), 3167–74.

Suloway, C., Pulokas, J., Fellmann, D., Cheng, A., Guerra, F., Quispe, J., Stagg, S., Potter, C. S., & Carragher, B. (2005): Automated molecular microscopy: the new Leginon system. *Journal of Structural Biology*, 151 (1), 41–60.

Szymczak, P. (2013): Tight knots in proteins: can they block the mitochondrial pores? *Biochemical Society Transactions*, 41, 620–624.

Takusagawa, F. & Kamitori, S. (1996): A real knot in protein. *Journal of the American Chemical Society*, 118 (37), 8945–8946.

Tamano, K., Aizawa, S., Katayama, E., Nonaka, T., Imajoh-Ohmi, S., Kuwae, A., Nagai, S., & Sasakawa, C. (2000): Supramolecular structure of the Shigella type III secretion machinery: the needle part is changeable in length and essential for delivery of effectors. *The EMBO journal*, 19 (15), 3876–87.

Tamano, K., Katayama, E., Toyotome, T., & Sasakawa, C. (2002): Shigella Spa32 is an essential secretory protein for functional type III secretion machinery and uniformity of its needle length. *Journal of Bacteriology*, 184 (5), 1244–52.

Tang, G., Peng, L., Baldwin, P. R., Mann, D. S., Jiang, W., Rees, I., & Ludtke, S. J. (2007): EMAN2: an extensible image processing suite for electron microscopy. *Journal of Structural Biology*, 157 (1), 38–46.

Taylor, W. R. (2000): A deeply knotted protein structure and how it might fold. *Nature*, 406 (6798), 916–9.

Taylor, W. R. (2007): Protein knots and fold complexity: some new twists. *Computational Biology and Chemistry*, 31 (3), 151–62.

Team, R. D. C. (2003): R: a language and environment for statistical computing.

Tiller, T., Busse, C. E., & Wardemann, H. (2009): Cloning and expression of murine Ig genes from single B cells. *Journal of Immunological Methods*, 350 (1-2), 183–93.

Tiller, T., Meffre, E., Yurasov, S., Tsuiji, M., Nussenzweig, M. C., & H., W. (2008): Efficient generation of monoclonal antibodies from single human B cells by single cell RT-PCR and expression vector cloning. *Journal of Immunological Methods*, 329 (1-2), 112–24.

Towbin, H., Staehelin, T., & Gordon, J. (1979): Electrophoretic transfer of proteins from polyacrylamide gels to nitrocellulose sheets: procedure and some applications. *Proceedings of the National Academy of Sciences of the United States of America*, 76 (9), 4350–4.

Troisfontaines, P. & Cornelis, G. R. (2005): Type III secretion: more systems than you think. *Physiology*, 20, 326–39.

Vasselon, T., Mounier, J., Hellio, R., & Sansonetti, P. J. (1992): Movement along actin filaments of the perijunctional area and de novo polymerization of cellular actin are required for Shigella flexneri colonization of epithelial Caco-2 cell monolayers. *Infection and Immunity*, 60 (3), 1031–40.

Veenendaal, A. K., Hodgkinson, J. L., Schwarzer, L., Stabat, D., Zenk, S. F., & Blocker, A. J. (2007): The type III secretion system needle tip complex mediates host cell sensing and translocon insertion. *Molecular Microbiology*, 63 (6), 1719–30.

Venkatesan, M. M., Goldberg, M. B., Rose, D. J., Grotbeck, E. J., Burland, V., & Blattner, F. R. (2001): Complete dna sequence and analysis of the large virulence plasmid of shigella flexneri. *Infection and Immunity*, 69 (5), 3271–85.

Virnau, P., Mallam, A., & Jackson, S. (2011): Structures and folding pathways of topologically knotted proteins. *Journal of physics. Condensed matter : an Institute of Physics journal*, 23 (3), 033101.

von Seidlein, L., Kim, D. R., Ali, M., Lee, H., Wang, X., Thiem, V. D., Canh do, G., Chaicumpa, W., Agtini, M. D., Hossain, A., Bhutta, Z. A., Mason, C., Sethabutr, O., Talukder, K., Nair, G. B., Deen, J. L., Kotloff, K., & Clemens, J. (2006): A multicentre study of Shigella diarrhoea in six Asian countries: disease burden, clinical manifestations, and microbiology. *PLoS Medicine*, 3 (9), e353.

Wassef, J. S., Keren, D. F., & Mailloux, J. L. (1989): Role of M cells in initial antigen uptake and in ulcer formation in the rabbit intestinal loop model of shigellosis. *Infection and Immunity*, 57 (3), 858–63.

West, N. P., Sansonetti, P., Mounier, J., Exley, R. M., Parsot, C., Guadagnini, S., Prevost, M. C., Prochnicka-Chalufour, A., Delepierre, M., Tanguy, M., & Tang, C. M. (2005): Optimization of virulence functions through glucosylation of Shigella LPS. *Science*, 307 (5713), 1313–7.

Wilharm, G., Dittmann, S., Schmid, A., & Heesemann, J. (2007): On the role of specific chaperones, the specific ATPase, and the proton motive force in type III secretion. *International Journal of Medical Microbiology : IJMM*, 297 (1), 27–36.

Wilharm, G., Lehmann, V., Krauss, K., Lehnert, B., Richter, S., Ruckdeschel, K., Heesemann, J., & Trulzsch, K. (2004a): Yersinia enterocolitica type III secretion depends on the proton motive force but not on the flagellar motor components MotA and MotB. *Infection and Immunity*, 72 (7), 4004–9.

Wilharm, G., Lehmann, V., Neumayer, W., Trcek, J., & Heesemann, J. (2004b): Yersinia enterocolitica type III secretion: evidence for the ability to transport proteins that are folded prior to secretion. *BMC microbiology*, 4, 27.

Yang, Y., Zhao, J., Morgan, R. L., Ma, W., & Jiang, T. (2010): Computational prediction of type III secreted proteins from gram-negative bacteria. *BMC bioinformatics*, 11 Suppl 1, S47.

Yeates, T. O., Norcross, T. S., & King, N. P. (2007): Knotted and topologically complex proteins as models for studying folding and stability. *Current Opinion in Chemical Biology*, 11 (6), 595–603.

Zarembinski, T. I., Kim, Y., Peterson, K., Christendat, D., Dharamsi, A., Arrowsmith, C. H., Edwards, A. M., & Joachimiak, A. (2003): Deep trefoil knot implicated in RNA binding found in an archaebacterial protein. *Proteins*, 50 (2), 177–83.

Zychlinsky, A., Kenny, B., Menard, R., Prevost, M. C., Holland, I. B., & Sansonetti, P. J. (1994): IpaB mediates macrophage apoptosis induced by Shigella flexneri. *Molecular Microbiology*, 11 (4), 619–27.

Zychlinsky, A., Prevost, M. C., & Sansonetti, P. J. (1992): Shigella flexneri induces apoptosis in infected macrophages. *Nature*, 358 (6382), 167–9.

List of Figures

List of Tables

6 Appendix

6.1 Abbreviations

	General abbreviations
α	alpha
β	beta
Δ	gene deletion mutant
A	adenine
APS	ammonium persulfate
ATP	adenosine triphosphate
bp	base pair
BSA	bovine serum albumin
C	cytosine
C-terminus	carboxy terminal end of polypetide or protein
Da	Dalton (molecular weight unit)
DMEM	Dulbeccos modified Eagle medium
DNA	desoxyribonucleic acid
EDTA	ethylene diamine tetraacetate
FCS	fetal calf serum
FPLC	fast performance liquid chromatography
G	guanine
HEK	human embryonic kidney (cell line)
HEPES	2-[4-(2-hydroxyethyl)-1-piperazino]-ethansulfonic acid
Inv	invasion
Ipa	invasion plasmid antigen
IpgC	invasion plasmid gene C
IPTG	isopropyl thiogalactoside
kb	kilo base
kDa	kilo Dalton
LB	lysogeny broth (medium)
MALDI	matrix assisted laser desorption/ionization
MOI	multiplicity of infection
MS	mass spectrometry
Mxi	membrane expression of invasion
N-terminus	amino terminal end of polypetide or protein

	General abbreviations
NC	needle complex
OD	optical density
PAGE	polyacrylamide gel electrophoresis
PCR	polymerase chain reaction
PBS	phosphate-buffered saline
PDB	Protein Data Bank
PEG	polyethylene glycol
PFA	para-formaldehyde
pI	isoelectric point
psi	pressure unit, Pascal
rcf	relative centrifugal force
rpm	revolution per minute
RT	room temperature
SDS	sodium dodecylsulfate
SEC	size exclusion chromatography
Spa	surface presentation of antigen
T	thymine
TCA	trichloroacetic acid
TEMED	N,N,N’,N’-tetramethylethylenediamine
TRIS	Tris(hydroxymethyl)-aminomethane
T3SS	type three secretion system
wt	wildtype
Yop	Yersinia outer protein
Ysc	Yersinia secretion

	Amino acids		
G	Glycine (Gly)	W	Tryptophan (Trp)
P	Proline (Pro)	H	Histidine (His)
A	Alanine (Ala)	K	Lysine (Lys)
V	Valine (Val)	R	Arginine (Arg)
L	Leucine (Leu)	Q	Glutamine (Gln)
I	Isoleucine (Ile)	N	Asparagine (Asn)
M	Methionine (Met)	E	Glutamic acid (Glu)
C	Cysteine (Cys)	D	Aspartic acid (Asp)
F	Phenylalanine (Phe)	S	Serine (Ser)
Y	Tyrosine (Tyr)	T	Threonine (Thr)

6.2 Sourcecode for R: Nearest-neighbor analysis

```
require(Biobase)
# Set parameters
config.image.size.x <- 2045
config.image.size.y <- 2045
config.factor.nm_per_pixel <- 200/176
config.histo.breaks <- 50
config.path<-"#folder with images"
# Define functions
simulate.events <- function(events){
    matrix(
        trunc(
            runif(events*2) * c(config.image.size.x,config.image.size.y)
        ),
        ncol=2,
1        byrow=TRUE
    )
}
files.input <- list.files(config.path, pattern=".*txt$")
list.input <- lapply(files.input,function(file.in)
{read.csv(paste(config.path,file.in,sep=""),sep="",header=TRUE)})
data.coord_dist <- sapply(list.input,function(data.input){
    pos.needle <- data.input[data.input$Type==1,c("X","Y")]
    pos.gold <- data.input[data.input$Type==2,c("X","Y")]
    pos.needle<-matrix(as.double(c(pos.needle$X,pos.needle$Y)),ncol=2,
        dimnames=list(NULL,colnames(pos.needle)))
    pos.gold<-matrix(as.double(c(pos.gold$X,pos.gold$Y)),ncol=2,dimnames=
        list(NULL,colnames(pos.gold)))
    count.needle <- dim(pos.needle)[1]
    count.gold <- dim(pos.gold)[1]
# Find nearest neighbors (nn)
    nn.gold.needle <- matchpt(pos.gold,pos.needle)
    nn.segments <- cbind(pos.gold,pos.needle[nn.gold.needle$index,])
    list(nn.gold.needle$distance,pos.needle[,"X"],pos.needle[,"Y"],pos.gold
        [,"X"],pos.gold[,"Y"],c(count.needle,count.gold))
})
histo.data.lin <- hist(unlist(data.coord_dist[1, ])*config.factor.nm_per_
    pixel, breaks=config.histo.breaks, plot=FALSE)
histo.data.log <- hist(log(unlist(data.coord_dist[1, ])*config.factor.nm_per
    _pixel,10), breaks=config.histo.breaks, plot=FALSE)
```

```
data.simulation <- replicate(50,sapply(data.coord_dist[6,], function(counts_
    needle_gold){
     matchpt(
          simulate.events(counts_needle_gold[2]),
          simulate.events(counts_needle_gold[1])
     )$distance
}))
histo.simulation.lin <- hist(unlist(data.simulation)*config.factor.nm_per_
    pixel, breaks=config.histo.breaks, plot=FALSE)
histo.simulation.log <- hist(log(unlist(data.simulation)*config.factor.nm_
    per_pixel,10), breaks=config.histo.breaks, plot=FALSE)
#output
postscript(file="P:/foo.ps",paper="a4")
par(mfrow=c(2,1))
plot(histo.data.log,
     xlim = range(histo.data.log$breaks, histo.simulation.log$breaks),
     xlab = "Distance␣(nm)",
     ylab = "Counts",
     col = "00000080",
     freq = FALSE,
     main = "Distribution␣of␣nearest␣neighbors"
)
plot(histo.simulation.log,
     col = "#80808080",
     freq = FALSE,
     add = TRUE
)
legend("topright",
     c("Data", "Simulation"),
     fill = c("black", "darkgrey"),
     bty = "n",
     border = NA
)
dev.off()
```